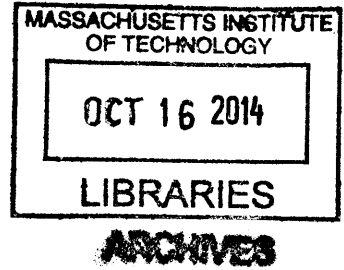Boundary Condition Effects On Vibrating Cantilever Beams

By

Jonathan David Monti

Sc.B. Mechanical Engineering
United States Naval Academy, 2012

Submitted to the Department of Mechanical Engineering
in Partial Fulfillment of the Requirements for the Degree of
Master of Science in Mechanical Engineering

at the

Massachusetts Institute of Technology

September 2014

Signature redacted

Signature of Author..
Department of Mechanical Engineering
August 8, 2014

Signature redacted

Certified by. ....
Martin L. Culpepper
Professor of Mechanical Engineering
Thesis Supervisor

Signature redacted

Accepted by.......................
David E. Hardt
Professor of Mechanical Engineering
Graduate Officer

THIS PAGE INTENTIONALLY LEFT BLANK

Boundary Condition Effects On Vibrating Cantilever Beams

By

Jonathan David Monti

ABSTRACT

Compliant mechanisms continue to see increased used in many areas of modern engineering. Their low cost, ease of production and manufacturing, and precision of motion have made them attractive solutions to many controlled motion systems such as nanopositioners or linear platforms. However, in some applications the stiffness requirements for the devices to function properly and the stiffness requirements for devices to survive outside effects such at vibration or impulse create a conflict which cannot be rectified with traditional engineering approaches. By utilizing boundary controls which acted only when a flexure reached a certain deflection, the original purpose of the device could be preserved while also reducing or eliminating the risk of failure from plastic deformation or brittle failure. By starting with the most basic of compliant mechanisms, the cantilever beam, and utilizing Buckingham Pi theory the dynamic behavior of the vibrating beams could be quantified and the associated variables used to tailor the design of a flexure and boundary control system. This research details the primary correlation between variables in a flexure system during natural frequency excitation and provides the mathematics necessary to implement boundary controls to prevent flexure failure. With this new information, cantilever style flexures can now be designed to operate in environments which previously would have put them at risk of catastrophic failure, and can allow for three to four times the increased range performance of a compliant mechanism in these environments without risk of failure. Furthermore, this research lays the foundation for the study of more complex flexures and multi degree-of-freedom systems.

Thesis Supervisor: Martin L. Culpepper
Title: Professor of Mechanical Engineering

THIS PAGE INTENTIONALLY LEFT BLANK

ACKNOWLEDGEMENTS

CONTENTS

7

8

FIGURES

11

TABLES

1

INTRODUCTION

1.1 Introduction

The purpose of this research is to lay the foundation for implementing boundary control features in compliant mechanisms to prevent catastrophic failure due to vibrational forces. Current design methods do not include a tool to develop compliant mechanisms which will have boundary condition interaction over only a portion of their flexing range. The flexing range is defined as the range of motion which a mechanism can bend throughout without causing plastic deformation or catastrophic failure. This research focused on creating a way to predict the performance of a vibrating cantilever beam that contacts a boundary condition during its range of motion. This thesis seeks to create design guidelines for boundary conditions in compliant mechanisms, specifically cantilever beams, to allow them to maintain desired functions while mitigating survivability issues by introducing suitable boundary conditions. This will be accomplished by utilizing the Buckingham Pi method and a large set of test data. The implementation of boundary controls, which only interact with the mechanism when it reaches a point beyond its functional range, will allow designers to ensure a failure does not occur while preserving the desired static design performance. This research lays a foundation by analyzing a cantilever beam system exposed to vibration and provides a path for continued research into more complex compliant structures.

1.2 Background

1.2.1 Introduction to Final Product

Figure 1.1 is a basic graphic of the physical system and illustrates exactly how it functions as well as what the pertinent variables are in the test setup. A cantilever beam driven at

a frequency ω_D, with an amplitude δ_D, will cause the cantilever beam of length L with mass m to bend and deflect, specifically at the resonant frequency. If left unchecked this motion would eventually cause the failure in the beam either through plastic deformation or complete failure in a brittle material. Utilizing Buckingham Pi Theory and
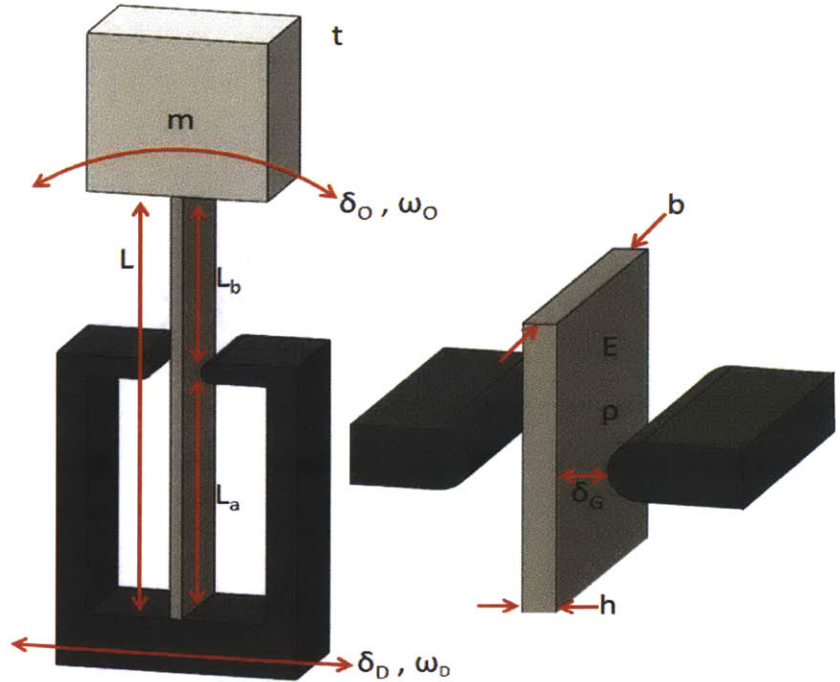
Figure 1.1: Full System Diagram

test data, we sought to determine what the exact effect of δ_G, L_b, and L_a would be, and how to utilize the variables in the system to prevent a catastrophic failure. Following the Pi term derivation we discovered one major correlation which led to the creation of an operating line between two Pi terms (Figure 1.2: π_5- π_1 Correlation). This allowed variables in a system to be properly adjusted to maintain original performance and also prevent the device from failing if exposed to random vibration.

Figure 1.2: π_5- π_1 Correlation

14

1.2.2 Specific Motivation for Research

The Lunar Laser Communication Demonstration (LLCD) is a collaborative effort between NASA and MIT Lincoln Laboratory which sought to develop the first fully functional spaced based laser communications system [1]. The purpose of this project was to develop a communications system designed around lasers instead of the traditional RF technology. As designed the LLCD can transmit data at rates of up to 622 Mbps download and 20 Mbps upload. The system is comprised of two major components; the Lunar Lasercomm Space Terminal, and the Lunar Lasercomm Ground Terminal (Figure 1.3) [2].
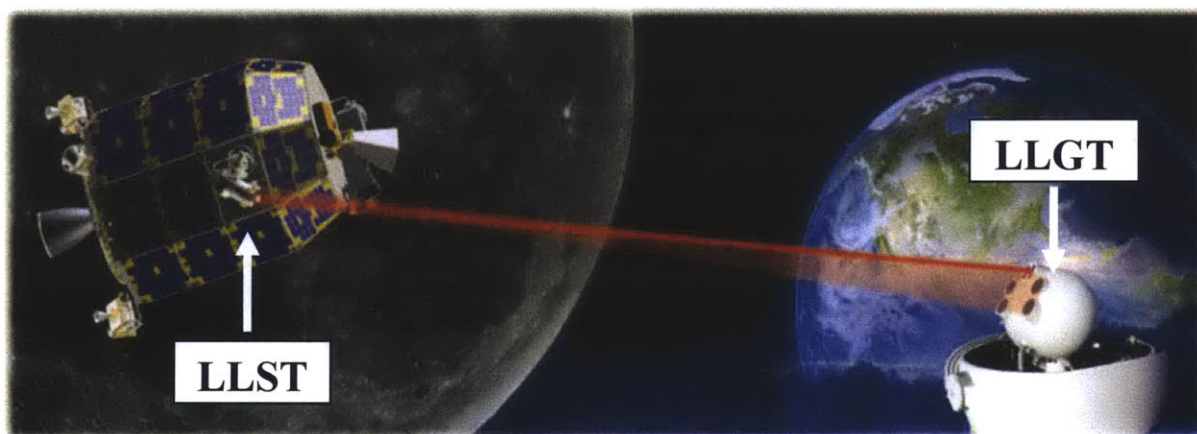
Figure 1.3: LLCD System Graphic

The Lunar Lasercomm Space Terminal (LLST) which sits aboard the LADEE spacecraft and has three sub modules; the optical module, modern module, and controller electronics module. The second component, the Lunar Lasercomm Ground Terminal (LLGT) consists of eight transreceivers and receiver telescopes and is built on a mobile platform allowing for deployment at various locations [2]. The nanopositioner, which motivated this research, is a subcomponent of the optical module on the LLST and is responsible for the Point-Ahead capability of the system by utilizing piezo-electric crystals on a compliant stage [3]. Due to relative motions of the LLST and the LLGT this nanopositioner must direct the outgoing beam with a Point-Ahead Angle (PAA). The greater the range of the PAA the greater the relative speed can be between the platforms while maintaining communications capabilities [4]. A greater PAA capability increases the overall capability of the platform by both increasing coverage area and

15

decreasing amount of LLST's required, or by allowing the same number of satellites to create redundancy coverage.

1.2.3 Current Technology

In order to increase the performance of each optical module, a PAA 4-6 times greater than the current capability was desired. This was not possible with the original nanopositioner due to its development around stacked piezo actuators. These actuators provide for high force outputs at the cost of total range (~1kN blocking force, ~15μm free deflection, manufacturer dependent) [5]. Even using amplification arms, the stacked piezos would not be able to compensate for the limited deflection ranges they provided. The use of stacked piezos was motivated by the need for the nanopositioner to have a high natural frequency to avoid catastrophic failure during launch. The LADEE spacecraft is launched via the United States Air Force's Minotaur V rocket. Technical documents released by the U.S. Air Force indicate the random vibration frequency envelope and spectral energy density can reach range from 2-2000Hz and 0.002-.012g^2/Hz respectively with 3.5344gRMS as seen in Figure 1.4 [6].

Breakpoints	
Frequency (Hz)	PSD (g2/Hz)
20	0.002
60	0.004
300	0.004
800	0.012
1000	0.012
2000	0.002
3.5344 gRMS 60 Sec Duration	

TM14025_069
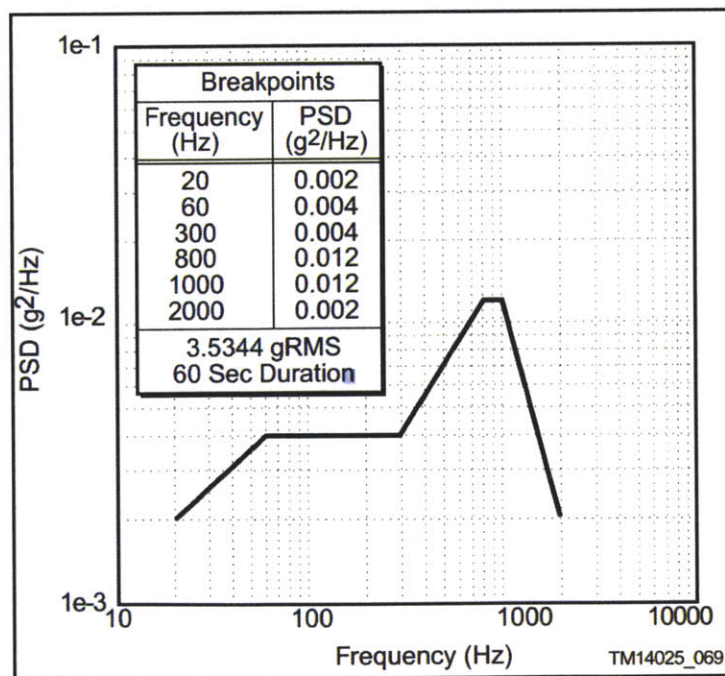
Figure 1.4: Minotaur Payload Random Vibration During Flight

16

The random vibration frequencies and spectral energy density mandate the nanopositioner platform must have a certain stiffness and natural frequency in order to survive the 60 second launch window, beyond which vibration is negligible (Figure 1.4). For this reason, stacked piezos with low range and high force output had previously been utilized, which greatly limits the PAA.

1.2.4 Large PAA Nanopositioner

In order to get the desired increase in PAA while abiding by the geometric constraints of the original system, stacked piezo actuators had to be replaced with bending piezo actuators. These bending piezos would allow for PAA's 4-6 times higher than the current solution, at the cost of overall stiffness. Table 1.1 lists the requirements and constraints put forth for new the nanopositioner design.

Table 1.1: Nanopositioner Design Requirements

Nanopositioner Property	Required	Units
Translation X	+/- 50	μm
Translation Y	+/- 50	μm
Length (Z)	<22.8	mm
Width (X)	<20	mm
Height (Y)	<17	mm
Natural Frequency	>1000	Hz
Drive Voltage	⁻50-200	Volts

With these design requirements in mind the nanopositioner in Figure 1.5 was designed utilizing CMBP03 Bending Piezo Actuators manufactured by Noliac. These bending piezos are capable of +/-85μm free deflections and have a blocking force of 5.5N [6], which was the largest range and blocking force available from an off-the-shelf plate bender with suitable geometry. With these piezos at the heart of the design, the nanopositioner was capable of meeting or exceeding all design requirements from Table 1.1 as can be seen in Table 1.2.

17

Figure 1.5: Large PAA Nanopositioner
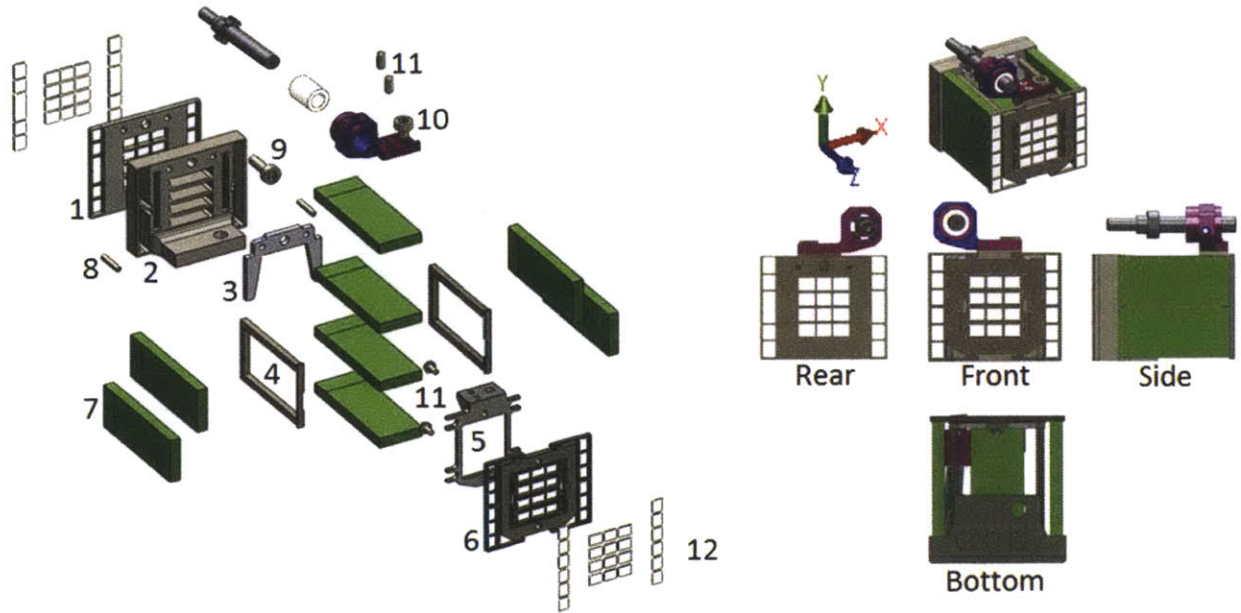
Part #	Description	Material	Part #	Description	Material
1	Base Piezo Retainer	Aluminum	7	CMBP03 Piezo	PZT
2	Base	Aluminum	8	5x1 mm Pin	Aluminum
3	Base Leg Retainer	Aluminum	9	M1.6x0.35 Screw	Steel
4	Flexure Legs	Titanium	10	M1.06x0.35 Screw	Steel
5	Ferrule Mount Connector	Aluminum	11	M1x0.25 Screw	Steel
6	Decoupling Flexure	Titanium	12	Epoxy	Epoxy

Table 1.2: Nanopositioner Performance

Nanopositioner Property	As Designed	Units
Translation X	+/- 57	μm
Translation Y	+/- 58	μm
Length (Z)	<21.7	mm
Width (X)	<20	mm
Height (Y)	<17	mm
Natural Frequency	2095	Hz
Drive Voltage	0-200	Volts

18

Although the large PAA nanopositioner meets or exceeds all desired properties, vibration platform testing must still be performed to ensure survivability in a launch scenario. Early FEA indicates the platform has a factor of safety just over 1, with failure occurring at the base of the piezos in the corners as indicated in Figure 1.6. With a factor of safety just over 1 and any failure in these piezos causing not only a major performance setback within the system but even larger problems due to fragmented piezo material free floating throughout the

Figure 1.6: Large PAA Failure Points

optic system, a more robust and effective survivability setup was preferred. This was the fundemental motive which drove the research conducted in this thesis.

1.3 The Endless Design Loop
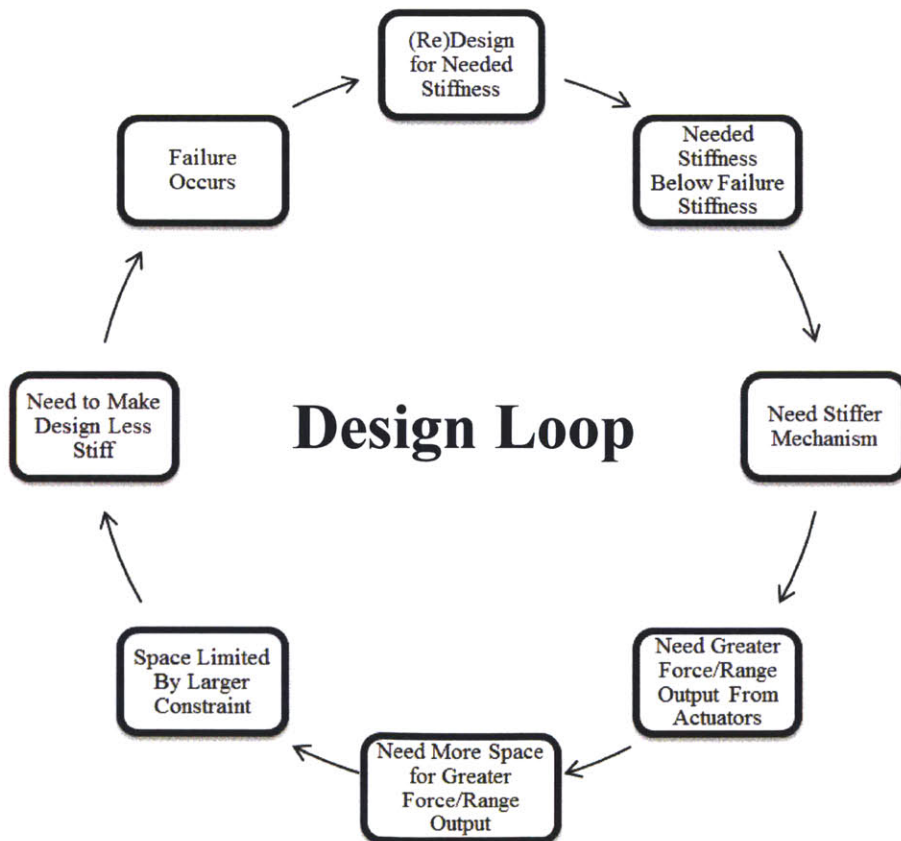
Figure 1.7: Endless Design Loop

The primary problem with current philosophy, especially in regards this area of design, is that if the stiffness needed for functionality is considerably lower than the stiffness needed for survivability it creates an endless loop (see Figure 1.7).

There are ways to break out of this loop; use higher force actuators, higher strength materials, etc. However, these break

point items are highly researched and movement is now incremental. It is unlikely that next year a company will introduce a piezo with all the same dimensions and characteristics of current ones only with double the force output. Same goes for the materials used in construction.

1.4 The Larger Picture

Although the motive behind this research was a specific application, increased survivability during rocket launch, the research has applications beyond this single area. Intelligently designed boundary control could be used not only for catastrophic failure mitigation, but stiffness zone designing, and controlled stiffness increases (to be discussed in further detail later). In the specific satellite situation discussed, proper implementation of the boundary condition controls could result in a satellite network performing anywhere from 4 to 6 times more effectively than currently designed. This means the total network cost for a full coverage satellite network could be reduced by 4 to 6 times, or there could multiple layers of redundancy in a lasercomm network. With a single Minotaur series rocket costing $50 million to procure and launch (each Minotaur rocket can carry up to seven satellites) [8], and the average cost of a satellite at nearly $100 million [9], the cost savings to this program alone could be in the billions (initial LLCD launch was lunar based, still yet to be determined how orbital satellite network would be arranged or how many of the current generation of LLST's would be required). This is the larger impact cost. In a more direct sense, the previous nanopositioner was in development for nearly half a decade by a team of engineers at Lincoln Lab. Boundary control research will give designers a clearer understanding of compliant mechanism design subjected to random vibrations.

Compliant mechanisms have become increasingly popular, especially in the area of precision control. As stated previously, compliant mechanisms are the choice platform for long range communications laser positioning. However, the larger application of compliant mechanisms includes surgical tools [10], precision machining [11], and automotive and aerospace applications [12], to name a few. Compliant mechanism are growing in popularity largely due to their reduction in production cost (many are designed and built as single piece structures without the need for assembly or multiple stages of production) and increase in performance due to the single unit design. The performance benefits come from reduced size

and weight, reduced wear [12], and little or no assembly means no friction, or error due to imprecise parts fit/alignment. All compliant mechanisms are built with a balance between overall stiffness needed for the device application, and stiffness required to ensure part reliability and survivability. This research seeks to give compliant mechanism designers a new tool to apply to a design which will preserve the stiffness required for application, while addressing the stiffness required to ensure reliability and survivability.

1.5 Prior Art

Very little work has been done previously in this area of research. Nearly all work containing similarities has to do with AFM or PCV research. The closest research content to what is contained in this thesis was conducted by Clemens T. Mueller-Falcke and has to do with variable stiffness in AFM cantilever beams (Figure 1.9 [13]). His research focused on utilizing external
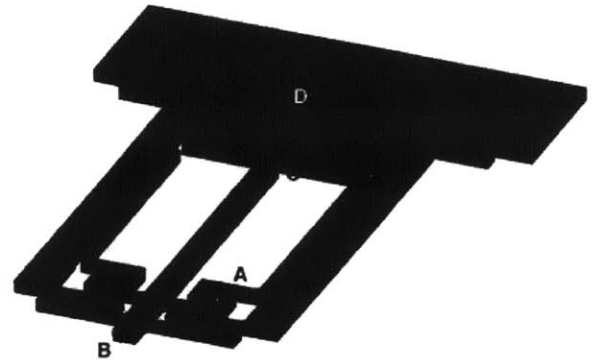
Figure 1.9: AFM Variable Stiffness

beams which would be electrostatically charged causing them to bond to the original beam, thus changing the stiffness of the beam. This research does directly apply to the issues being discussed in this thesis since the adjustments were made deliberately and at determined times and was used as an active system. Upon activation the system would merely take on a set new stiffness value, but still move and function as a cantilever beam (essentially the same as changing the geometry). This process would not apply to case being address in this since a passive step-function stiffness increase is required at a predetermined deflection. The other major research into this field was conducted by David Freeman. He characterized deflection in Pressure Control

Figure 1.8: PCV Non-Linear Motion

Valves contacting an external boundary, but his research deals with valve plates with large deformations into the non-linear region of motion, and that research is only concerned with static deformations (Figure 1.8 [14]). In most engineering practices, designing a deflecting part such that it will contact another body and continue deflecting would generally be avoided due to the friction, contact stress, shock etc. This could explain the limited amount of research in this area.

21

1.6 Preview of Thesis Contents

This thesis will:

- Lay the foundation for the research
    - o Introduce the fundamentals of flexure design
    - o Introduce the basic concept of boundary condition control fundamentals of boundary condition control and explain current boundary condition control styles
    - o Discuss the benefits of boundary condition control
- Discuss the math behind the proposed boundary condition controls
    - o Basic beam bending math
    - o Static beam bending with contact on a rigid body
    - o Beam dynamics and math limitations
- Introduce Buckingham Pi method
- Discuss vibrating beam test theory
    - o Scope
    - o Assumptions
- Detail vibrating beam test setup
    - o Vibration test bench design
    - o Beam sample design and test fixture design
    - o Test theory assumptions
- Discuss test process and data handling
- Analyze Buckingham Pi associations
- Complete a practical application example
- Introduce future work

2

Fundamentals of Flexure Design and Motivation for Specific Research

2.1 Compliant Systems Nanopositioner Design

2.1.1 Compliant Stage

Most compliant mechanism based positioner designs consist of a compliant stage and an actuator. The compliant stage is then broken up into 3 distinct zones; ground, flexures, and stage (Figure 2.2). Figure 2.1 shows three examples of modern piezo driven nanopositioners (for intellectual property reasons, exact design schematics not available); **1**. nPXY60-258 by nPoint Inc. [13], **2**. P-612.2 Compact XY Positioner by Physik Instrumente [16], **3**. PZ 250 CAP WL by Piezosystems Jena [17] . Indicated in the figure are the ground portions (solid black line) and actuated stage portions (dotted line) of each positioner, with the piezo and exact flexure system being enclosed within the shell of the device.

Figure 2.1: Example Nanopositioners

Ground indicates the portion of the device which is considered to be stationary, often locked or screwed to a bench or larger machine. The flexures are responsible for allowing, restricting, or directing the motion of the stage. The stage is where the object to be manipulated

would be secured, and the actuator (in the above cases a piezo), is responsible for supplying the force to move the stage into place. Figure 2.2 is a simplified diagram of what this would look like in a basic cantilever compliant mechanism.
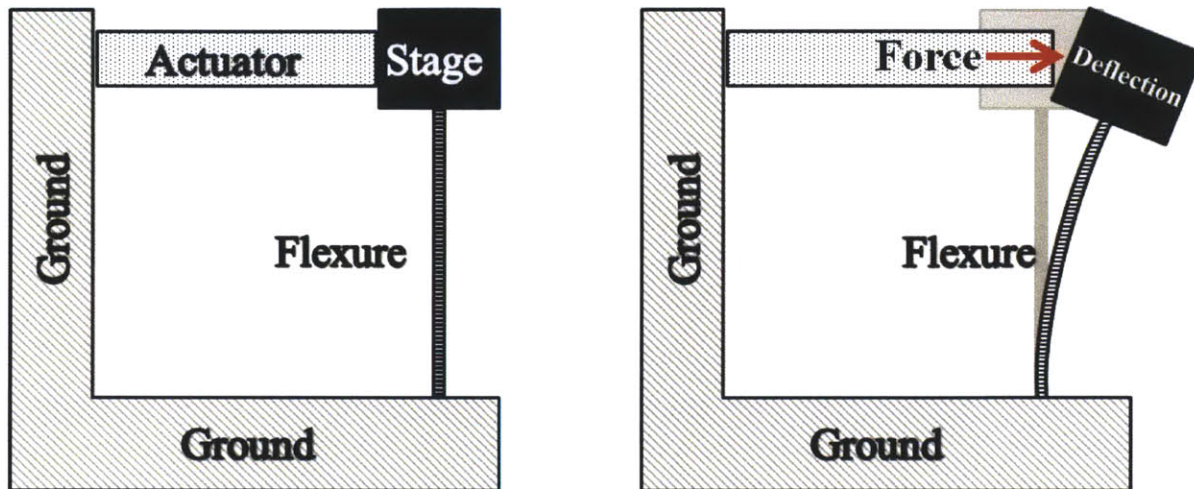
Figure 2.2: Basic Compliant Stage Diagram

The force and deflection values are mathematically tied together. In order to increase the stage deflection the force must be increased, assuming the max deflection of the actuator has not been reached, or the flexure stiffness must be decreased. In the case of the compliant stage in Figure 2.2 the governing mathematics are fairly basic and straightforward. If the compliant stage above is simplified into a single degree of freedom system, as can be seen in the free body diagram in Figure 2.3, and the deflections are large enough that internal stresses can be ignored (simplified beam equations instead of Timoshenko beam equations), then relating the actuator force (F_{Act}) with the static deflection requires it to be balanced with the spring force exerted by the flexure (F_{Spr}).
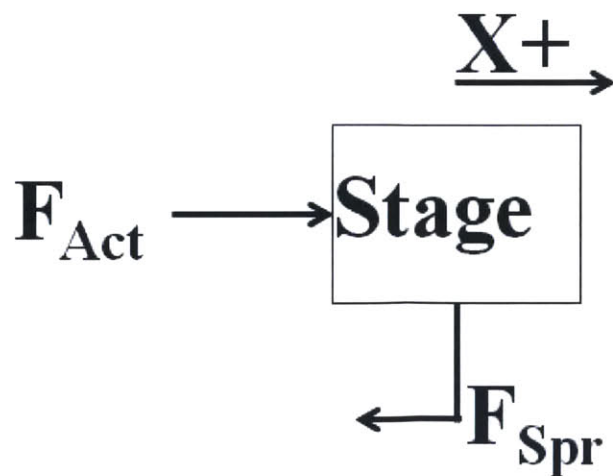
Figure 2.3: Basic Stage FBD

$$F_{Act} = F_{Spr}$$

24

And

$$F_{Spr} = K_{Spr}x$$

with x being the magnitude of deflection in the stage, then

$$F_{Act} = K_{Spr}x$$

The stiffness K_{Spr} has previously been determined to be

$$K_{Spr} = 3EI/L^3 \quad \text{and} \quad I = bh^3/12$$

with E, and L being the modulus of elasticity of the specific material used and the length of the beam respectively. I is the moment of inertia for the beam and consists of the beam dimensions both in line with the direction of motion, h, and perpendicular to the motion and the length, b, Figure 2.4.
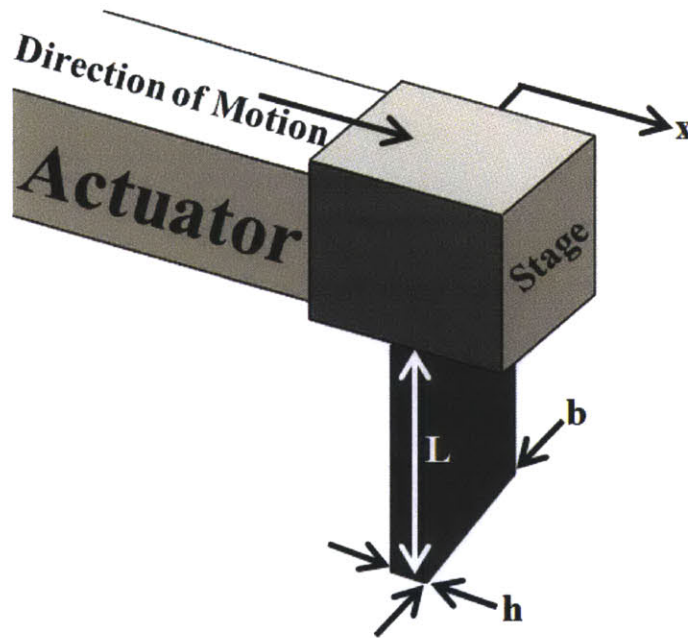
Figure 2.4: Beam Geometry Diagram

Therefore, the governing equation which relates the force output of the actuator to the stage's deflection in the X direction is

$$F_{Act} = x3EI/L^3$$

25

This is one of the most basic forms of a compliant mechanic being used as a positioning stage, and as such the mathematics are fairly straightforward as well. There are many more configurations of flexures that can be used to direct actuator motion in a specific axis. Figure 2.5 [16] shows three examples of flexure systems without an actuator, each with increasing complexity, and each with a different purpose.
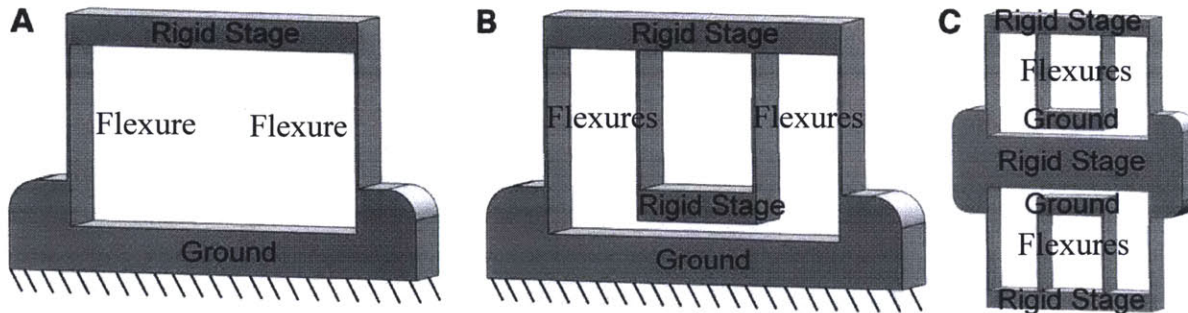
Figure 2.5: Parallel (A), Serial (B), Hybrid (C) Flexure Systems [18]

There is much literature detailing how to develop flexure systems, the math which governs specific configurations, and the expected performance and capability that can achieved with various flexure structures. These more complex systems will not be discussed in this thesis unless pertinent to the content of the chapter.

2.1.2 Nanopositioner Actuation Solutions

Although the design of most positioning stages is fairly straightforward, problems begin to arise when the requirements for a stage become contradictory. This is the case in the previously discussed Large PAA nanopositioner. Due the size constraints on the device, piezoelectric and voice coil actuators (Figure 2.6 [20]) are the only two widely available actuators which are suitable for this application. For voice coils the governing equations are

Figure 2.6: Voice Coil Actuator

$$F = kBLIN$$

Where F =force, k=constant, B=magnetic flux density, I=current, L=length of conductor, and N=number of conductors [19]. All things being constant this means that the force output on a

26

voice coil is directly proportional to the length of the conductor. Therefore, as the package size decreases the force output of the voice coil decreases as well, this causes a problem when designing for space-limited applications.

The second primary actuator used is the piezoelectric actuator. These break into many different types; stacked (1), plate (2), and bender (3), to name a few (Figure 2.7).
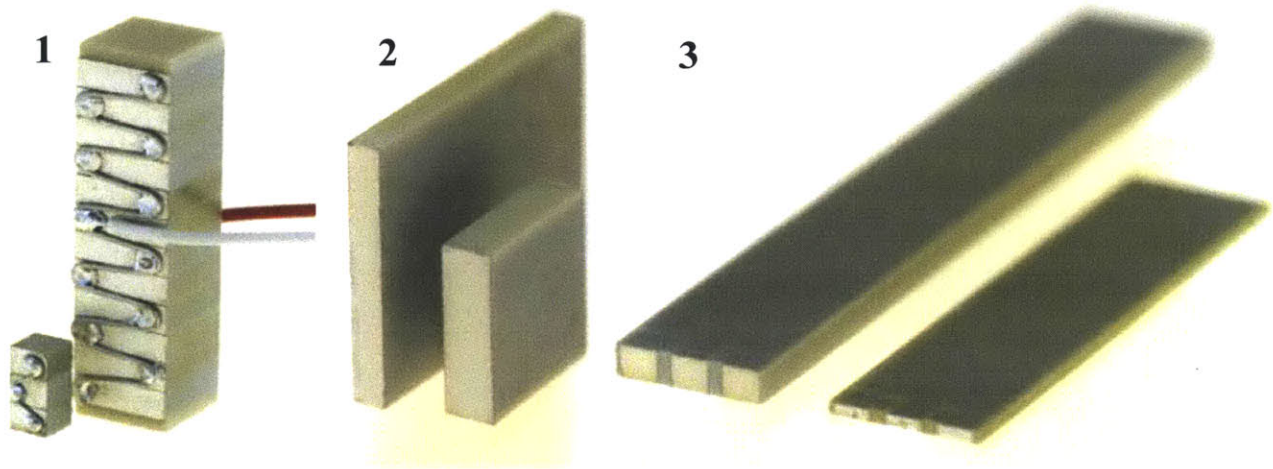
Figure 2.7: Piezoelectric Actuator Types

For piezoelectric actuators the general force equation for zero deflection (blocked force) is

$$F_{max} = k_T \Delta L_O$$

where k_T=piezo actuator stiffness, and ΔL_O=max displacement without external restraint [21], and

$$k_{T-axial} = AE/L$$

$$k_{T-transverse} = 3EI/L^3$$

and

$$A = wt \qquad I = bh^3/12$$

where E=modulus of elasticity for the specific material, and L, w, t, b, and h are illustrated in Figure 2.8.
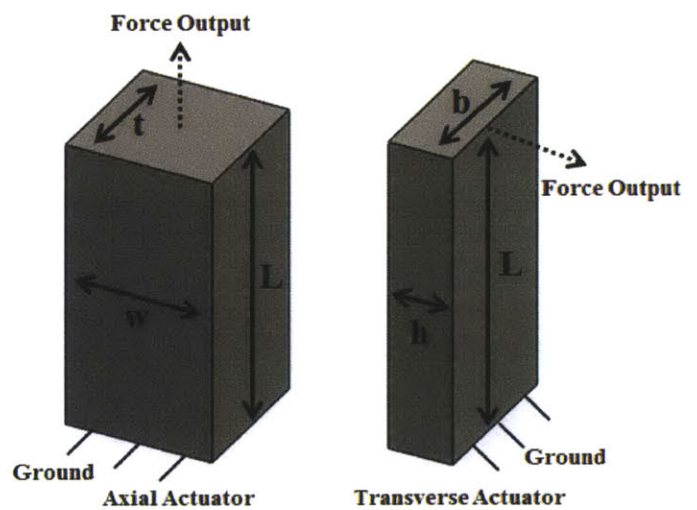
Figure 2.8: Piezo Geometry Diagram

Once again, as was the case with the voice coils, as the package size decreases the output force also decreases (depending on which element of the geometry is being reduced).This is without even taking into account the specifications for needed stroke length.

With the two primary actuation methods being governed by physics which limit force output based upon package size, designers are forced to develop a stage which can achieve the desired performance while staying at or below the force output threshold for the specific actuator chosen.

2.2 Contradicting Requirements for Compliant Stages in Harsh Environments

For many nanopositioner applications the environment will be well controlled with respect to vibration and in some cases will have unique requirements demanded of the device. The requirements may include waterproofing, electrical shielding, thermal insulating, or any one of a number of other requirements. For the most part these requirements can be met by a skilled engineer developing an intelligent design. Most requirements are ancillary and can be designed within or around the original device. In some instances the original device may need to be modified. However, none of these requirements are such that they must absolutely interfere with the device's operation to complete their purpose. In rare cases, these nanopositioners will be put into environments where there will be high levels of random vibration. In order for these positioners to survive the harsh environments they must be capable of withstanding the vibrational forces exerted on them. This is the where the contradiction arises.

In order to keep an object from failing in a high vibration environment, the designer has two options; make it more compliant, or make it stiffer. In the first case, make it more compliant, the designer assumes that the deflection in the device is such that rather than trying to fight it, it is wiser to allow the device to move freely. The designer can adjust the design of the device such that the maximum deflection felt by the positioner is less than the deflection required to reach the maximum allowable stress in any area of the device. The problem with

option is that most compliant stages require actuators which are fairly rigid, and the option to simply make them more compliant does not exist. For instance, if a designer chooses to modify the geometry of a bending piezo actuator he or she does so at the cost of performance (either free stroke or blocked force). In the second case, the designer can choose to increase the stiffness of the device. This is most easily done by adjusting the geometries of the flexure elements, or changing the material used in the positioner. However, changing the material is unlikely since the original material was chosen for its specific properties, likely its low modulus of elasticity and high yield stress. That leaves the designers one viable option; adjust the geometry of the flexures to make it stiffer.

In many cases in order to ensure the device will survive the vibration environment the designer must ensure the natural frequency of the device is above the range of vibration frequencies it will be exposed to. Any time a device is exposed to a vibrating frequency equal to its natural frequency the energy in the device builds and will manifest itself as large deformations within the device. Natural frequency is governed by the equation

$$f_n = \sqrt{k/m} \text{ (radians)} \qquad \text{or} \qquad f_n = \frac{1}{2\pi}\sqrt{k/m} \text{ (Hertz)}$$

Where f_n=natural frequency (radians/hertz respectively),

k=equivalent stiffness, and m=tip mass.

Stiffness must be increased or tip mass decreased in order to raise the natural frequency. This works assuming the designer can then adjust the actuation device to cope with the new stiffness values. In some cases this may not be possible due to power, geometry, cost, or a number of other limiting factors. If the designer is unable to adjust the actuation device, he or she is at an impasse. Figure 2.9 shows how the contradiction manifests itself in regards to stiffness, force required (to maintain the same max
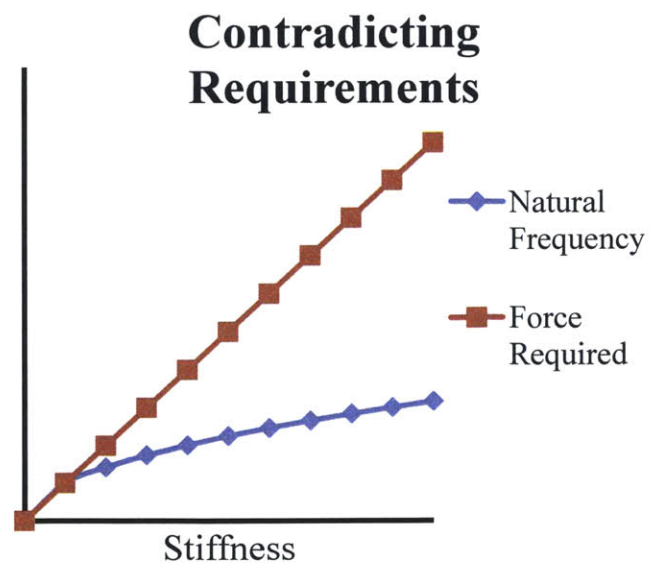
Figure 2.9: Contradicting Requirements

29

deflection), and natural frequency (assuming tip mass is constant) in a basic cantilever beam. The contradiction is the same in other more complex compliant mechanisms as well since fundamentally natural frequency is tied to stiffness and stiffness dictates force required. As can be seen in Figure 2.9, as stiffness increases the force required increases linearly and proportionally, however, natural frequency increases by the square root of the increase in stiffness. What this means for the designer is that any attempt to increase the natural frequency brings with it a severe increase in the force required. As previously discussed in Section 2.1.2 any increase in force required brings with it the mandate that the geometric size of the actuator must also be increased. For instance, if the designer attempts to raise the natural frequency of a device by a factor of 2, the force required increases by factor of 4, and the resulting changes in volume and deflection of commercially available piezos to meet this force requirement are illustrated in Figure 2.10 [22][23][24].
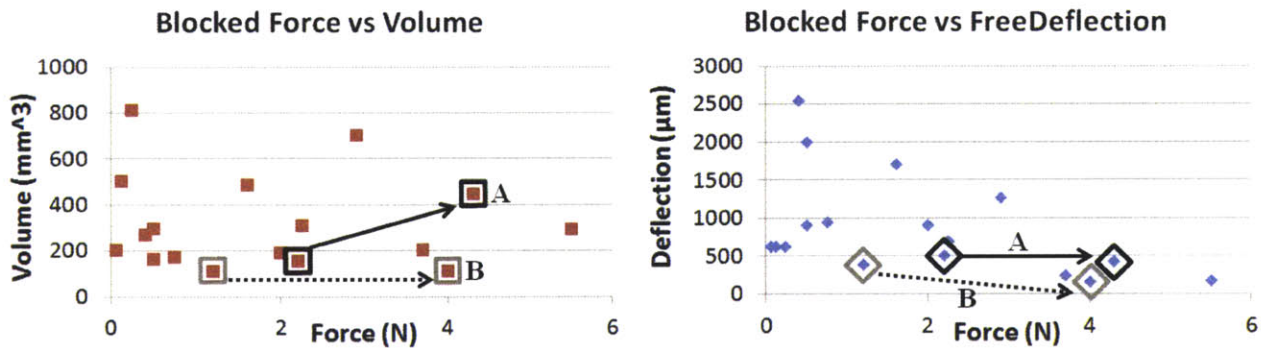
Figure 2.10: Commercially Available Piezo Volumes, Deflections, and Force Outputs

In case **A**, if the designer needs to double the blocked force and maintain a free deflection of ~500µm for the positioner to work properly then the volume of the piezo increases from 156mm³ to 450mm³. Even more significant is that due to the nature of piezoelectrics the volumetric increase will likely be the result of a large change in one aspect of the geometry rather than a proportional increase in all geometries. For case A the length and width remained relatively constant (max change of <20%), but the thickness increased nearly threefold from 0.65mm to 1.8mm. Conversely, in case **B** if the designer needs to maintain the piezo's volume while increasing the output force from 1.2N to 4N the loss to free deflection is nearly 60%, dropping from 390µm to 160µm. These two examples illustrate the fact that if the designer has to

decrease the vibrational sensitivity of a positioning stage in a space-limited application they are left with an impossible situation (see Figure 1.7: Endless Design Loop).

2.3   Finding a Mechanism to Interrupt the Endless Cycle

In order to break the endless design loop, we need to look at every unique element in the design phase and determine which one may still be manipulated. Figure 2.11 shows the basic cantilever beam with all major properties listed (ones that directly impact the problem needing to be addressed).
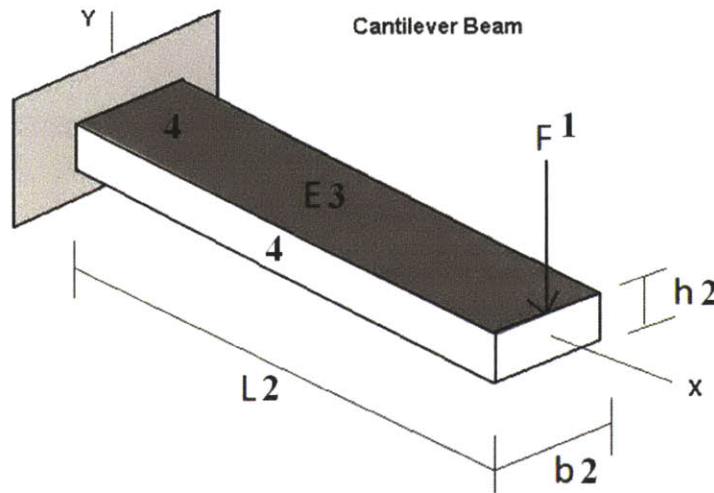
Figure 2.11: Basic Cantilever Beam

As previously discussed, $(F, 1)$ force is fixed or limited due to geometric constraints, the size of the beam $(L, b, h\ (2))$ is limited by both geometric constraints as well as stiffness limitations from the force output of the actuator, $(E, 3)$ modulus of elasticity has likely already been determined based on stage application and is also constrained by force limitations. This leaves no viable option within the system to effect change. However, one area we haven't considered is the surface areas of the flexure (4). In most flexures this surface is a smooth, flat surface, making it ideal for interaction with another body in order to limit its overall deflection. Having this surface area interact with another body at some point beyond its normal flexing range will cause a change in stiffness which can be used to prevent plastic deformation or catastrophic failure.

31

2.4 The Idea of Boundary Control

By using a boundary control mechanism which does not contact the stage during normal operation the stiffness of the device can be changed without interfering with its standard functions. A boundary control could be any body that interacts with the deflecting portions of the stage in such a way as to alter the behavior of the system. Generally speaking, it is unwise to have rigid bodies contacting in a compliant stage. This interaction leads to friction, contact stresses, and shock loading. None of these are desirable characteristics in a compliant stage, and should generally be avoided. But if a boundary control can be implemented in such a way as to prevent ultimate failure of the stage, then the tradeoff to a designer is worthwhile.

3

Boundary Condition Fundamentals

3.1 Previous Boundary Condition Use

3.1.1 Nonuse

The nonuse of a boundary condition in the applications discussed would result in a failure of the flexures or actuators either by plastic deformation, buckling, or brittle failure. When talking about the flexures themselves, plastic deformation will be the likely manner in which a beam fails. In regards to a piezo actuator, brittle failure is likely to occur due to its material properties.

Due to the design nature of the flexures in a compliant stage plastic deformation will occur at the very base first (Figure 3.1). The equation for the stress in a deflecting beam is

$$\sigma = \frac{Mc}{I} \quad \text{and} \quad I = \frac{bh^3}{12}$$

where σ=stress, M=moment at specific point, c=distance from neutral axis, I=area moment of inertia, (I defined in 2.1.1). For a uniform geometry cantilever beam the max stress is found in the very base of the beam, this is where the moment is highest. The equation to determine the max stress from the beam in Figure 3.1 is

$$\sigma_{max} = \frac{PLc}{I}$$
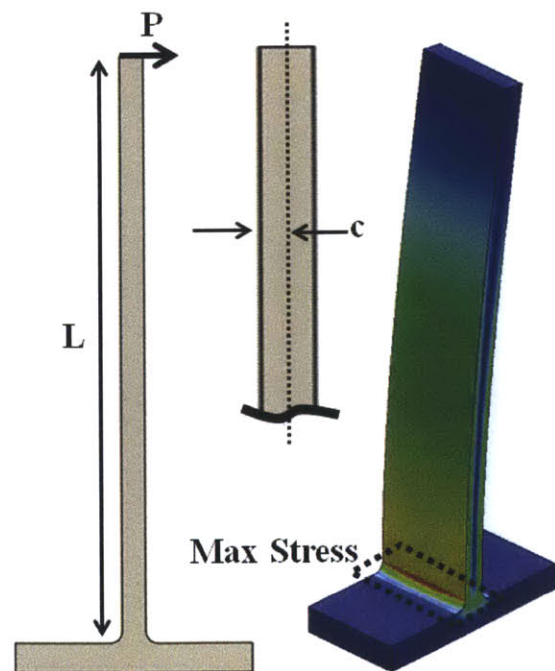
Figure 3.1: Stress in a Cantilever Beam

Looking at the stress-strain curves for two commonly used flexure and actuator materials (aluminum and PZT) (Figure 3.2) [25] [27], we see that the yield stress for a generic piezoceramic is far lower than the yield stress for a flexure. This makes the bending piezo stress the point which must be design around. Without any boundary condition interaction a compliant mechanism subject to a vibration force with enough energy will cause fracturing at the base of the bending piezo. The assumption of this

Figure 3.2: Stress-Strain Curves

research is that the vibrational forces the positioning stage will be subject to will cause the max stress in the base of the piezo actuator to be greater than the established yield stress for the specific piezo material used.

3.1.2 Soft Stops

A soft stop is probably the most commonly used means to prevent a bending element from reaching its yield stress. By inserting a material with a low stiffness the deflecting beam has some interaction with the soft stop which absorbs energy and limits the overall motion the beam can be subjected to. Soft stops can be broken down into two major categories; compliant materials and damping.

3.1.2.1 Compliant Material

A compliant material is any material which has a specifically selected stiffness such that when an object interacts with it there is a period where the compliant material exerts a reactive force to prevent the further motion of the original object. Compliant materials are also used to reduce the shock loading felt by a deflecting object or any object in motion. This concept is used in many every day applications. Common applications include airbags, race car head restraints,

34

football helmets, rubber stops on cabinets, and protective cell phone cases (Figure 3.3) [27][28][29][30][31].

Figure 3.3: Common Compliant Material Applications

The major issue with using compliant materials (rubbers, plastics, etc.) is the outgassing that occurs throughout the object's lifetime. Outgassing is the release of internally held gasses in rubbers, polycarbonates, and many other synthetic materials [32]. The effects of outgassing are amplified in the research specific case by the vacuum present in the space bound platforms. In sealed or controlled applications this outgassing can introduce particles to the atmosphere which are harmful to the overall performance of the system.

3.1.2.2   Damping

Unlike soft stops, which act upon an object with as set reactive force consistent with its stiffness properties, damping is the process which resists motion based upon its velocity at a given time. For instance water can be used a damping mechanism. If a person were to slip their hand into water slowly palm down, the hand would easily cut through the water and sink. However, if a person were to slap their hand against the water with a high velocity the water would exert a reactionary force on the hand to slow its speed; this is damping. A common example of a damping is the strut assembly in a motor vehicle. The strut assembly is comprised

of two major parts (Figure 3.4). First is the coil spring which acts as a compliant material and deforms when a load is placed on it. The problem with having only a coil spring is that when a vehicle hits a bump the force exerted on the spring is greater than the force which the spring can sustain. This is where the damping system begins to act. The shock absorber is the internal tube portion of the strut and acts to resist fast motions, like those induced when hitting a pothole. In general, damping is the preferred method of reducing and limiting the effects of shock on a system. Because the natural frequencies of most systems are relatively high (above single digit frequencies) the velocity of the oscillating mass is also high. This property makes it an ideal setup to introduce damping. However, the issue with damping is that most damping materials and systems include a viscous element (Figure 3.5) [33]. This means they require a housing mechanism or some way to control the damping substance. Since the designer is already working in a space limited capacity this poses a geometric problem. Also, because of the viscous nature of the damping substance, long term use and containment of the substance brings with it a whole new set of design complications.
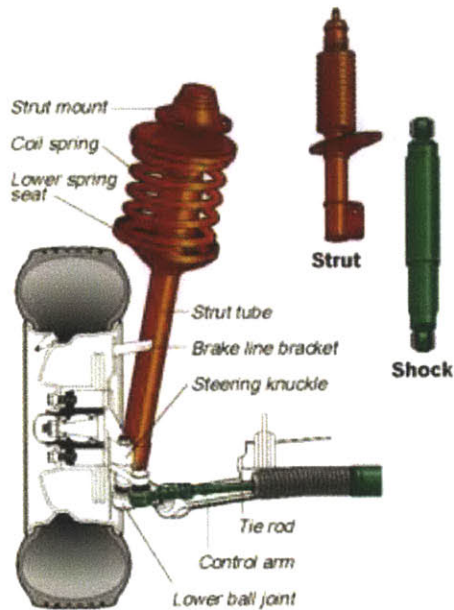
Figure 3.4: Automotive Strut Assembly

Figure 3.5: Oil Damper by ISOTECH

3.1.3 Hard Stop

Another commonly used method of preventing a bending element from reaching its yield stress is a basic hard stop. This is a solid material stop which essentially takes the beam element's stiffness to infinity upon contact. If a person opens a self-closing door at a business, this door has some stiffness associated with its operation. If the person continues to open the door until the handle on the other side smacks into a wall, this would be considered a hard stop. The problem with utilizing a hard stop is that it induces shock loading in the system. If a door is

slammed open into a wall, the door will begin the visibly vibrate after bouncing violently off the wall. Similarly, a deflecting stage will collide with a hard stop and induce further vibration and shock loading from the contact. Shock load is the common term for the force applied to an object which causes sudden acceleration or deceleration. A common way of analyzing the shock imparted on a system is the velocity change method. The shock transmitted when one rigid body collides with another is governs by the equation

$$G_t = \frac{V(2\pi f_n)}{g}$$

and the deflection caused by the shock is

$$\Delta d = \frac{V}{2\pi f_n}$$

where G_t=transmitted shock, V=velocity and is derived from Figure 3.6 [35] (specified for gravitationally controlled systems, can be modified for other accelerating forces), g=acceleration due to gravity (or any acceleration inducing mechanism), and f_n=natural frequency of the system.

Figure 3.6: Shock Excitations

Shock loading is influenced by three factors; mass of the system, the speed of the system just prior to impact, and the rate of change of the acceleration in the system [36]. The rate of change of the accelerations is related to the stopping distance of the system as seen by the basic motion equation

$$\Delta V = V_o + at$$

Where ΔV=change in object velocity, V_o=velocity of the system prior to impact, a=acceleration, t=time

To see a practical example of the forces induced in shock loading Figure 3.7 illustrates a 0.001kg aluminum ball on a negligible stiffness cantilever beam with 0.001m radius about to contact a grounded aluminum plate at 1m/s. To determine the stopping distance we need to know how far the ball travels following its initial contact with the wall. To get a general idea of this distance, we will use the equation for Hertzian contact deformation [37]
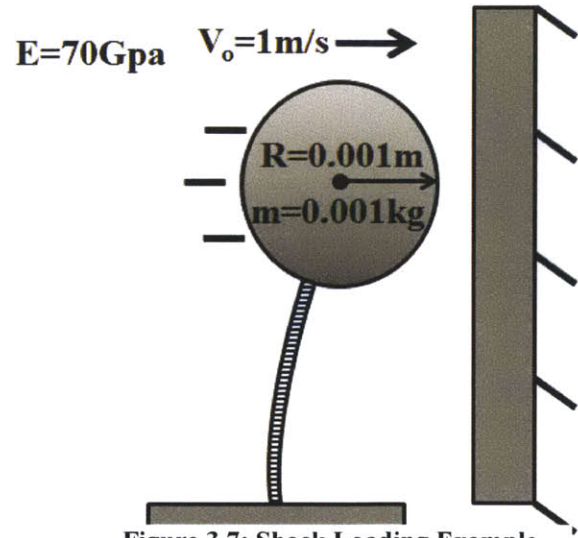
Figure 3.7: Shock Loading Example

$$\delta = \left(\frac{1}{2}\right)\left(\frac{1}{R_e}\right)^{\frac{1}{3}}\left(\frac{3F}{2E_e}\right)^{\frac{2}{3}} \quad \textbf{(I)}$$

and

$$R_e = \frac{1}{\frac{1}{R_1}+\frac{1}{R_2}}$$

where δ=deformed deflection, R_e=equivalent radius, R_{1-2}=radii of object 1 and 2 respectively, F=force of ball in motion, E_e=equivalent modulus of elasticity.

Combining the Hertzian contact equation with the basic displacement equation

$$x = V_o t + \frac{1}{2}at^2 \quad \textbf{(II)}$$

where x=center displaced distance of the ball (deflection), V_o=velocity upon impact, a=acceleration, t=time for ball to reach a zero velocity, results in the equation

$$V_o t + \frac{1}{2}at^2 = \left(\frac{1}{2}\right)\left(\frac{1}{R_e}\right)^{\frac{1}{3}}\left(\frac{3F}{2E_e}\right)^{\frac{2}{3}} \quad \textbf{(III)}$$

Using Newton's second law we can replace force with mass and acceleration, and we know that acceleration is merely the rate of change of velocity

$$F = ma \quad \textbf{(IV)} \quad \text{and} \quad a = \frac{dv}{dt} \textbf{(V)} \rightarrow \text{this case} \quad \frac{dv}{dt} = \frac{\left(-\frac{1m}{s}\right)}{t}$$

substituting **(IV)** and **(V)** into **(III)** results in

$$V_o t + \frac{1}{2}(\frac{dv}{dt})t^2 = \left(\frac{1}{2}\right)\left(\frac{1}{R_e}\right)^{\frac{1}{3}}\left(\frac{3m\frac{dv}{dt}}{2E_e}\right)^{\frac{2}{3}} \quad \textbf{(VI)}$$

leaving *t* as the single unknown variable.

Using all the givens from the original problem:

Variable	Value	Units
V_o	1	m/s
V_f	0	m/s
R_e	0.001	m
m	0.001	kg
E_e	7×10^{10}	N/m^2

we find that *t*=0.0136ms, which can use to calculate the acceleration of the object using

$$\Delta V = at$$

And we know ΔV=-1m/s, and *t*=13.6ns, thus a=-73000m/s^2 which can be plugged back into equation **(IV)** to solve for *F*=73N imparted on the ball during the collision. As a comparison this same ball sitting in the palm of your hand would only exert a force of 9.8mN, and the same collision at a one third reduction in velocity would reduce *F* to 48N. Furthermore, if the Δt value could be increased by a third, the force imparted could be reduced by one third as well. Because a pure contact has such small Δt it is not unreasonable to assume that it could be increased by a factor of 100 or more with a boundary contact which would allow motion to occur at a higher stiffness value beyond contact. These types of forces and loads should be avoided whenever possible, especially in compliant stages using piezo actuators due to the brittle nature of piezoceramic materials. For a further look at contact pressures and stresses see "Precision Machine Design" by Alexander Slocum [37].

In most cases a hard stop is used at the point of highest deflection. In the case of a cantilever beam, this would be the free end of the beam. The problem with this application is that the free end of a cantilever beam is also the point of highest velocity. Since the maximum

Free End

% Beam Length	% Tip Velocity
100	100
90	72.9
80	51.2
70	34.3
60	21.6
50	12.5
40	6.4
30	2.7
20	0.8
10	0.1
0	0

Fixed Base
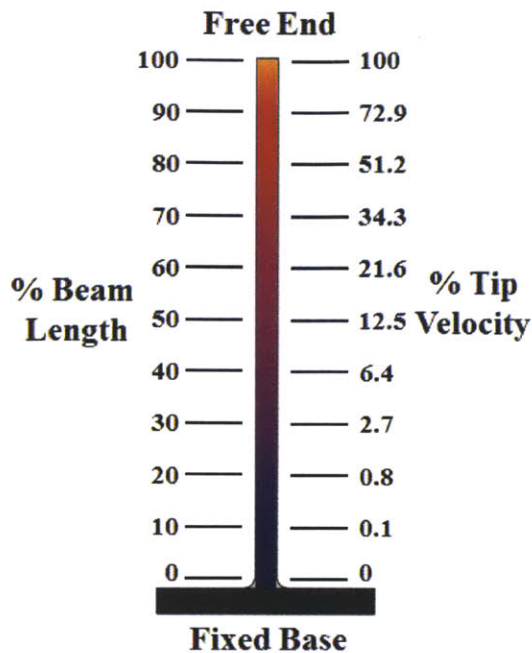
Figure 3.8: Cantilever Beam Velocity Profile

deflection of any point on a cantilever beam is proportional to the velocity at that same point, it would follow that the further you get from the base of the beam the higher the velocity at that point. Since deflection is a properly of the length of the beam cubed, the velocity at a given point on the beam increases by that factor as well. Figure 3.8 illustrates the velocity of a beam at various points as a percent of max tip velocity. If the hard stop were to be moved one third the way down the beam, the induced shock would be reduced by over 70%. Furthermore, if the hard stop is moved down the beam towards the fixed end, there will be a mass above the hard stop which will continue its motion after contact has occurred with the hard stop. This means that stopping time is greatly reduced, thus reducing the force exerted on the beam from the hard stop.

3.1.4 Boundary Condition Control: The Space Between Hard Stop and No Stop

As was discussed in the previous sections, if a designer is at a point where a compliant mechanism will fail due to vibrational forces a "no stop" is not an option. Conversely, a hard stop would impart extremely high forces on to the deflecting stage. However, if a hard stop is moved away from the point of maximum deflection on a beam or stage, this greatly reduces the shock loading as well as increasing the stiffness of the device thus resisting further motion. We will call this implementation of a hard stop a boundary control, and illuminate the effects and proper use of this new concept.
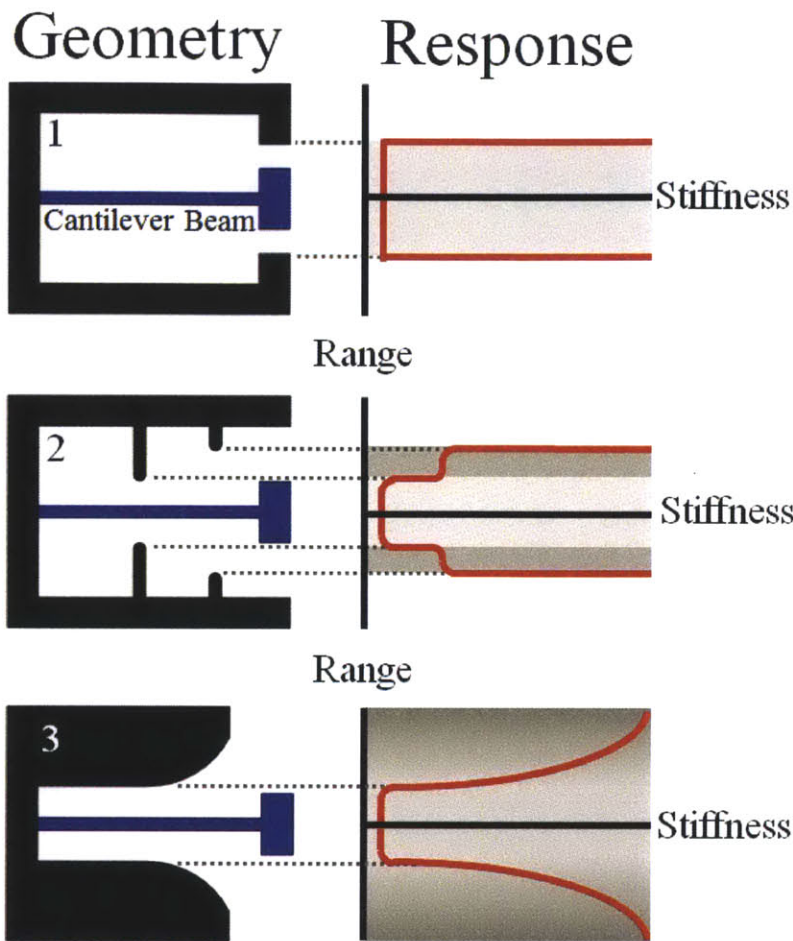
Figure 3.9: Boundary Condition Styles

In the case of a deflecting beam, Figure 3.9 illustrates several design concepts incorporating the new boundary control theory. **Geometry 1** indicates a traditional hard stop. As the center cantilever beam deflects and strikes the outer geometry the stiffness theoretically goes to infinity. **Geometry 2** idicates a boundary condition which creates stiffness zones. As the cantilever beam deflects it contacts the boundary condition points in sequence, with each causing the beam to take on a new stiffness property. This research will focuse on **Geometry 2** using only a single stiffness zone change. **Geometry 3** is a rolling boundary condition in which beam stiffness is directly related to its exact deformed position at any time after contact. Using **Geometries 2** and **3**, a designer could not only prevent a catastrophic failure, but design in specific stiffness zones.

4

Boundary Condition Math

4.1 Static Behavior

4.1.1 4 Static Cases

We must analyze 4 different cases In order to explore the mathematics behind the static operation of a boundary control. Figure 4.1 illustrates the four cases which when analyzed make up the full extent of static boundary control mathematics. For the content in this thesis, all external forces are treated as purely perpendicular. **Case 0** indicates a standard cantilever
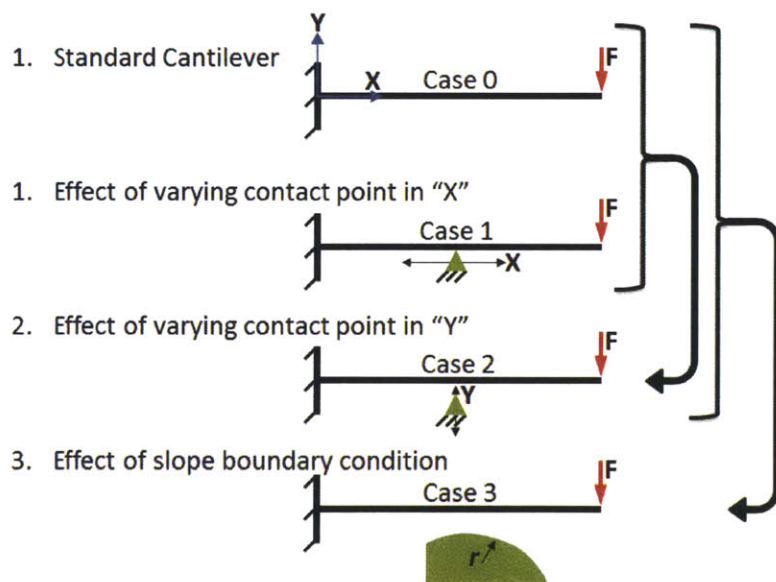
Figure 4.1: 4 Boundary Control Cases

beam with linear deflection. **Case 1** occurs when the deflecting beam in **Case 0** is combined with a support at some point along the length of the beam. **Case 2** is a support that is not initially in contact with the deflecting beam; as such its mathematical equivalent is a combination of **Case 0** (prior to contact) and **Case 1** (after contact). **Case 3** is a combination of all three with the X-Y contact point being a product of the total tip deflection, for this research we will not address this style of boundary condition and will instead focus primarily on **Case 2**.

4.1.2 Superposition Method

The superposition method is used when several different forces are acting on an object simultaneously and rather than using a single equation to account for all forces, each force/deflection pair is computed individually [38]. These individual deflection solutions are then combined back to represent the final deflection of the original beam. Figure 4.2 shows an example of how the superposition method would be used with a cantilever beam with two separate forces being applied. By separating the forces each deflection is a basic cantilever beam deflection.
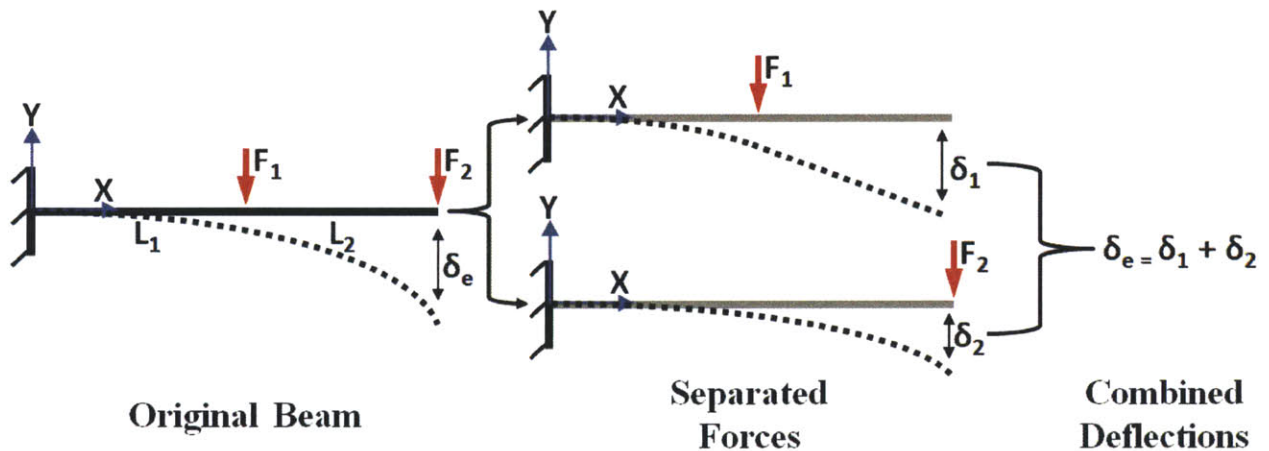
Figure 4.2: Superposition Method Illustration

4.1.3 Cantilever Beam with Offset Support Static Solution

Figure 4.3 illustrates the cantilever beam deflection which is the fundamental static operation of a boundary control (point a). When a purely lateral force F acts on the cantilever beam it begins to deflect. Once the tip deflection reaches a point such that the deflection at L_a equals d, a induces a reactionary force such to keep the deflection at L_a equal to d indefinitely (assuming no contact surface compliance).
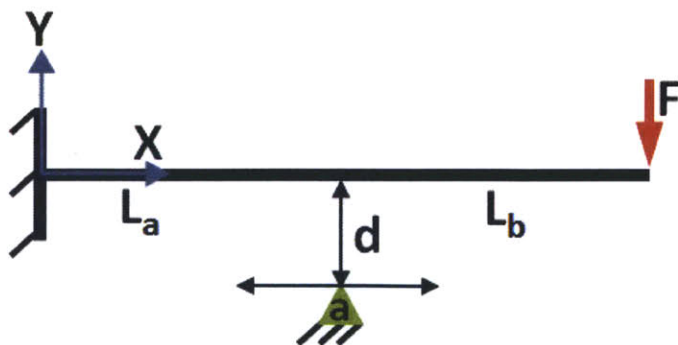
Figure 4.3: Cantilever Beam with Boundary Control

Following contact with point a, the beam must be separated into three different cases in order to solve for the static deflection. Figure 4.4 illustrates that the problem in Figure

4.3 breaks into the three deflection cases which must be combined to solve for the equivalent tip deflection of the original beam. **Case I** is the free deflecting beam prior to contact, **Case II** is a free deflecting beam after contact, **Case III** is the reaction deflection caused by the boundary control.
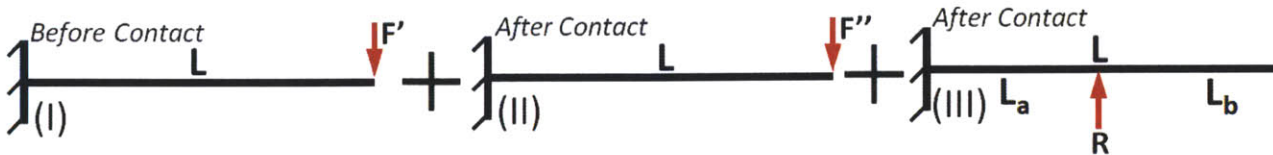
Figure 4.4: Superposition Boundary Control Superposition Cases

Figure 4.5 is a full representation of the static boundary condition problem with the complete set of important variables and parameters. Following will be a step-by-step solution of the static deflection of the beam.
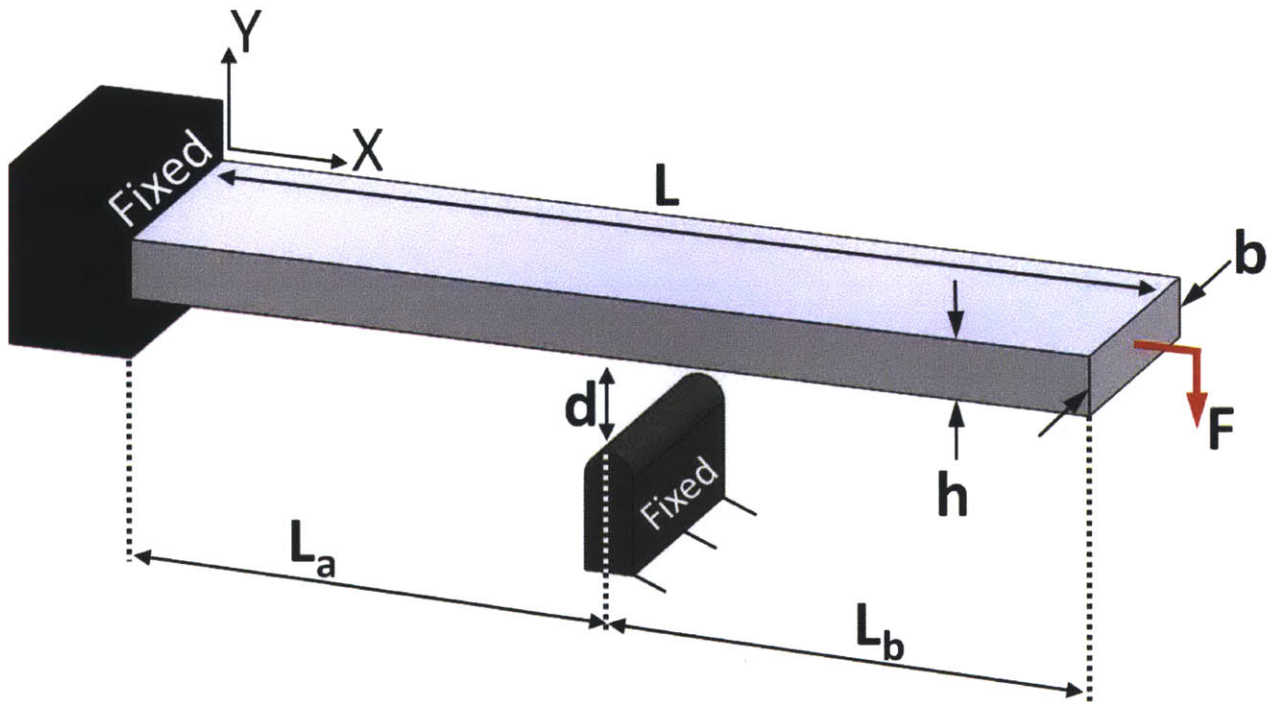
Figure 4.5: Full Diagram of Cantilever Beam with Boundary Control

Static Solution for Tip Deflection*:

1) Solve for F', the force required for the deflecting beam to contact the boundary control

$$F' = d \frac{6EI}{L_a^2(3L-L_a)} \quad \text{with} \quad I = \frac{bh^3}{12}$$

2) Determing if contact occurs

if $\quad F' > F \quad$ no contact occurs and the tip deflection is governed by $\delta_{Tip} = \frac{FL^3}{3EI}$

if $\quad F' < F \quad$ then contact does occur, continue to Step 3

3) Solve for F''

$$F'' = F - F'$$

4) Solve for R, rection force

$$R = F'' \frac{L_a - 3L}{2L_a}$$

5) Solve for deflection caused by F' (before contact)

$$\delta_I = \frac{F_I L^3}{3EI} \text{ (I)}$$

6) Solve for deflection caused by F'' (after contact)

$$\delta_{II} = \frac{F_{II} L^3}{3EI} \text{ (II)}$$

7) Solve for deflection caused by R (reaction force from boundary control)

$$\delta_{III} = \frac{R L_a^3}{3EI} + \frac{R L_a^2 L_b}{2EI} \text{ (III)}$$

or

$$\delta_{III} = \frac{F''\left(\frac{L_a-3L}{2L_a}\right)L_a^3}{3EI} + \frac{F''\left(\frac{L_a-3L}{2L_a}\right)L_a^2 L_b}{2EI} \text{ (III)}$$

8) Combine δ_I, δ_{II}, and δ_{III} to solve for tip deflection δ

$$\delta = \delta_I + \delta_{II} + \delta_{III}$$

*To solve for the deflection point at any part along the beam if contact has occurred (Step 2), the process is the same as calculating the tip deflection except equations **(I)**, **(II)**, and **(III)** will be raplaced in Steps 4, 5, and 6 with the respective equations below

$$\delta_{Ix} = \frac{F'x^2(3L - x)}{6EI}$$

$$\delta_{IIx} = \frac{F''x^2(3L - x)}{6EI}$$

and

$$\delta_{IIIx} = \delta_{IIIa} + \delta_{IIIb} \begin{cases} \text{for} \quad x<=L_a \quad \delta_{IIIa} = \frac{Rx^2(3L_a-x)}{6EI} \\[3em] \text{for} \quad x>L_a \quad \delta_{IIIb} = \frac{RL_a^2(3x-L_a)}{6EI} \end{cases}$$

or

$$\delta_{IIIx} = \delta_{IIIa} + \delta_{IIIb} \begin{cases} \text{for} \quad x<=L_a \quad \delta_{IIIa} = \frac{F''\left(\frac{L_a-3L}{2L_a}\right)x^2(3L_a-x)}{6EI} \\[3em] \text{for} \quad x>L_a \quad \delta_{IIIb} = \frac{F''\left(\frac{L_a-3L}{2L_a}\right)L_a^2(3x-L_a)}{6EI} \end{cases}$$

For a the same beam in Figure 4.5 with boundary controls on both sides, all equations are the same, except d changes between a positive or negative value depending on the direction of F.

46

4.2 Dynamic Behavior

4.2.1 Standard Cantilever Beam with Tip Mass
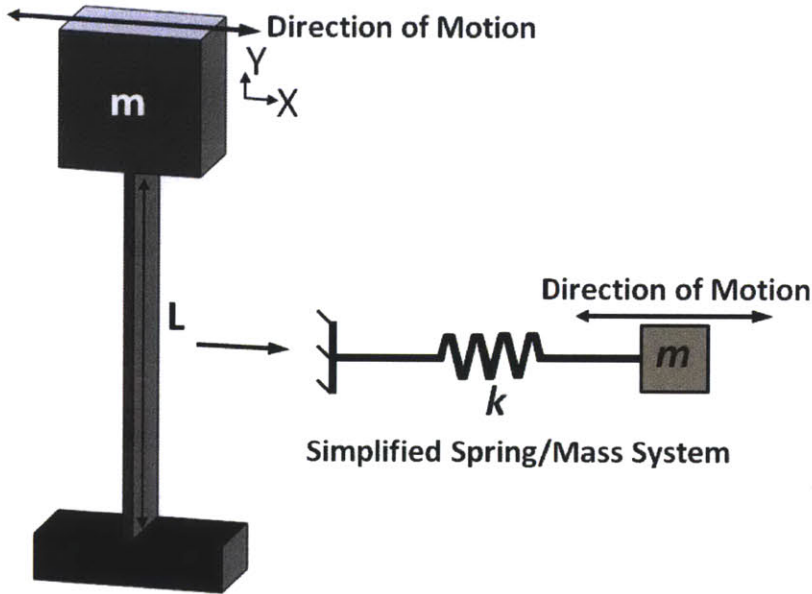
Figure 4.6: Cantilever Beam with Tip Mass

For the cantilever beam in Figure 4.6 the dynamic behavior is fairly easy to compute, specifically the natural frequency. Figure 4.6 shows the original system, along with the siplified spring mass system which is based upon two primary assumptions; the tip mass is the only mass in the system, motion is purely in the X-direction. With these two assumptions, the natural frequency is governed by the equation

$$f_n = \sqrt{k/m} \text{ (radians)} \qquad \text{or} \qquad f_n = \frac{1}{2\pi}\sqrt{k/m} \text{ (Hertz)}$$

and k is beam stiffness governed by the equation

$$k = 3EI/L^3$$

4.2.2 Dynamic Behavior with Boundary Controls

4.2.2.1 Basic Concept

Unlike the standard cantilever beam with tip mass discussed in the previous section, a cantilever beam with tip mass exposed to boundary condition controls does not have a elegant equation to solve for the natural frequency of the system. Figure 4.7 shows what occurs when a cantilever beam with tip mass vibrates back and forth (either driven or impulse excited).

Figure 4.7: Cantilever Beam with Tip Mass Exposed to Boundary Conditions

The stiffness of the beam, k term of natural frequency, is subjected to a step function. $\delta_{+/-}$ are the positive and negative deflections of the tip mass at which the beam goes from free moving to in contact with the boundary conditions. At the moment of contact (when $\delta=\delta_+$ or δ_-) the stiffness changes from the original k_a value, to a new k_b value. Because of this instantaneous jump there is no real "natural frequency" of the system, and thus we cannot determine the magnitude of the deflections that will occur.

4.2.2.2   Limitations with Mathematical Approach

When trying to approach the cantilever beam with tip mass and step function boundary controls from a pure math standpoint several problems arise which make the solving the system with certainty highly difficult. These issues will be discussed and detailed in the next few pages.

1) One proposed method of determining the natural frequency and subsequent tip motion was to "weigh" each of the k values based upon how long the system was exposed to each. For instance, in Figure 4.8 the complete arc of motion is broken up into the k_a an k_b zones, since k_b makes up roughly four times the area of the arc as compared to k_a, the equivalent k_e would be determined by the equation

$$\frac{1}{k_e} = \frac{1}{\frac{1}{k_a}+\frac{4}{k_b}}$$

The problem with that approach is that we cannot simply take the free motion of a cantilever beam with tip mass and assume this is represensentative of the actual motion of the beam once boundary controls are introduced. The moment the beam contacts the boundary controls the stiffness is decreases greatly (for a 50% reduction in beam length the stiffness increases by a factor of 8). Because of the massive disparity between the two stiffnesses, even a small error in in the weight of each would greatly affect the subsequent natural frequency and deflection calculations.

Figure 4.8: Weighted Stiffness Zones

2) The Raleigh quotient would normally be applicable in dynamic analysis of a system. By removing the row and column which represent the point on the beam that is now "fixed" we could determing the eigenvalues of the new system [39]. However, this process assumes that

those points are always fixed, and cannot account for a step function in the stiffness according the displacement of a point on the beam. If the boundary controls were affixed to the beam in its nuetral state this process would work, but that would have the same effect as merely stiffnening the beam and would defeat the ability of the beam to complete its original function.

3) The actual contact behavior between the deflecting beam and the sidewall is difficult to predict. In a macro sense, the beam will deflect until it contacts the boundary control surface, at which time it will take on a new stiffness value (as seen in Figure 4.9). However, on a micro scale, this beam is a non-rigid body contacting another non-rigid body, thus making the stiffness value not just the single value of the new beam stiffness, but that stiffness in parallel with with the beam sidewall stiffness, and the boundary control stiffness in series (k_1 and k_2). Since k_1 an k_2 are non-linear stiffnesses they increase the complexity of the system greatly.
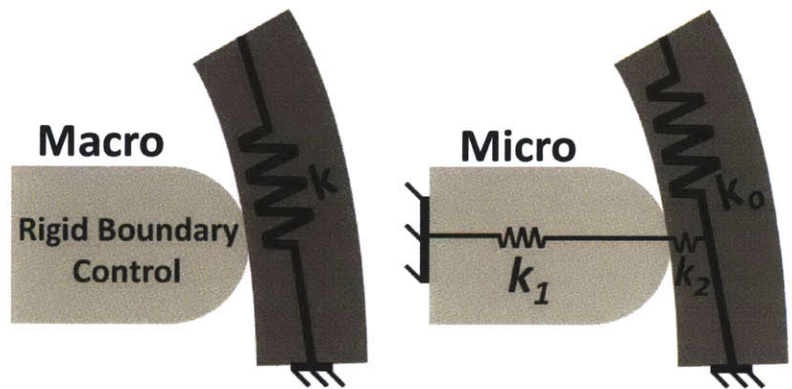
Figure 4.9: Macro vs Micro Scale Stiffness

4) Another aspect of the beam sidewall and boundary control contact interaction is the bounce that may occur upon contact. A elegant way to describe this is to use an electrical analogy. When a switch a thrown in an electrical system, we assume the circuit goes from being open to be closed, as basic as that. However, the mechanical switches in a circuit (much like this beam

Switch Bounce (Going from Off to On)
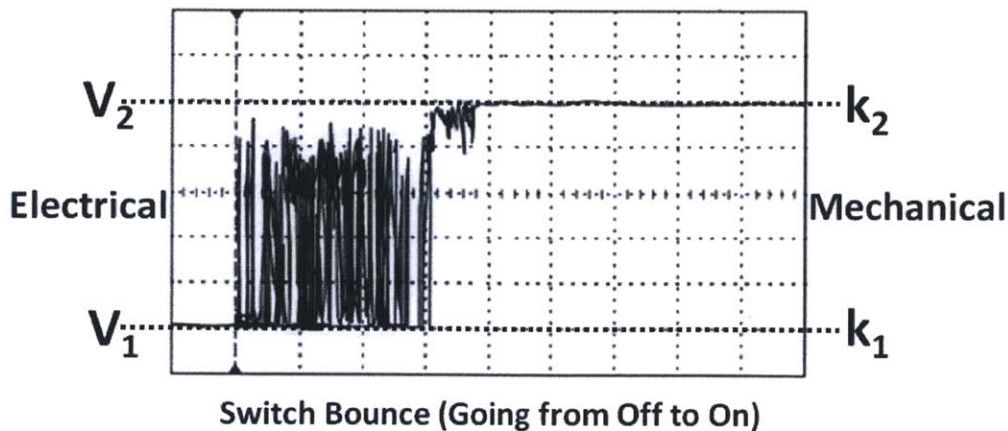
Figure 4.10: Switch Bounce

50

contacting the sidewall) do not simply go from open to closed, they "bounce". Figure 4.10 [40] shows the read out from an oscilloscope as a mechanical switch is thrown Although this is an electrical readout, the physics and contact iteraction which causes this phenomenon is just as present in the bending beam system. And just as with the electrical system oscillating rapidly between V_1 and V_2, the cantilever beam system will oscillate between k_1 an k_2. This bouncing phonomenon is very hard to mathematically predict, and each time the two bodies contact each other the frequency and number of oscillations changes.

5) All the previous stated issues are going to be highly affected by the input frequencies and amplitudes. Since this research is designed to prevent failure in environments that have irregular frequies and amplitudes, it does the designer no good for the research to be narrowly focused on a few discreet numbers in each category. For the research to be worthwhile, it would need to be able to track the behavior of the system as it moves into and out of the lowest natural frequency zone (this research does not address the natural frequencies above the first mode).

4.2.2.3 Decision to Use Buckingham Pi Theorem

The many uncertainties and complexities discussed in the previous section led the decision to utilize the Buckingham Pi theorem to properly characterize the cantilever beam with boundary control system. This approach allows many of the uncertainties or unknown system elements to be absorbed by the larger factors in the system and accounted for via dimensionless terms.

5

Buckingham Pi Theory

5.1 Intro to Buckingham Pi Theory

Bucking Pi theory is a method of conducting a dimensional analysis on a complex problem [41]. By starting with a complete list of variables involved in the system then reducing them to dimensionless groups and conducting experiments we can build a set of data which dictates the behavior of the system under given conditions. This theory is used often in fluid dynamics where all the major variables are known, but the exact interaction between those variables is either unknown or too complex for traditional math.

5.2 Variables in the System

Table 5.1 lists and explains all variables present in the system, Figure 5.1 (Note: we have swapped f for ω and will be working in Hz for the remainder of this research).
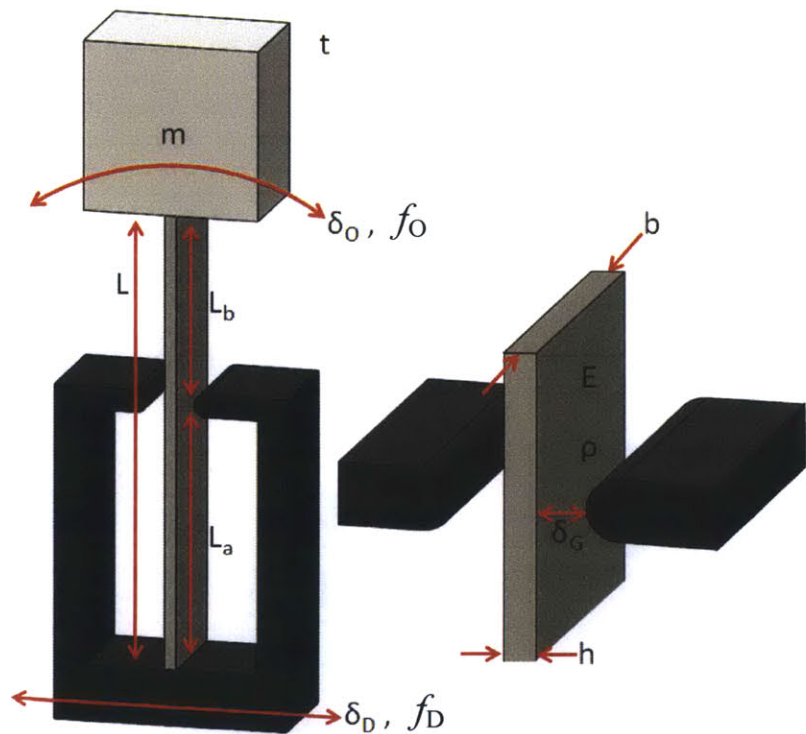
Figure 5.1: Complete System Diagram

Table 5.1: System Variables

Symbol	Description	Units	Dimensions
m	Tip mass	g	M
t	Time	s	T
L	Beam length	mm	L
La	Length below boundary control	mm	L
Lb	Length above boundary control	mm	L
δ_O	Tip mass deflection (total range)	μm	L
f_O	Tip mass frequency	Hz	1/T
δ_D	Driven deflection (total range)	μm	L
f_D	Driven frequency	Hz	1/T
δ_G	Boundary control gap	μm	L
b	Beam thickness	mm	L
h	Beam width	mm	L
E	Material modulus of elasticity	N/mm^2	M/LT^2
ρ	Material density	g/mm^3	M/L^3

5.3 Formulation of Pi Terms

5.3.1 Assumptions

1) The tip mass is at least ten times greater than beam mass, making the beam mass' impact on the system negligible, thus the density term (ρ) will be dropped.

2) Because we are only concerned about the max deflections and not the location of the tip mass at any specific point, time is not a concern and the time variable (t) will be removed.

3) We will only be concerned with the max deflection in the X direction, as such all motion will be treated as moving purely on the X axis.

4) The boundary control walls are infinitely rigid, move with the base motion, and have not effect on the system other than stopping beam motion at a predetermined point.

5.3.2 Deriving Pi Terms

We will use M (mass), L (length), T (time), as our primary dimensions. Following the removal of t, and ρ from the variable list, we are left with

$$m \quad L \quad L_a \quad L_b \quad \delta_O \quad f_O \quad \delta_D \quad f_D \quad \delta_G \quad h \quad b \quad E$$

$$[M] \quad [L] \quad [L] \quad [L] \quad [L] \quad \left[\frac{1}{T}\right] \quad [L] \quad \left[\frac{1}{T}\right] \quad [L] \quad [L] \quad [L] \quad \left[\frac{M}{LT^2}\right]$$

From here we can combine single variables into larger related groups h, b, and E, can be combined to form a new term, rigidity (R) which is governed by the eqution

$$R = EI \qquad \text{and} \qquad I = \frac{bh^3}{12}$$

R (not to be confused with the reaction force from 4.1.3) can then be combined with L, La, Lb to determine k_{free} (stiffness of beam when not in contact with boundary control), and $k_{contact}$ (stiffness of the beam when in contact with boundary control), these equations are

$$k_{free} = \frac{3EI}{L^3}$$

and

$$k_{contact} = \frac{12EI}{4L^3 - 3LL_a(2L_a + 3L_b) + L_a{}^2(2L_a + 3L_b)}$$

by combining these variables we are left with

$$m \quad k_{free} \quad k_{contact} \quad \delta_O \quad f_O \quad \delta_D \quad f_D \quad \delta_G$$

$$[M] \quad \left[\frac{M}{T^2}\right] \quad \left[\frac{M}{T^2}\right] \quad [M] \quad \left[\frac{1}{T}\right] \quad [M] \quad \left[\frac{1}{T}\right] \quad [M]$$

the amount of Pi terms required to represent the sytem is governed by the equation

$$\#Pi\,Terms = n - m$$

where n=total number of independent variables, and m=number of primary dimensions involved. Therefore, we need five Pi terms to adequately represent the system. Next we choose k_{free} (k_f), δ_G, and m as our repeating variables. This leaves $k_{contact}$ (k_c), δ_D, δ_O, f_D, f_O to be used to develop our Pi terms (Table 5.2).

54

Table 5.2: Pi Term Formulation

π_1: k_c k_c + k_f^a + δ_G^b + m^c

	k_c	k_f^a	δ_G^b	m^c	=				
M	1	1a	0	1c	=	0	c	=	0
L	0	0	1b	0	=	0	b	=	0
T	-2	-2a	0	0	=	0	a	=	-1

$\pi_1 = k_c/k_f$

π_2: f_D f_D + k_f^a + δ_G^b + m^c

	f_D	k_f^a	δ_G^b	m^c	=				
M	0	1a	0	1c	=	0	c	=	1/2
L	0	0	1b	0	=	0	b	=	0
T	-1	-2a	0	0	=	0	a	=	-1/2

$\pi_2 = f_D(m/k_f)^{1/2}$

π_3: δ_D δ_D + k_f^a + δ_G^b + m^c

	δ_D	k_f^a	δ_G^b	m^c	=				
M	0	1a	0	1c	=	0	c	=	0
L	1	0	1b	0	=	0	b	=	-1
T	0	-2a	0	0	=	0	a	=	0

$\pi_3 = \delta_D/\delta_G$

π_4: f_O f_O + k_f^a + δ_G^b + m^c

	f_O	k_f^a	δ_G^b	m^c	=				
M	0	1a	0	1c	=	0	c	=	1/2
L	0	0	1b	0	=	0	b	=	0
T	-1	-2a	0	0	=	0	a	=	-1/2

$\pi_4 = f_O(m/k_f)^{1/2}$

π_5: δ_O δ_O + k_f^a + δ_G^b + m^c

	δ_O	k_f^a	δ_G^b	m^c	=				
M	0	1a	0	1c	=	0	c	=	0
L	1	0	1b	0	=	0	b	=	-1
T	0	-2a	0	0	=	0	a	=	0

$\pi_3 = \delta_O/\delta_G$

this leaves us with the five Pi terms required to characterize the system

$$\pi_1 = \frac{k_c}{k_f} \qquad \pi_2 = f_D\sqrt{\frac{m}{k_f}} \qquad \pi_3 = \frac{\delta_D}{\delta_G} \qquad \pi_4 = f_O\sqrt{\frac{m}{k_f}} \qquad \pi_5 = \frac{\delta_O}{\delta_G}$$

5.4 Acquiring Pi Term Data

With the five Pi terms derived, we must now develop a test setup which will accurately track and control each of the variables contained within each of the terms. This set of data will then allow us to build the charts which will define and illustrate the behavior of each term when associated with each other term. For the input variables f_D, and δ_D and we need to develop a linearly oscillating platform. For the k and m values we needed various beam geometries and tip mass values. Lastly for δ_G we need an adjustable external boundary control system.

CHAPTER

6

Test Theory and Design

6.1 Scope

1) The current test setup will only analyze the behavior of a cantilever beam with tip mass.

2) The test setup will have sidewall point contacts that can be varied in both the X (gap distance) and Y (height on the beam) directions.

3) Focus will be on frequencies from within the range of the natural frequency of a sample, generally +/-2-+/-12Hz

4) Test will not include sloped boundary conditions.

5) Test will only deal with 6061-T1 aluminum samples.

6) Only single boundary condition will be applied, resulting in only one stiffness change.

6.2 Vibration Bench Design

6.2.1 Test Setup Specifications

A basic vibration platform was needed to excite the cantilever beams in a single direction and be able to precisely control the f_D and δ_D values. In order for the vibration bench to properly run the tests it needed to adhere to the specifications in Table 6.1.

Table 6.1: Vibration Platform Specifications

Vibration Bench Property	Desired	Actual	Units
Amplitude (@ 5Hz)	+/- 2.5	+/- 2.5+	μm
Drive Frequency	0-500	0-1000+	Hz
Length (Z)	180	172	mm
Width (X)	180	120.65	mm
Height (Y)	50	22.5	mm
Natural Frequency	>1000	1384	Hz
Drive Voltage	0-200	100	Volts

6.2.2 Linear Stage Design

The best design for the vibration platform was two four bar parallel flexures in parallel (Figure 6.1). This setup provides a high level of linearity in the desired platform motion while restricting all other motions. The flexure geometries will all be the same, thus the stiffness of all flexures will be the same. With this assumption the stiffness of the system is two springs in parallel, in series with two more springs in parallel, then parallel again. The equation is easier to understand and is

A: $k_A = k + k$ B: $k_B = k + k$

Side1: $\dfrac{1}{k_1} = \dfrac{1}{k_a} + \dfrac{1}{k_b}$ Side 2: $\dfrac{1}{k_1} = \dfrac{1}{k_a} + \dfrac{1}{k_b}$

Equivalent Stiffness: $k_{eq} = k_1 + k_2$
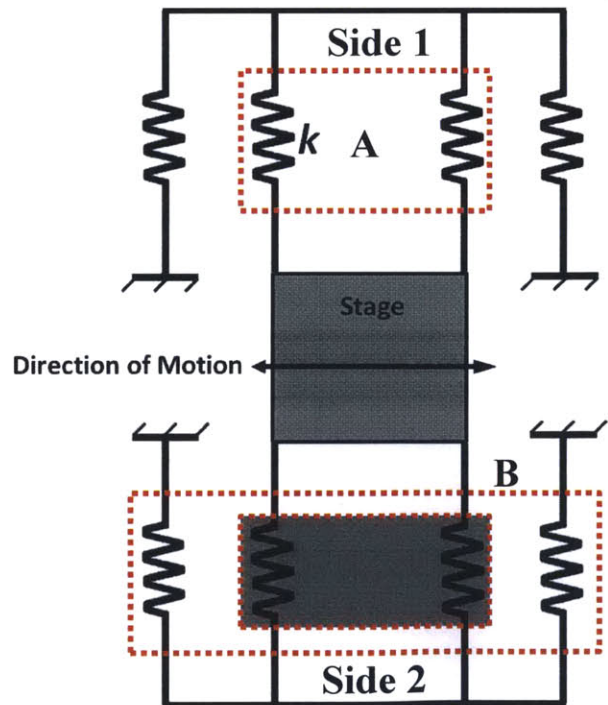
Figure 6.1: Linear Actuation Stage

Since all flexures are the same stiffness, the equivalent stiffness for the stage is simply $2k$. Now that we have derived the stiffness of the system we will use it to meet the frequency needs for the test setup.

6.2.3 Actuator Selection

The best method of driving this platform was to use a stacked piezo actuator. The low displacement and high force output fit the needs of the system. We chose a TS18-H5-104 stacked piezo manufactured by Piezo Systems, Inc. as the drive actuator for the system. This actuator was capable of 14.5μm free deflection and 840N blocked force. As can be seen in Figure 6.2, when desiring 5μm of total deflection this meant our upper and lower bound of useable

TS18-H5-104 Piezo Performance
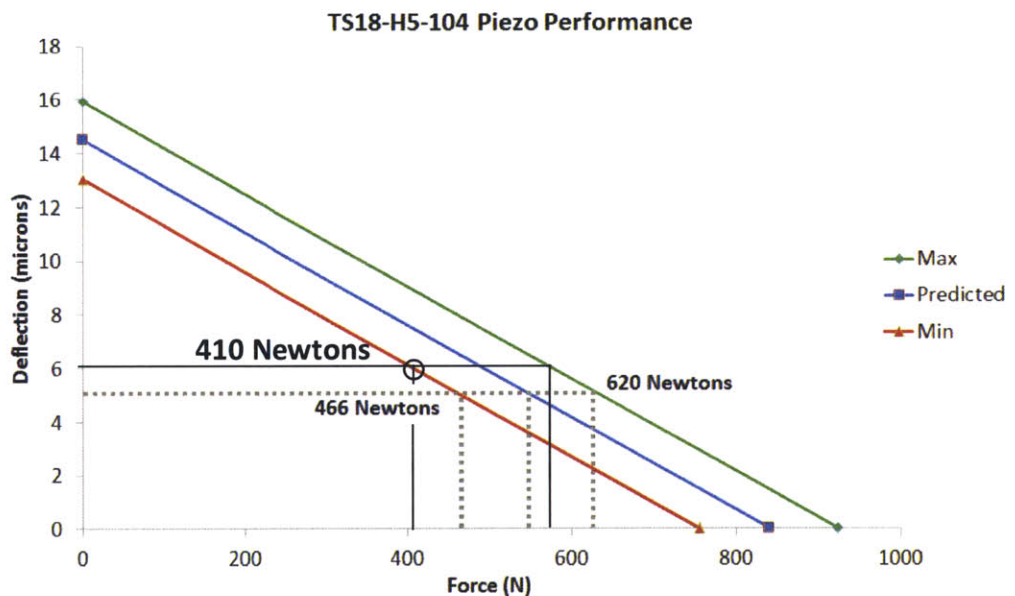
Figure 6.2: Stacked Piezo Performance

force was 466-620N. However, in order to avoid the piezo "bottoming out" we assumed there to be at least a 1μm offset from its zero deflection point (blocked force point). This then moved the max deflection required to 6μm, thus reducing our useable force output to minimum of 410N which we used as our design point force.

6.2.4 Dynamic Design

500Hz was chosen as the max frequency which put it a minimum of 4 times higher than any frequency we would be testing. This ensured that the platform would be capable of conducting the tests without causing any undesired effects. The function of the platform is

59

broken up into two phases (Figure 6.3) with the actuator driving the first phase, and the spring stiffness of the linear stage driving the second.
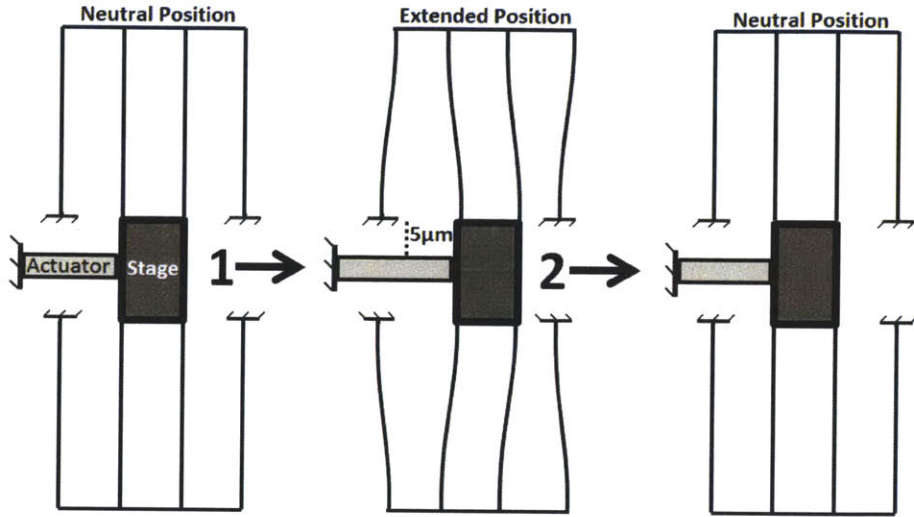
Figure 6.3: Phases of Linear Motion

Since we know the piezo is capable of transition from the neutral position to the extended position with enough force and speed to meet the design requirements (from manufacture's specifications), we now need to ensure the spring stiffness in the linear stage is such that it can return the platform to its neutral position at least fast enough to keep up with a 500Hz cycle rate. Ignoring damping effects, and starting from Newton's 2nd Law and Hooke's Law we know

$$F = ma \quad \text{and} \quad F = -kx \quad \text{therefore} \quad ma = -kx$$

thus

$$m\frac{d^2x}{dt^2} = -kx \quad \text{or} \quad m\frac{d^2x}{dt^2} - kx = 0$$

since this is a second-order linear differential with auxiliary equation

$$mr^2 + k = 0 \quad \text{and roots} \quad r = \mp\omega i$$

the general solution is

$$x_{(t)} = c_1 \cos(\omega t) + c_2 \sin(\omega t)$$

And the specific response of the system is

$$x_{(t)} = A\cos(\omega t) \quad \text{with} \quad \omega = \sqrt{\frac{k}{m}} \quad [42]$$

60

we know A=5μm, and t=2ms, $x_{(t)}$=0, and m=0.5kg (max total setup mass), leaving k as the only unknown. Solving for k gives us a total platform stiffness required of ~4950kN/m or ~5N/μm. Since the stiffness of the platform required is far below the max stiffness capable of being actuated (~80N/μm), we will disregard the stiffness required to maintain this frequency and instead use the actuator max output force and other considerations to design the platform stiffness.

Since we need a minimum platform stiffness of 5N/μm and a maximum of 80N/μm we have a large design range. For the sake of incorporating manufacturing errors, material inconsistencies, and other unforeseen issues, we will start by roughly splitting the difference between these two numbers, giving us a stiffness of 40N/μm. However, when it comes to actually manufacturing and assembling the vibration platform, the closer the platform stiffness is to the max stiffness than be actuated, the less tolerance there exists in the final assembly between the actuator and the vibration stage. For instance, if we chose a stiffness of 80N/μm, and during assembly the piezo caused a 1μm offset in the stage, then the platform would be exerting a -80N force on the piezo, and we would require a total force output of 480N at 5μm to complete an oscillation. This would put the piezo output force above the minimum specified force and could cause the platform to not work. The closer we get to the minimum stiffness required, the greater the error can be in final assembly and still have a fully functioning system. For this reason we chose a stiffness that was three times higher than the minimum, but still 5 times lower than the maximum. A stiffness of 15N/μm would give us plenty of lower bound room to account for unforeseen issues in manufacturing, as well as leave us with a large acceptable range for the final placement of the actuator and vibration stage. This stiffness also kept the natural frequency of the system above the 1kHz minimum. To put it simply, the platform will perform to specification as long as the neutral position offset was anywhere from ~5-25μm.

6.2.5 Linear Platform Design
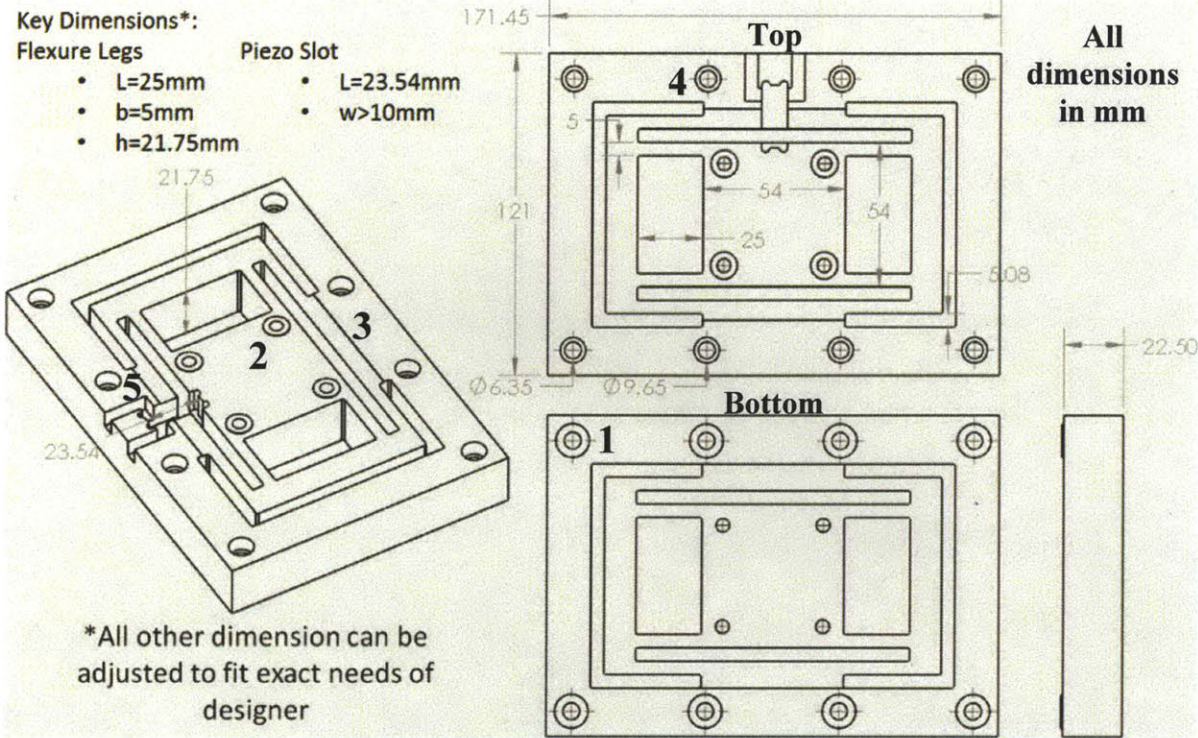
Figure 6.4: Linear Platform Dimensions

Figure 6.4 illustrates the platform design and indicates the few critical dimensions required to allow the operation to occur successfully (exact stiffness was determined via finite element analysis). Figure 6.5 shows the actual platform after fabrication. Also annotated on Figure 6.4 are several design features which allow the larger setup to run smoothly:

1. Small raised circles around the grounding screw holes prevent the stage from bending or warping if attached to a slightly uneven surface

2. Small raised circles on the stage prevent an attached test setup from bending or warping due to and uneven surface.

3. Both sides of the flexure system had a small amount of material removed (~.5mm) to prevent any rubbing if something is attached to the top of the stage.

4. 4 grounding holes used on each side to prevent the sidewall from acting a compliant wall and not maintaining ground.

5. Small channels cut for the drive wires of the piezo.
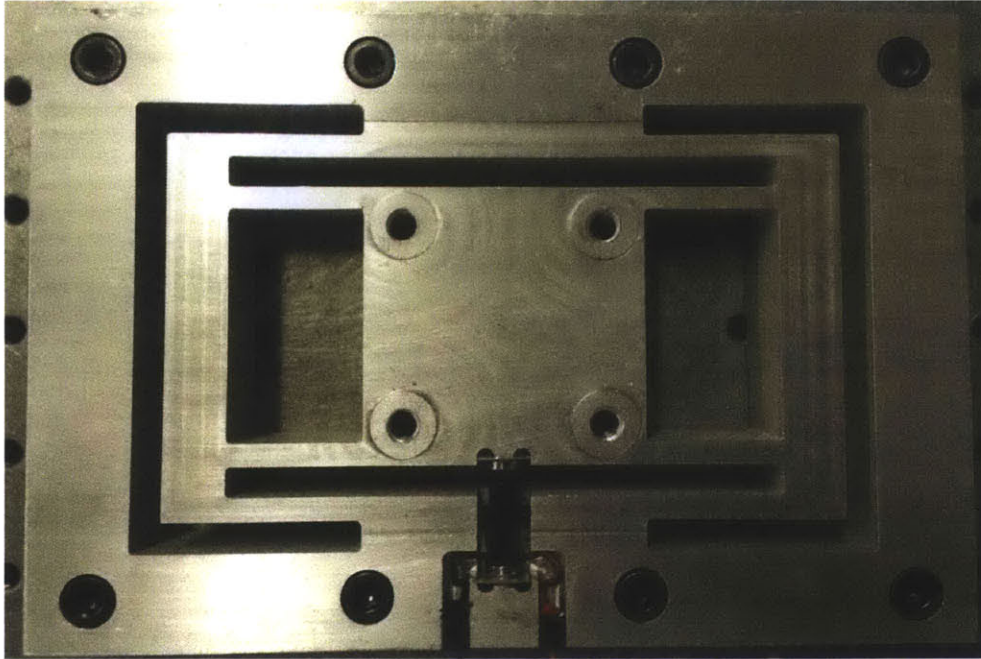
Figure 6.5: Physical Vibration Platform

6.2.6 Actuator and Stage Connection

In order for the vibration stage to properly function, the stage had to be offset from its neutral position by no less than 5µm and no more than 25µm, to allow for maximum error on either side we designed such that the offset would be 15µm. This required the final assembly between the stacked piezo and the linear stage to be precisely planned. Furthermore, in order to eliminate the risk of a shear load being placed on the piezo which would cause immediate and complete failure of the PZT material, large radius rounded tips had to be affixed to each end which would allow the piezo to roll on a contact plate if any transverse loads were applied. Figure 6.7 is a diagram of what the final assembly would look like (note, diagram is not drawn to scale) and Figure 6.6 shows the actual assembly.
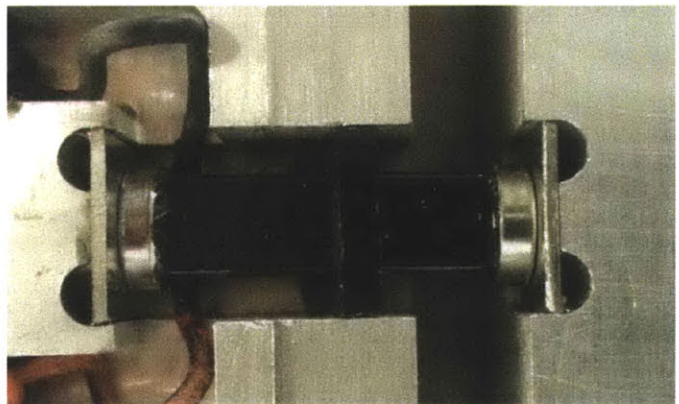
Figure 6.6: Piezo Actuator Integration
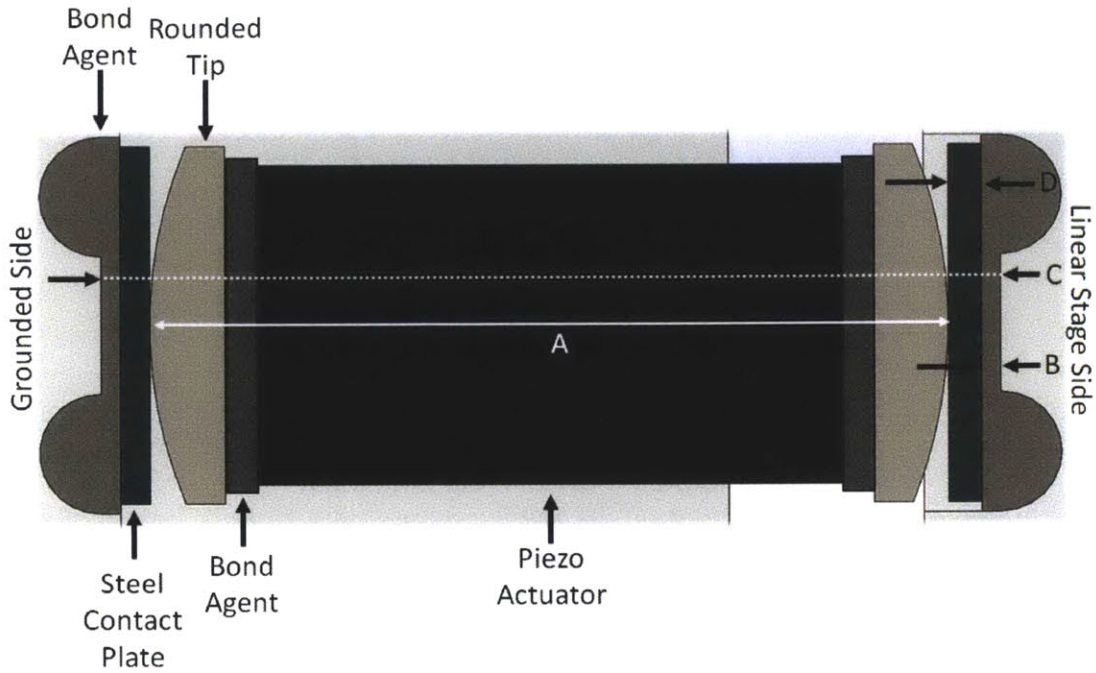
Figure 6.7: Piezo and Compliant Stage Assembly

The rounded tips which were used to eliminate the shear forces on the piezo also introduced Hertzian deformation into the system which would need to be accounted for in order to ensure proper alignment. The deformation from Hertzian contact is governed by [37]

$$\delta = \left(\frac{1}{2}\right)\left(\frac{1}{R_e}\right)^{\frac{1}{3}}\left(\frac{3F}{2E_e}\right)^{\frac{2}{3}}$$

With R_e=1000mm (the radius of the rounded tips), F=225N (15μm offset), and E=200000N/m^2 the deflection from Hertzian contact is 5.22μm at a 15μm offset. Also, from experimental setups, the bonding agent had a nominal dry thickness between two plates of 39μm, and showed negligible compression under the loads required for normal use. With the piezo already bonded the rounded tips, the final dimension yet to be accounted for is the thickness of the contact plates which could be sanded down to whatever thickness was needed to achieve the required offset. The equation to determine the thickness of the contact plates is (variables from Figure 6.7)

$$C + 0.015mm = A + 2B + 2D - 2\delta_{Hertzian}$$

with C=23.535mm, A=22.048mm, B=0.039mm, $H_{ertzian}$=0.005mm, contact plate thickness needed to be 0.717mm.

6.2.7 Test Sample Design

The primary concerns when developing the test sample were that it be:

- Easily excited in only single direction (10:1 thickness to width ratio)
- Tip mass be at least ten times greater than the beam mass to allow for a simplified spring-mass system assumption.
- Beam length be at least 20 times the beam thickness and two and half times the beam width to ensure the beam had enough motion to ignore shear stress factors and for boundary controls to be effectively implemented.
- Had to have various tip mass (m) (achieved with variable mass inserts) and stiffness values (k) (achieved by varying the beam geometry).

Figure 6.8 shows the final design of the beam and mass test samples, and Figure 6.8 shows the 4 physical beam and mass samples created. The beams were broken up into 5mm length increments from 30-45mm (including fillets), the tip mass with no variable mass insert was greater than ten times the beam mass, and in order to fit the test
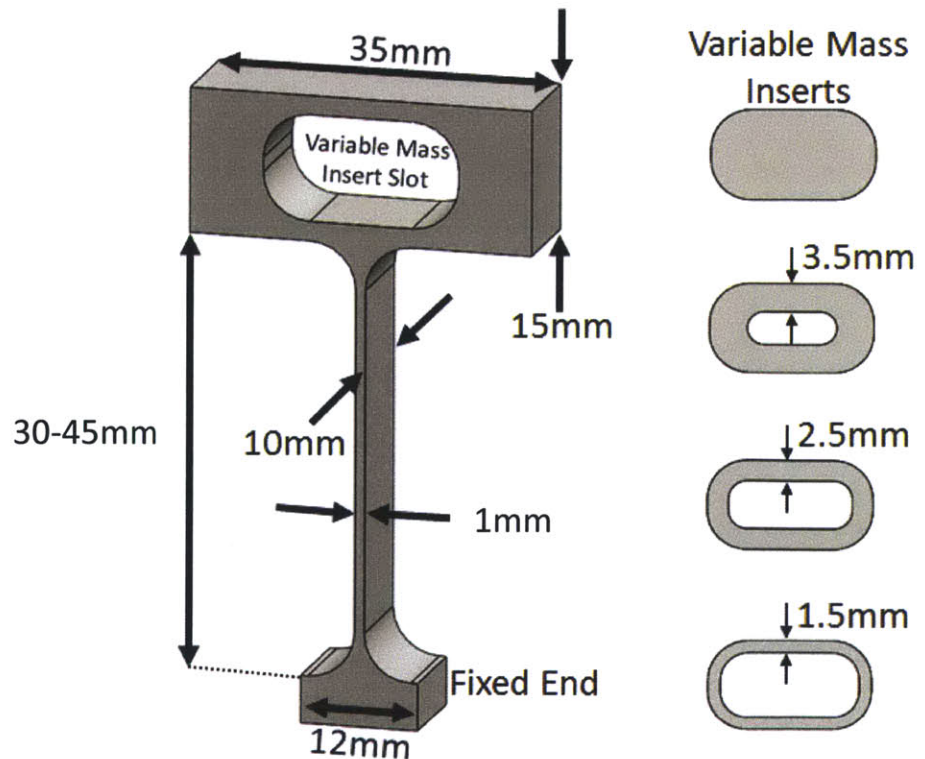
Figure 6.8: Beam Test Sample Design

65

setup all beams had a width of 10mm. All samples were made from 6061-T1 due to material properties and ease of machining.
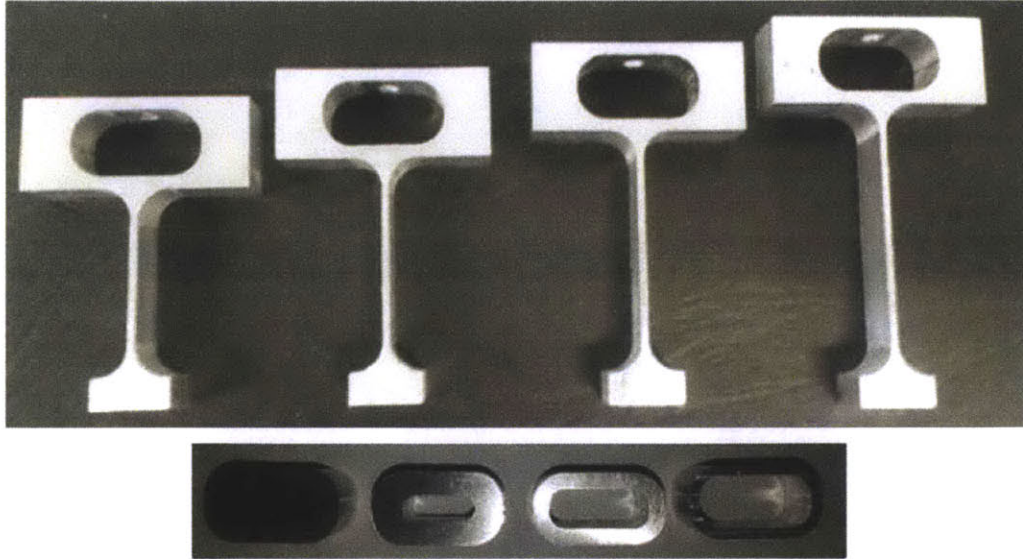
Figure 6.9: Physical Beam and Mass Test Samples

6.2.8 Boundary Control Design

The last piece needed to have complete control over the variables in our Pi terms was the boundary control system. This would control the δ_G terms as well as adjust L_a and L_b values (length of beam below and above the boundary control) to vary the beam stiffness. Figure 6.10 shows the design of the boundary control system. The minimum natural frequency for the boundary control setup was 1.2kHz, which was above the design minimum of 1kHz (same as vibration platform) to ensure the boundary controls would not be effected by the induced vibration. Something to note in the boundary control setup is that the boundary condition contacts are a point contact rather than a line contact which has been used in illustrations up to this point. The reason why the 4.8mm ball contact was used was to reduce the torque on the cantilever beam and limit the rotation in the tip mass.
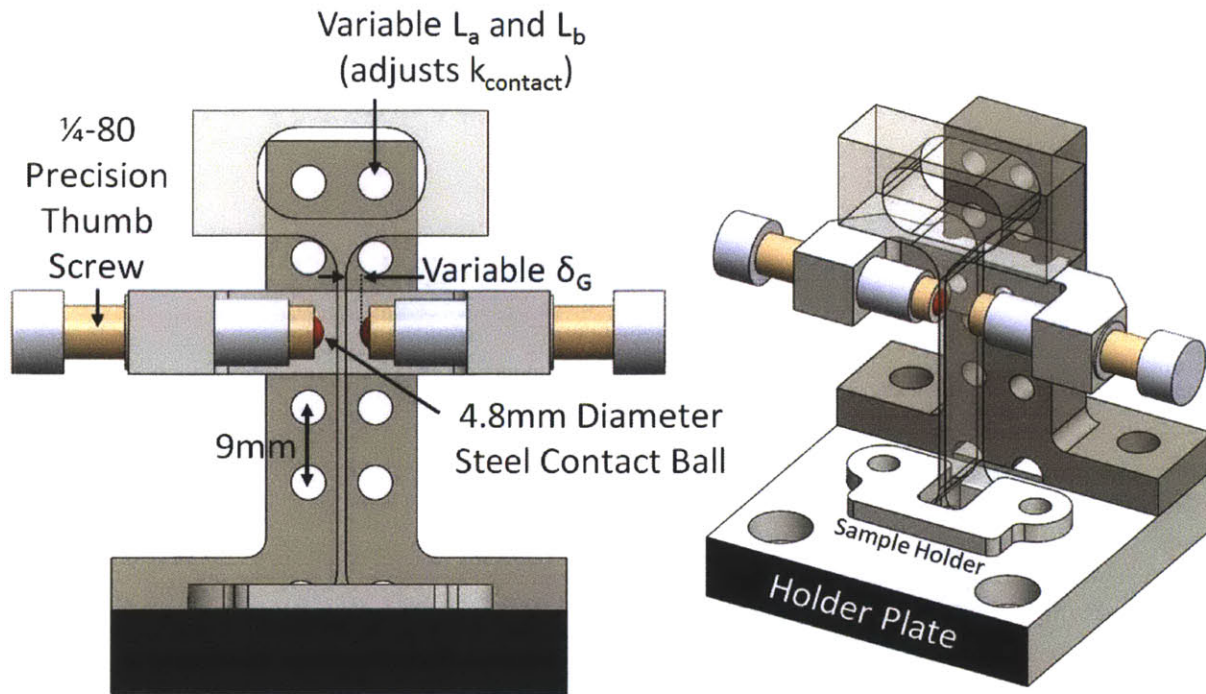
Figure 6.10: Boundary Control System

The boundary contact was originally designed to be a line contact along the face of the beam as seen in Figure 6.11. This was the original design as it was thought that it would eliminate any torque on the cantilever system. However, because the system motions are so small, the line contact actually induces a much larger torque and as such caused more rotation at the tip mass.
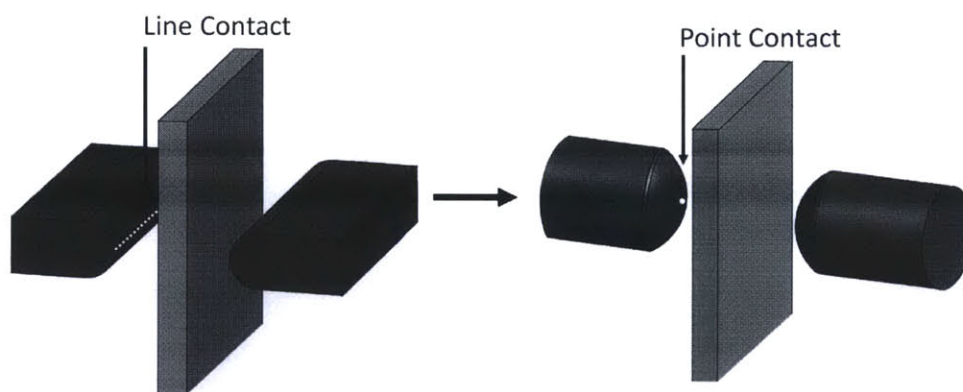
Figure 6.11: Line and Point Contact

The cause of this induced rotation was the inability of the boundary control and beam sidewall to be exactly parallel (Figure 6.12). In an ideal setup the side wall and the deflecting
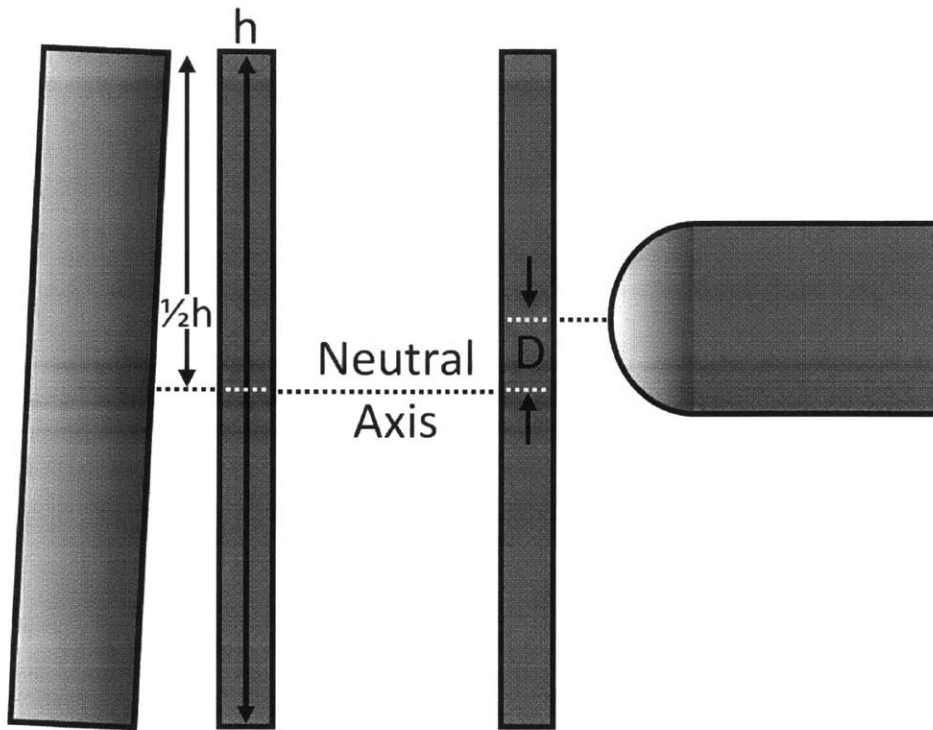
Figure 6.12: Boundary Control Induced Torque

beam would contact across the whole face simultaneously and no torque would be applied. However, in actual application it is impossible to achieve an absolute parallel between these two surfaces. This means that the beam side wall with contact either the left or right end of the wall first and cause a large rotational torque equal to

$$\tau_{LineContact} = F_{Contact}\left(\frac{1}{2}\right)h$$

and this induced torque would last until the sidewall and boundary control were in complete contact. If we use a point contact, we will inevitably have a misalignment from the neutral axis of the beam, and this will cause a torque equal to

$$\tau_{PointContact} = F_{Contact}D$$

If we know h=10mm, then the torque are for a line contact equals 5mm. Although it is impossible to align the point contact directly to the neutral axis of the beam, we can realistically assume we will be at most 100μm off if everything is precision machined and aligned. This means with an assumed equal contact force we will have a torque value for a line contact fifty times greater than a point contact. The one trade off of a point contact is that the torque is applied during the entire period of contact between the side wall and the boundary condition, whereas it is only applied on the line contact from the time the beam first contacts the boundary control until there is complete contact between the surfaces. Using a simplified assumption this means that the beam would need to be in contact with the point contact fifty times longer than it takes

for the beam to have complete contact with the line contact to exert more torsional energy, which is unlikely. In order to ensure the point contact created less rotation a series of tests were done with both boundary control styles. Ultimately the point contact induced only one third as much tip rotation as the line contact (0.035µRads verse 0.120µRads).

6.2.9 Measurement Points

Figure 6.13 shows the six points on the test setup that will be measured using five small range capacitive probes (~100µm range, <0.01% full scale error), and one large scale capacitive probe (~0.5mm range, <2% full scale error). Table 6.2 indicates what variables each probe is responsible to track. Figure 6.13 shows the physical setup with measurement probes attached.
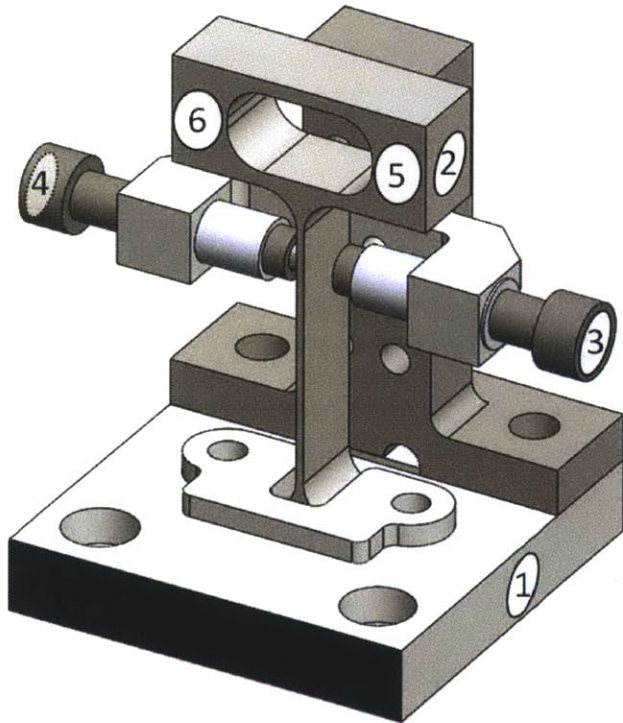
Figure 6.13: Test Setup Measurement Points

Table 6.2: Measurement Point Variables

Point	Variables
1	δ_D, f_D
2	δ_O, f_O
3	δ_{GRight}
4	δ_{GLeft}
5	Rotation Right
6	Rotation Left
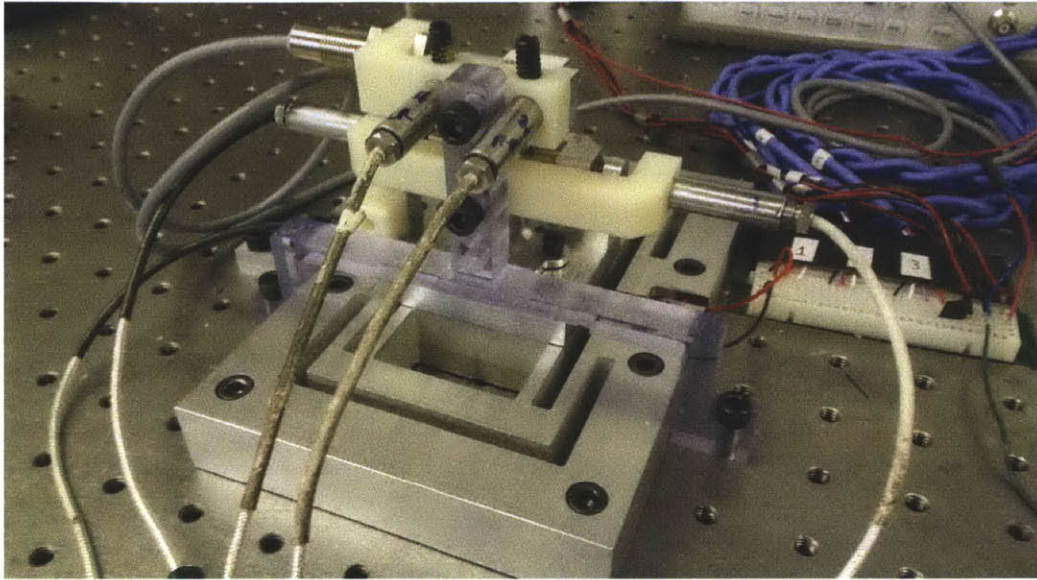
Figure 6.14: Physical Measurement Probe Setup

6.3   Test Setup Assumptions/Error Management

- Hertzian contact between cantilever beam and sidewall is negligible.

- The boundary control points are infinitely stiff both in Hertzian contact and bending/overall stiffness.

- 4.8mm diameter ball tip contact is a pure point contact and any surface roll that changes the length of the beam above and below the contact point is negligible.

- The effective beam length is from fillet end to fillet end (does not include filleted area).

- Slope on measurement point during deflection has no effect on probe accuracy (tests showed at maximum deflection, error due to the angle of the face was <0.3% of total deflection).

- ¼-80 Thumb screws have zero backlash, tests showed nanometer level motions when 5N force was applied.

- Excitable frequencies in the test setup were to be avoided; Figure 6.15 indicates no excitable frequencies in the desired range of frequencies of the platform.
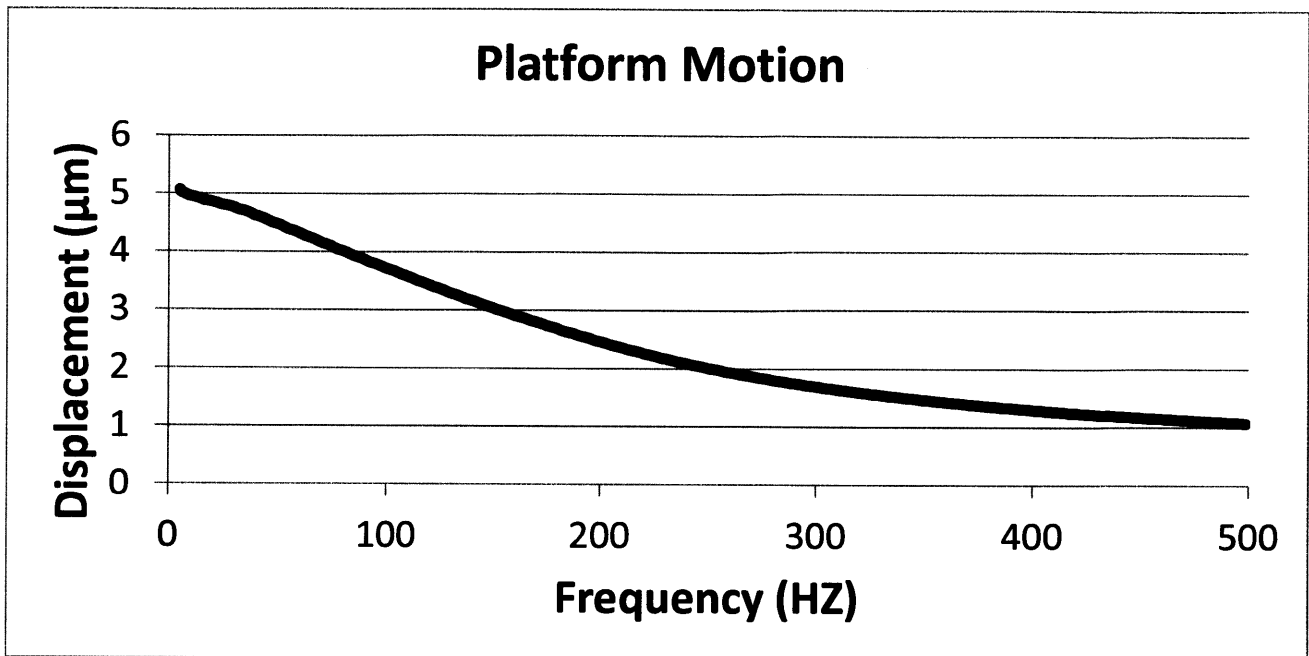
Platform Motion

Figure 6.15: Platform Motion over Frequency Spectrum

CHAPTER

7

Test Process

7.1 Cantilever Beam Characterization

Beam width and thickness were each measured in five spots along the beam and averaged to determine the exact width and thickness value that would be used.

Table 7.1 lists the precise static values for each beam.

Table 7.1: Static Cantilever Beam Properties

Sample	h (mm)	b (mm)	L_{Eff} (mm)	k_{free} (N/mm)
1	1.052	9.820	20.5	22.9
2	1.057	9.837	25.5	12.1
3	1.072	9.967	30.5	7.5
4	1.068	9.856	35.5	4.6

Table 7.2: Variable Mass Values

Mass Properties	m (g)
0 (No Tip Mass Inserted)	9.960
1	2.17
2	3.228
3	4.357
4	5.390

The exact mass values for the variable mass inserts are listed in Table 7.2. These masses are able to be swapped out in order to adjust the m variable for each test.

The dynamic properties of each beam with each of the variable mass inserts used had to be determined prior to testing. Table 7.3 lists the dynamic properties of each beam-mass combo ($1\mu m\ \delta_D$).

Table 7.3: Sample Natural Frequencies and Max Deflections

Sample-Mass	f_n (Hz)	δ_O @ f_n (μm)	Sample-Mass	f_n (Hz)	δ_O @ f_n (μm)
1-0	109.4	173	2-0	91.2	251
1-1	97.3	245	2-1	80.7	260
1-2	93.6	253	2-2	77.5	275
1-3	90.1	255	2-3	74.5	289
1-4	87.3	261	2-4	72.1	294

Sample-Mass	f_n (Hz)	δ_O @ f_n (μm)	Sample-Mass	f_n (Hz)	δ_O @ f_n (μm)
3-0	76.8	365	4-0	66.2	366
3-1	70.0	377	4-1	59.5	370
3-2	66.2	388	4-2	57.0	386
3-3	63.5	393	4-3	54.8	403
3-4	61.4	419	4-4	53	410

7.2 Test Process

Various types of tests needed to be run in order to gather the amount of data required to properly build the Pi term associations. The general test process went as follows (Note, all probe values are μm).

1. Insert the sample into to the vibration platform base and secure it using two M8x32 screws and the sample base retainer.
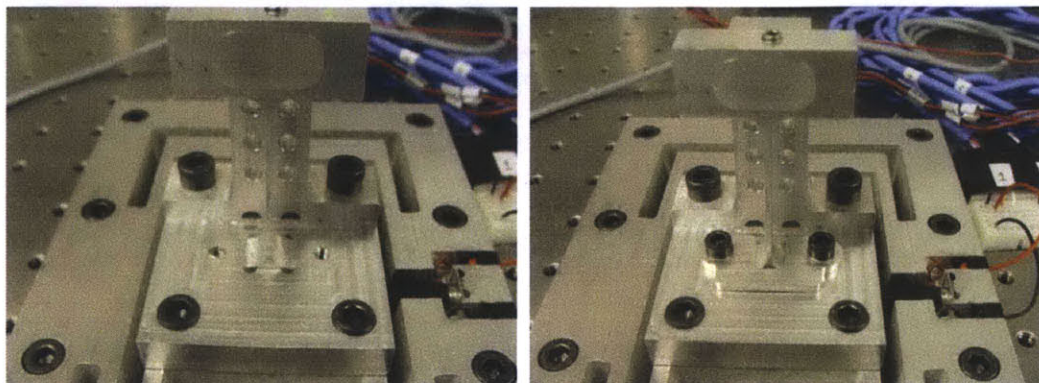
2. Determine which height the boundary controls and attach the boundary control holder to the proper set of holes on the vertical holder using two M8x32 screws.
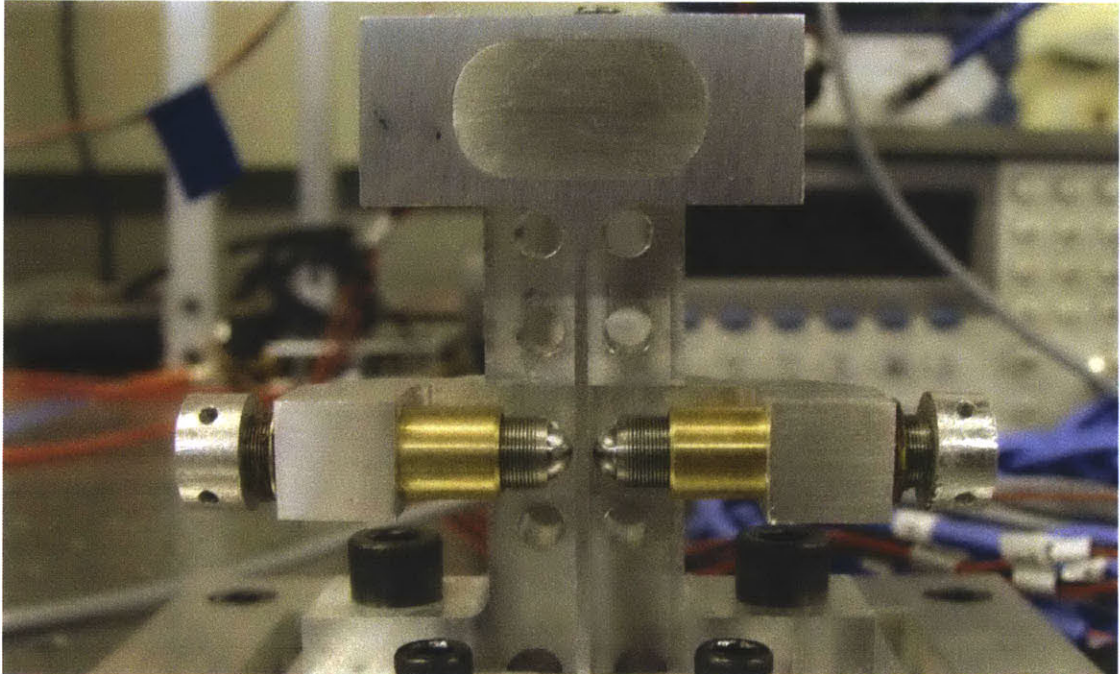
3. Insert desired variable mass and secure using M8x32 set screw.
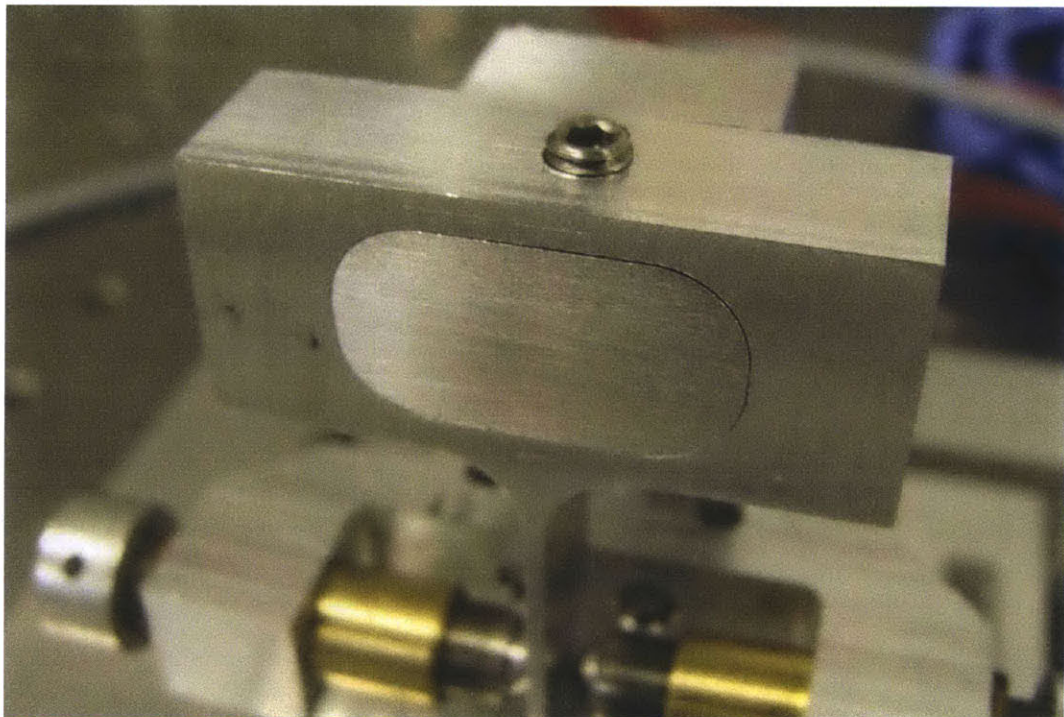
4. Put the capacitive probe holder into position and set the upper and lower sensor holder attachments at the proper height.
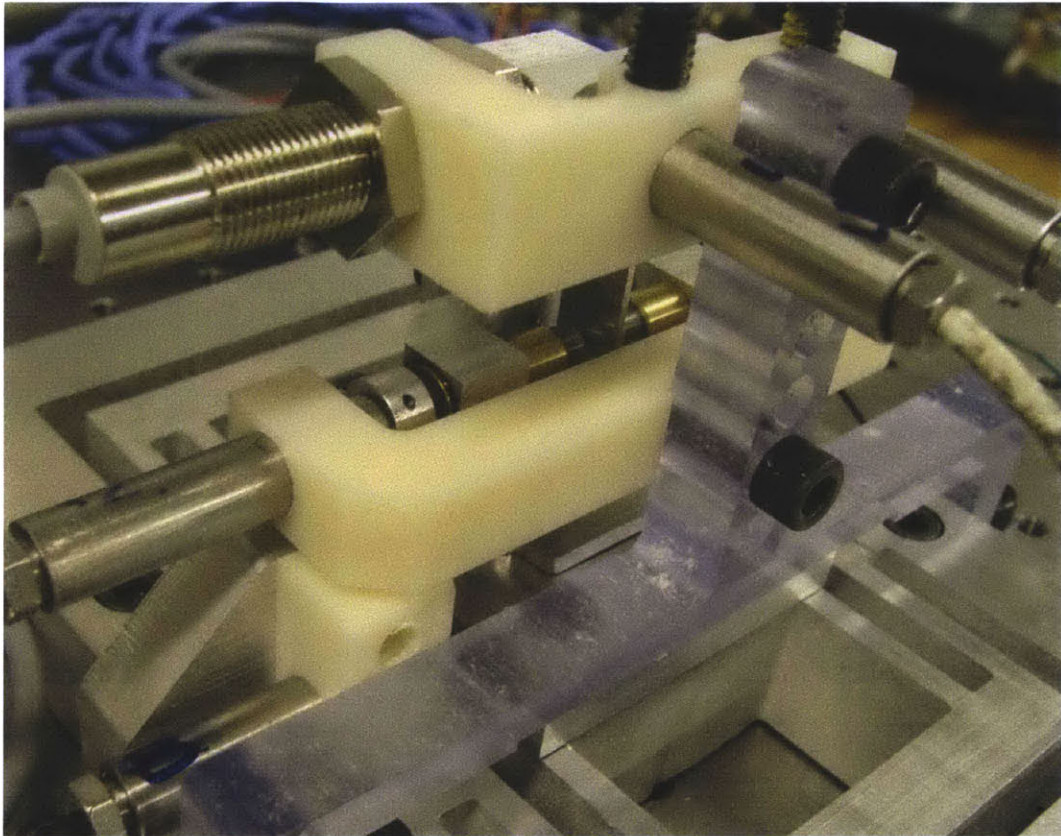
5. Align probes such that all are reading near the center of their complete range of motion (~100μm for small probes, ~500μm for large tip measurement probe).

6. Using LabView, apply an offset such that the large probe is reading "0" at the tip's neutral position.
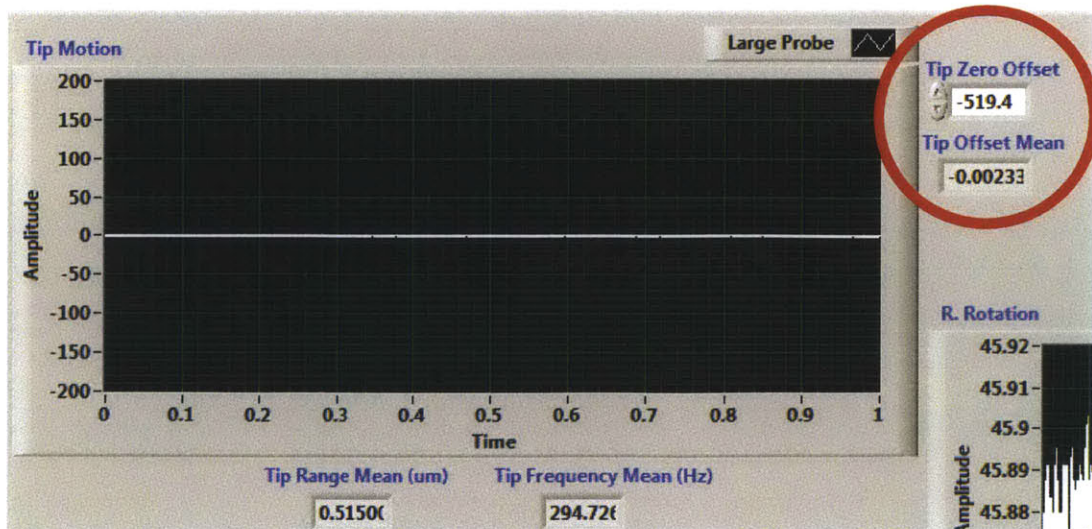
7. Screw right boundary control in towards the beam until the tip position is pushed away from neutral position by using adjustment holes and long scribe (allowed for precision motion of sidewall down to 0.25µm). Once contact occurred, the sidewall was backed off until the tip returned to its neutral position.

8. Set right wall offset such that it is reading a zero position for the right wall.

L. Rotation Zeroer			R. Rotation Zeroer
130.33!			129.78
L. Rotation Mean			R. Rotation Mean
7.77E-5			50.044

| L. Wall Zeroer | L. Wall Mean | R. Wall Mean | R. Wall Zeroer |
| 26.13 | 147.403 | -0.002 | 129.37? |
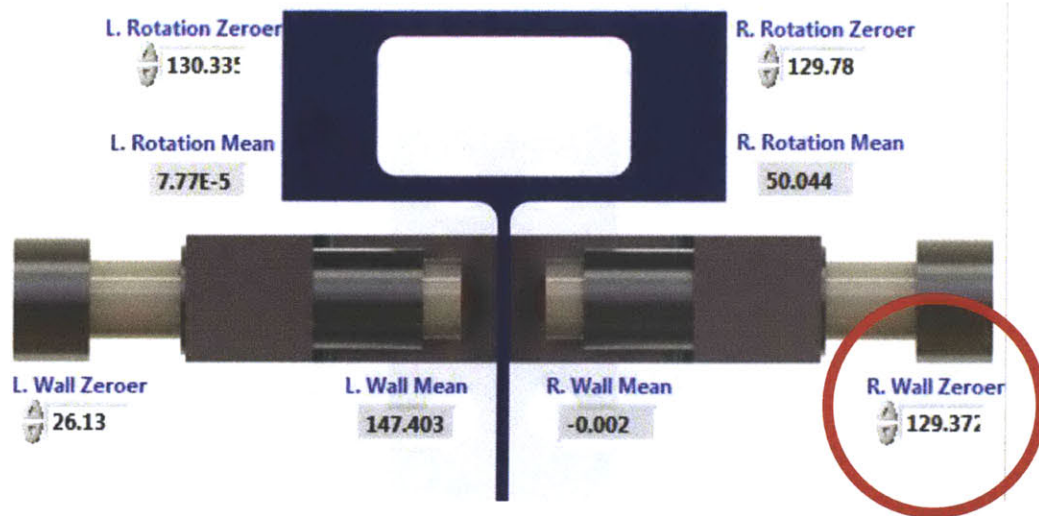
9. Back the right boundary control off the beam sidewall by >10µm (back-off value, record this number) to allow for the process to be repeated for the left boundary control without "pinching" the beam and causing an indent which would increase the gap distance value.

L. Rotation Zeroer			R. Rotation Zeroer
130.33!			129.78
L. Rotation Mean			R. Rotation Mean
7.77E-5			55.031

| L. Wall Zeroer | L. Wall Mean | R. Wall Mean | | R. Wall Zeroe |
| 26.13 | -102.249 | 14.719 | Back-off Value | 129.37? |
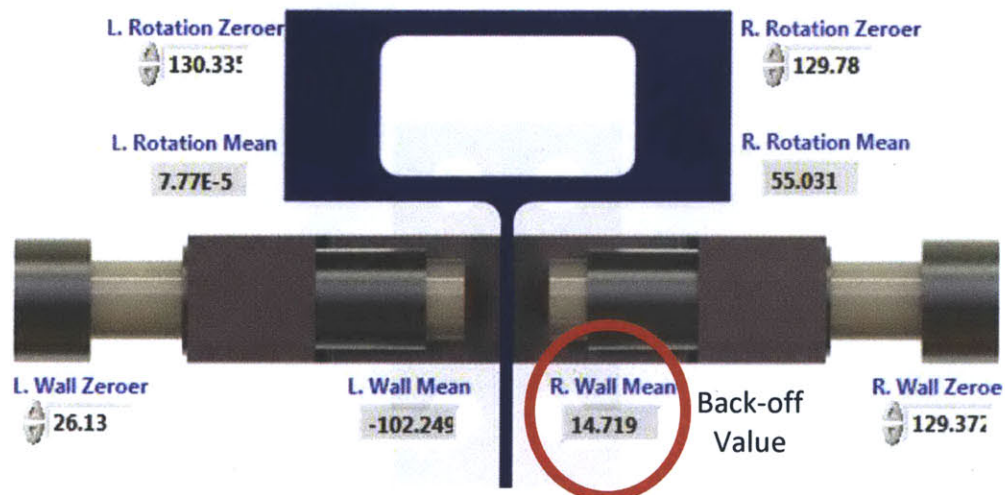
10. Repeat Steps 7 and 8 for left boundary control.
11. Power on function generator and piezo driver.

12. Set the function generator to natural frequency of sample being tested, and apply a 1.5V DC offset (to prevent the piezo from bottoming out), and Vpp for desired base range.
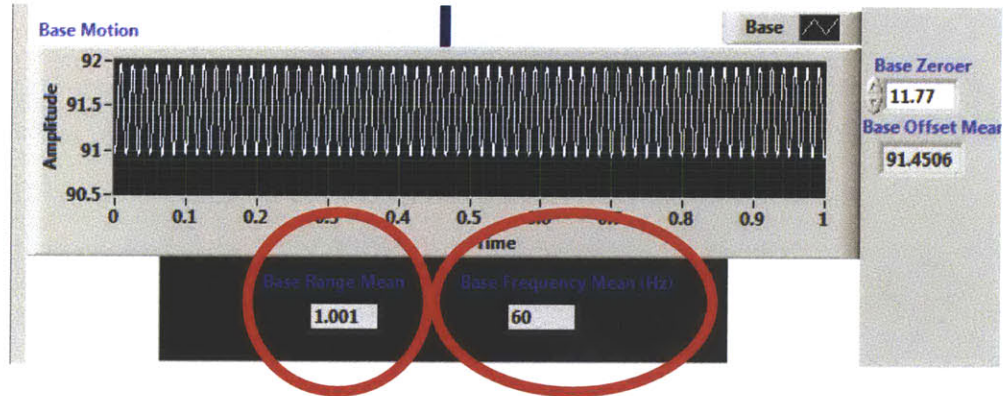
13. At this point the entire test platform has shifted relative to the sensors, generally 5-10µm depending out how far the piezo is extending and what the driving frequency is. For the large range probe this does not matter since it is reading a range via a max and min value, not an absolute location. However the sidewall sensors now show improper values. To rectify this, the left wall probe offset is set such that the probe is reading zero (it is still in contact with the sidewall). The right probe is recalibrated to reflect the back-off value we used in Step 9. We know have both sidewalls properly set to reflect the exact gap distance between their tip and the beam sidewall.

77
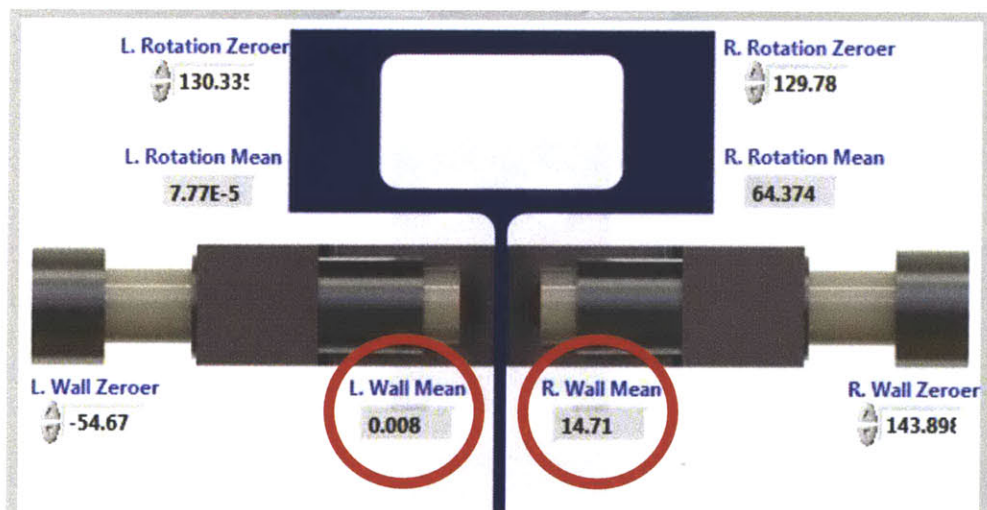
14. Rotational probes are adjusted such that they actively read the rotation of the tip (note: these values are not used in the testing and were only used to ensure the tip was not being excited in a rotational motion).

15. At this point all probes are calibrated and reading the setup properly and the base set to the natural frequency of the sample being tested. From here the process split into two types of tests. Early tests showed that the π_2-π_5 and π_1-π_5 relationships showing correlations. Each of these relationships required a different test procedure.

Test 1: π_2-π_5 Relationship (Required Frequency Sweep)

1. Set the function generator to the natural frequency of the sample beam and mass insert combination, apply a sweep of +/-3Hz to +/-12Hz (the smaller the boundary control gap the larger the sweep needed to adequate capture the behavior of the tip leading up to and after contact). Note: All sweeps started at a higher frequency and descended past the natural frequency and ended at some value below it. This was due to an excitation that occurred if the sweep started below the natural frequency and ascended (discussed in Section 8.1). The sweep time was no less than 20s/Hz, a separate test showed that any sweep faster than ~10s/Hz did not allow the beam to properly excite and passed over the natural frequency without allowing full resonance.

2. Set both boundary control screws to desired gap distance, (+/-50nm variation max). Although the platform is vibrating, the probes readings were combined into a mean value which nullified the motion of the platform. The gap distance used in procuring Pi numbers was an average of the two side wall values, thus if any point during a test the piezo strayed from its current position the gap value recorded was unaffected.

eroer

Mean

R. Ro

R. Ro
6

L. Wall Mean
8.252

R. Wall Mean
8.246
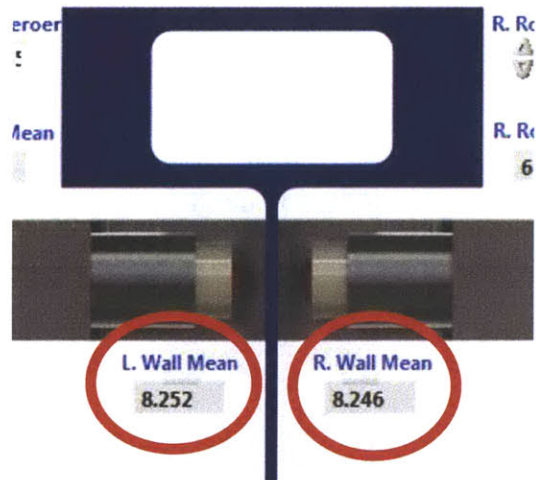
3. Once the physical setup was fully ready, the proper values were set into LabView to produce the 5 Pi terms throughout the test. Applying the sample #, mass #, and height notch automatically calculated all variables and produced the proper Pi values.

Sample #	Mass #	Height Notch #	Mass (g)	h (mm)
2	4	0	15.35	1.068

L (mm)	b (mm)
35.5	9.856

La (mm)	E (N/mm^2)
0	69000

Lb (mm)	I mm^4
35.5	1.00054

Sigma O (mm)	R (EI) N*mm^2
NaN	69037.1

Omega O (Hz)	Kfree N/mm
0	4.6293

Sigma D (mm)	Kcontact N/mm
0	4.6293

Omega D (Hz)	Sigma G (mm)
0	0

Pi 1	Pi 2	Pi 3
1	202.849	0.001

Pi 4	Pi 5
129.57	0.063

4. Once the LabView values were properly set both the frequency sweep and data collection were simultaneously activated. All tests were conducted with a 10kHz

sampling rate and the mean values from each one second interval were recorded directly to an Excel file.

5. Once the sweep was concluded data collection was turned off and a new test was set up. Below is how the test flow was conducted
    a. Set a gap distance (most time consuming and tedious step)
    b. Cycle all 4 masses through the setup with the proper natural frequency for each.
    c. Continue (a) and (b) until beam no longer contacted the sidewall.
    d. Adjust height notch
    e. Repeat steps (a), (b), and (c)
    f. Once all gap distance-height notch-mass combos had been tested, a new sample was inserted and the process was started over again at "TEST PROCESS Step 1".

Test 1: π_1-π_5 Relationship (Required Frequency Hold at Natural Frequency)

This test followed all previously established procedures, with the test flow being:

1. Attach test sample.
2. Set the function generator to the desired natural frequency.
3. Record the π_1-π_5 term values.
4. Repeat Steps 2 and 3 for all masses.
5. Adjust gap distance and repeat Steps 2 through 4 until beam no longer contacts boundary controls.
6. Adjust height notch and repeat Steps 2 through 5 for all height notches.
7. Swap samples and repeat Steps 2 through 6.

8

Buckingham Pi Results

8.1 System Recap

Figure 8.1 shows the complete list of variables in the system along with the associated Pi terms (for reference throughout this chapter). Note: the process for calculating k_c and k_f can be found in Section 4.1.2.

$$\pi_1 = \frac{k_c}{k_f} \qquad \pi_2 = f_D \sqrt{\frac{m}{k_f}} \qquad \pi_3 = \frac{\delta_D}{\delta_G} \qquad \pi_4 = f_O \sqrt{\frac{m}{k_f}} \qquad \pi_5 = \frac{\delta_O}{\delta_G}$$
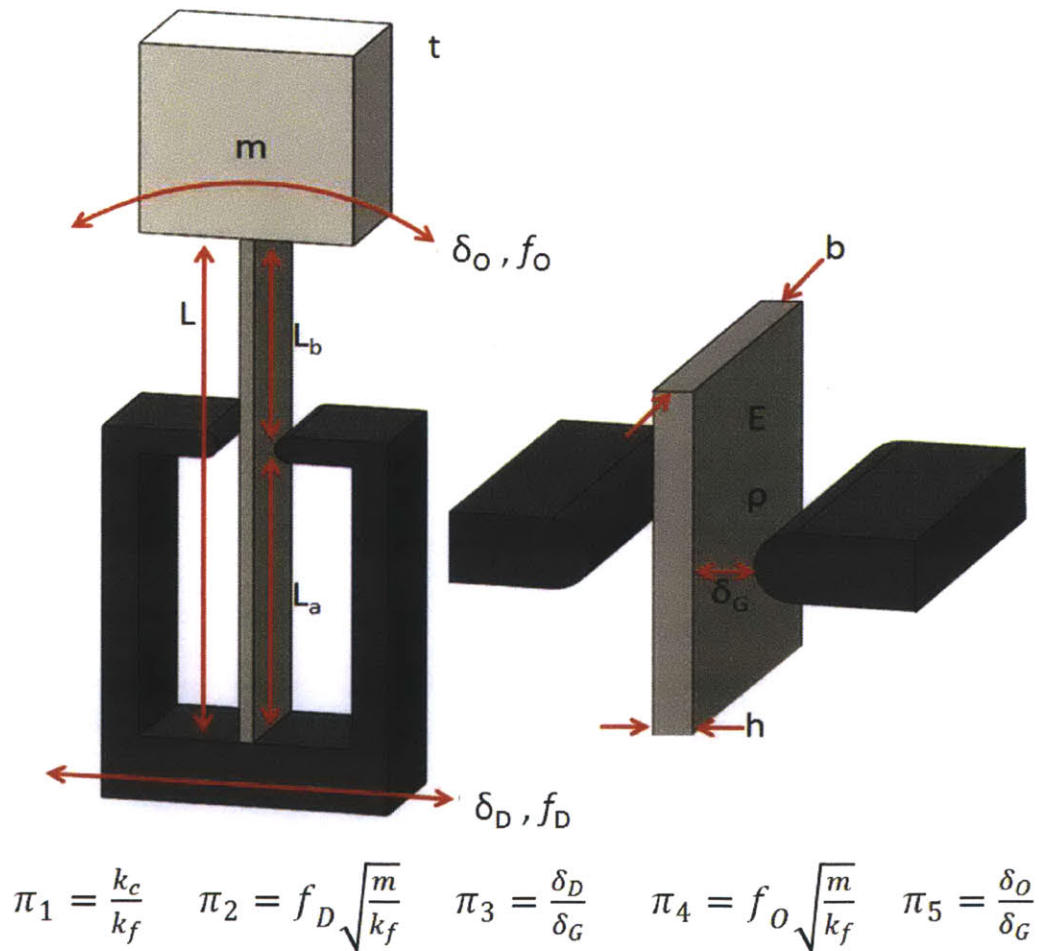
Figure 8.1: System Variables and Pi Terms

8.2 New Natural Frequency

Adding the boundary conditions did not create a new natural frequency for the system. The system excited at the same natural frequency as before, which makes sense since the boundary control points don't come into effect until the beam has been excited by its original natural frequency. However, during operation it was possible to get up to three subsequent "mode locks" at higher frequencies.
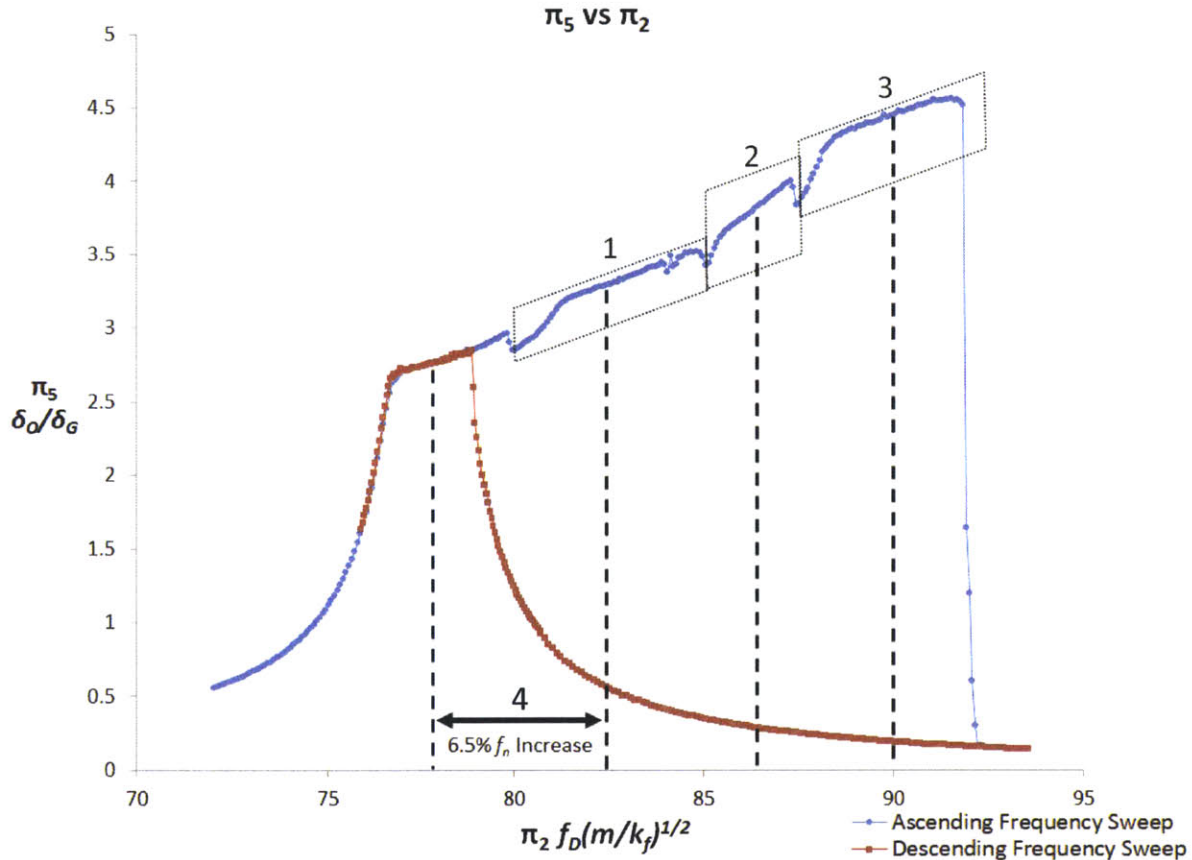
Figure 8.2: Higher Frequency Mode Locks

These mode locks are seen in **1, 2, 3** on Figure 8.2, and the centers of these mode locks appear to be nearly evenly spaced at 6.5% (**4** on Figure 8.2) increase intervals of the original natural frequency. This phenomenon was repeatable and only occurred in two specific cases; the system was subject to a slow, steadily ascending sweep, or there was an impulse while the beam was in an excitable region. If the system was subjected to ascending frequency sweep at a slow rate (<1Hz/25s sweep rate) it would continue through one to three (Figure 8.2, max seen during

82

testing) different mode lock regions before finally disengaging from any sidewall contact and returning to its low energy vibration state.
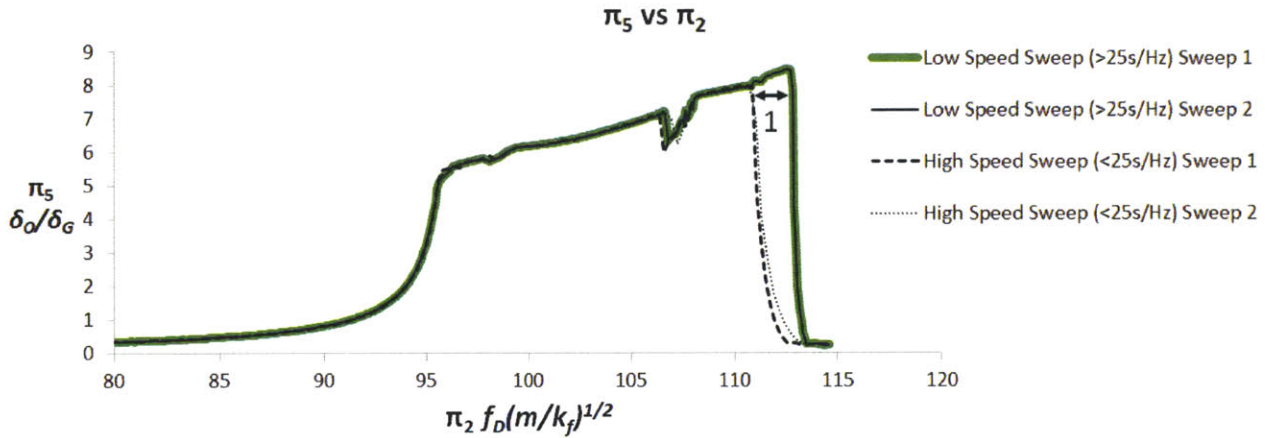
Figure 8.3: Mode Locks and Sweep Rates

If the rate of the sweep was increased it caused the mode lock to disengage early. Tests showed that the higher the sweep rate the lower the π_2 value (essentially frequency) when the beam would disengage from the new mode lock, **1** Figure 8.3. The higher the sweep rate, the earlier this disengagement would occur. Figure 8.4 shows that in **Region 1** the system is in a metastable state and during this time the system can drop from the high energy state to the low energy state rapidly. However, system can never of its own accord move from the low energy state the high energy state. If an impulse is applied properly with sufficient energy, the system can be kicked from the low energy state to the high energy state. Although an interesting phenomenon, and worth noting due its possible interference with the application of this research, this specific behavior of the system is parallel to the research discussed in this thesis. This behavior will not occur in a system exposed to random vibration and only applies when the input vibration is steadily ascending, or when the input vibration is stable such that the beam is in the metastable region and a subsequent impulse force is applied.
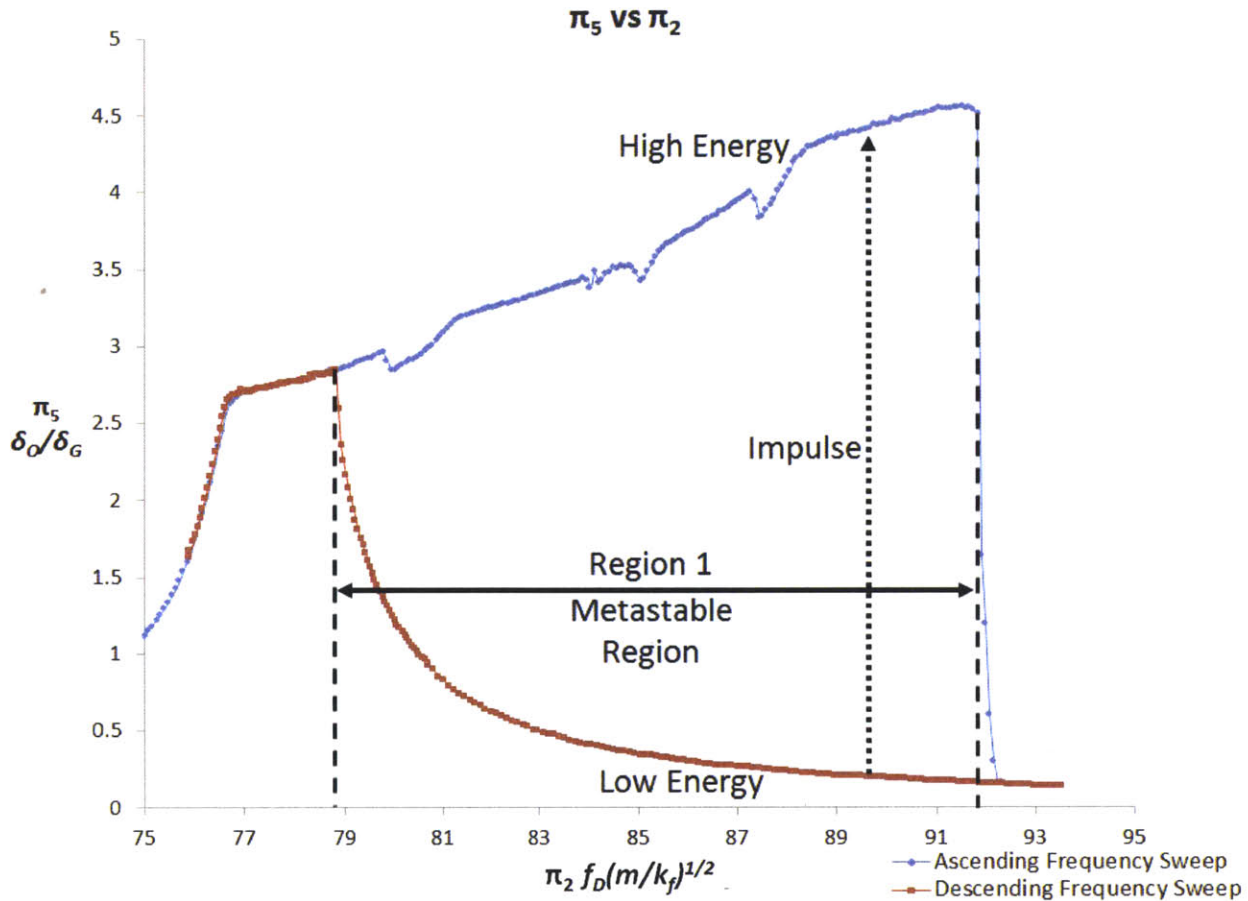
Figure 8.4: Metastable Region

8.3 π_5-π_2 Association

Tests show no direct correlation between π_5 and π_2, but the graph does reveal several important attributes of a boundary control system. Figure 8.5 is a graph of sixty-four separate frequency sweep tests. Each sample was tested at three different gap values (δ_G) and one time with no boundary interaction (free oscillation). At each of these gap conditions all four mass variations were inserted and tested. Each test frequency was centered on the natural frequency of the mass-sample combo and varied from +/-2Hz to +/-10Hz in a downward sweep depending on the size of the sweep needed to capture free oscillations prior to boundary contact, boundary contact, and free oscillations after boundary contact ended. Following the graph are sections discussion the importance of each of the numbered items noted on the graph.

84

π_5 vs π_2

Figure 8.5: $\pi 5$ vs $\pi 2$

85
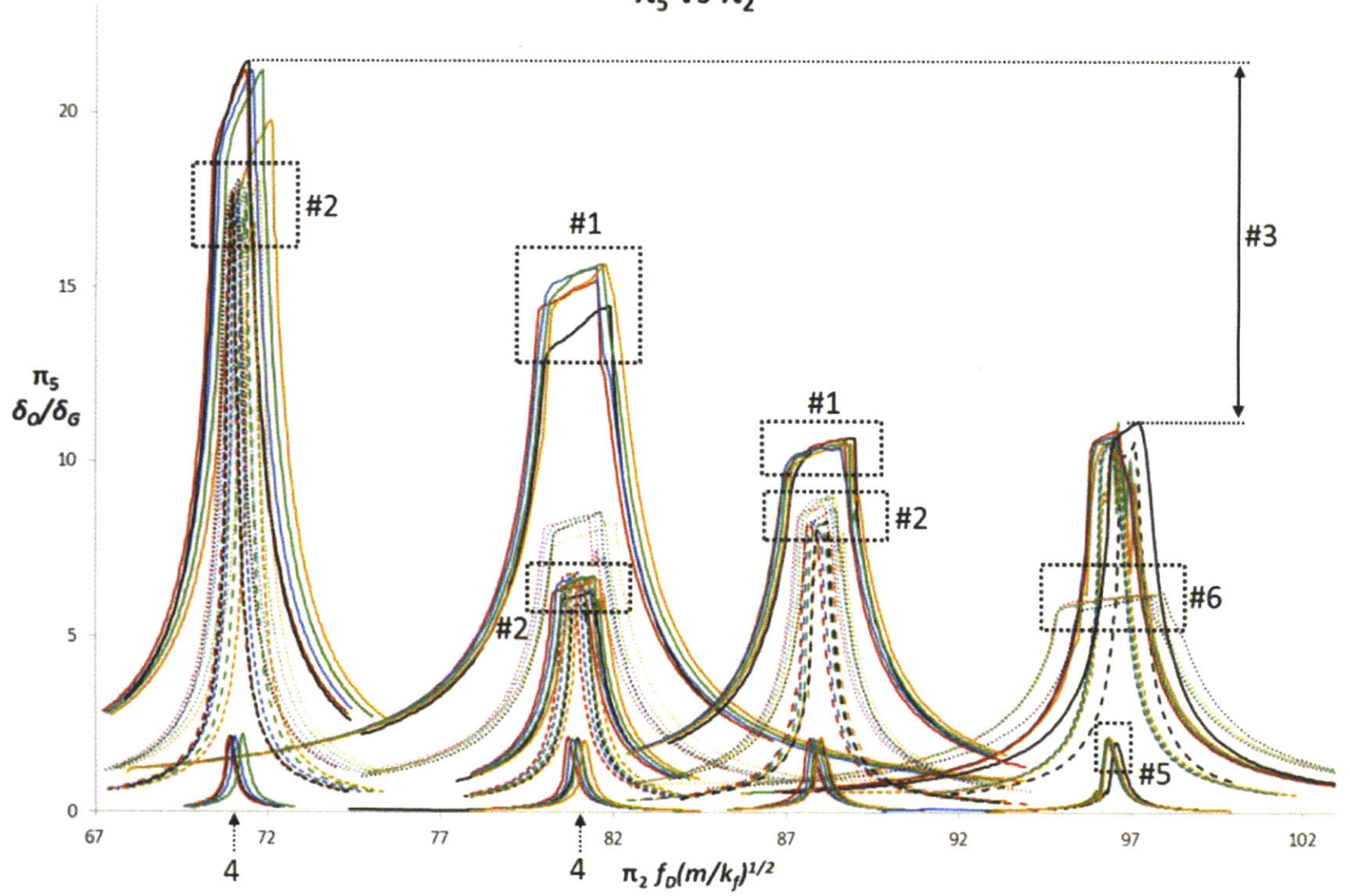
Figure 8.5: **Note 1**

Mass has no effect on the output-to-gap ratio (π_5). Each of the five different plateaus contained in the two boxes labeled **#1** are the same sample, boundary control height, and boundary control gap distance. The only variable that has been altered is the mass which ranged from 9.96-15.35g. Although there is some minor separation in the plateus, there is no discernable trend in the separation and is likely due to other inacuracies in the test process. The reason the mass has no appreciable effect on π_5 is likely because upon contact the beam stiffness increases by 10-250 times the original stiffness, thus rendering the inertial effects of the increased mass negligible when it comes to output deflection (δ_O).

Figure 8.5: **Note 2**

Although several of the samples had one large peak in the series of test (see the peaks noted in item **#1**) all four samples reached a steady π_5 once the gap distance was expanded beyond a few microns. Each of the four samples has two or three sets of tests that overlapped and had essentially the same output-to-gap (π_5) ratio. This indicated some "steady state" that could be reached with the system, such that there was a predicable ratio no matter what gap distance was chosen (this will be discussed further in the next section).

Figure 8.5: **Note 3**

Although the difference in the peaks between sample 1 and sample 4 appear to be quite large, this is a byproduct of the gap distance and contact height, and appears to have no direct correlation with the π_2 value. If a small gap (on the order of 1%-3% of total output) is used low on the beam, the π_5 will be large due the large output displacement at the tip and will show the same behavior regardless of the sample used. None of the tests appears to show a correlation between peak size and specific sample used.

Figure 8.5: **Note 4**

Each sample has a single π_2 value. As the gap distance, contact height, masses, etc were changed the tests all stayed on the same π_2. This makes sense since the mass which changes the natural frequency is in the denominator, and in the π_2 equation it is in the numerator. This shows

that the test setup was repeatable and that the π_2 term adequately captured the relationship between beam sample-mass combos.

Figure 8.5: **Note 5**

These low peaks indicate the beam samples when they are allowed to vibrate freely. There was no boudary control interation, which is essentially the same as a gap distance equal to one half the max deflection of the beam tip during resonance. The tight grouping once again indicated the both the repeatability and stability of the system.

Figure 8.5: **Note 6**

The flatness and width of the plateaus is a product of the gap distance and contact height. There are four distinct types of peaks. Figure 8.6 shows the four peak and boundary conditions which cause those peaks. The width of the plateau is indicative of span of frequencies that will cause contact between the sidewall and the boundary controls.
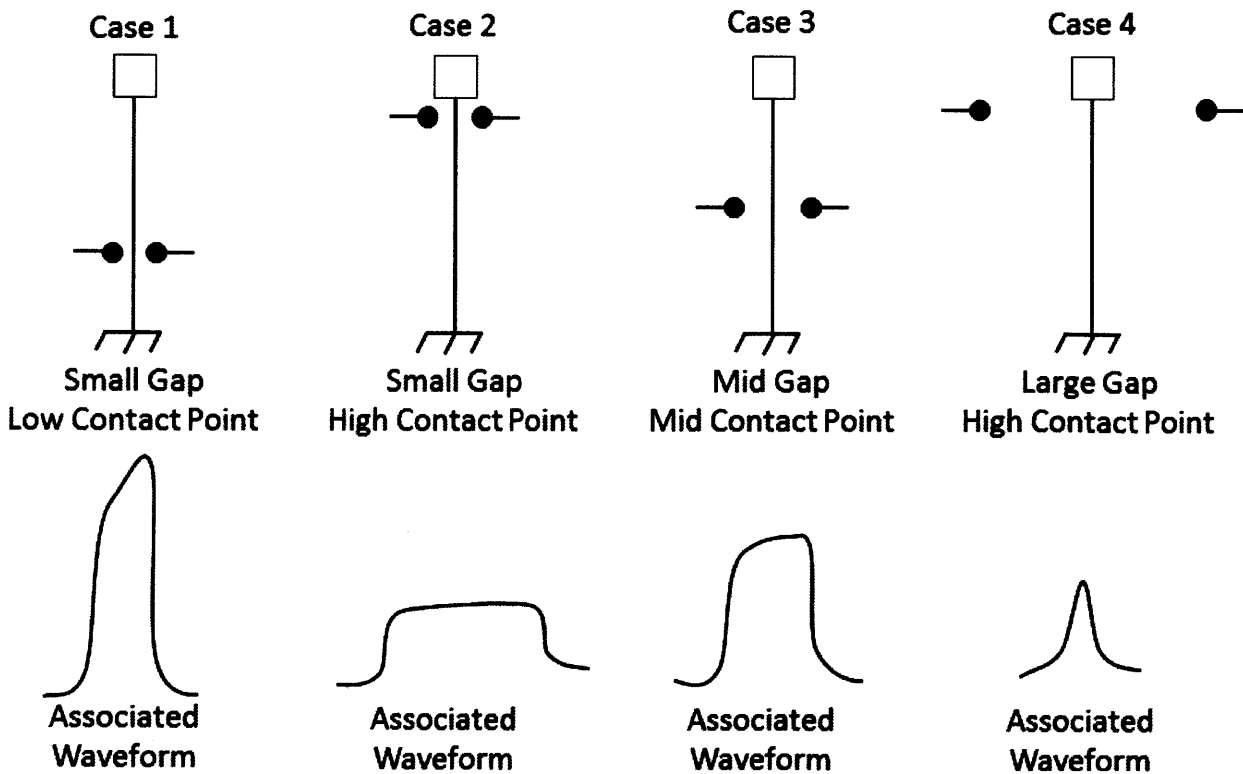
Figure 8.6: Boundary Contact Waveform Types

8.4 π_5-π_1 Association

Figure 8.7 is the graph of π_5 vs δ_G, and shows a unique feature of boundary control implementation. Below 10μm (~3% of maximum tip deflection) the π_5 value is a bit erratic, but stabilizes once the gap distance is greater than 3% of the total deflection value. This is likely due to inaccuracies in the gap distance measurement at such small values, and these inaccuracies become far less influential as the gap distance grows. Figure 8.7 shows that the π_5 is very stable despite gap distance (δ_G), mass (m), or driven amplitude (δ_D) changes. The two exceptions to statement are the two lowest contact point lines. However, even with their downward and upward slope the total range variation for either one above the 10μm gap distance was still less than 10% of the mean value. As was the case discussed earlier with the mass, the stability of the ratio is likely due to the stiffness after contact being so much higher than before contact, which means the mass or driven displacement which would normally have a large effect on output deflection are

far less impactful.

Figure 8.7:π_5 vs δ_G
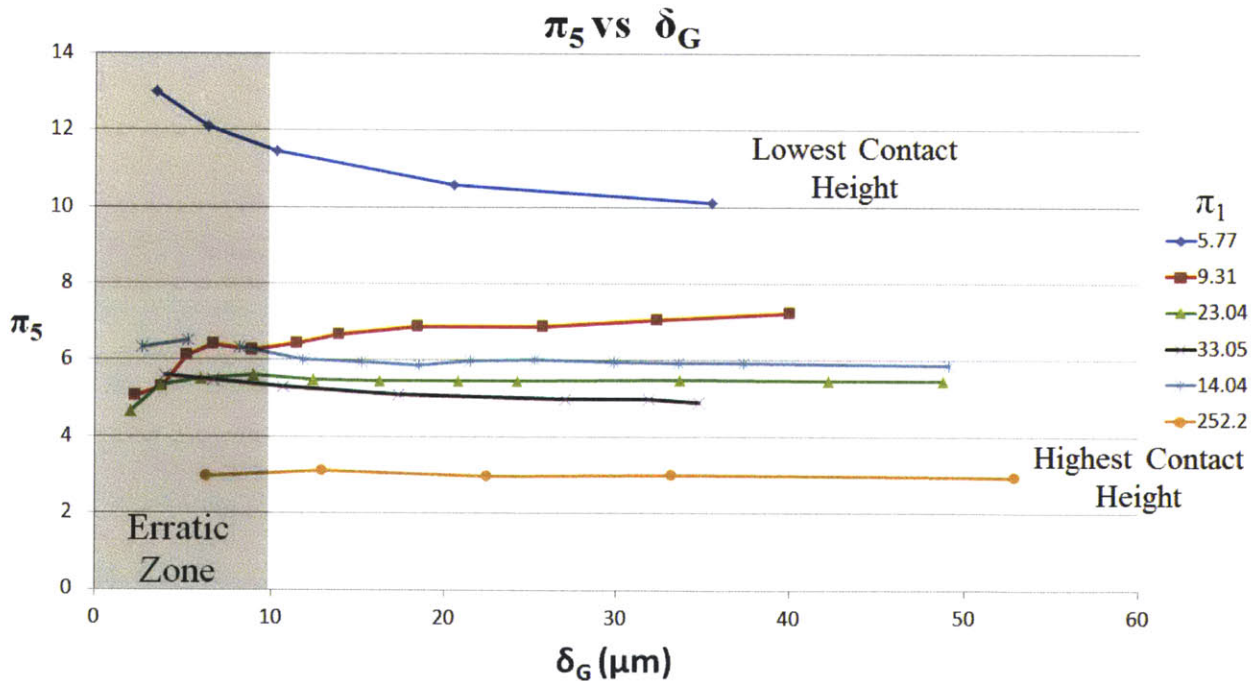
If the π_5 values on Figure 8.7 are averaged and plotted against π_1 (k_c/k_f), Figure 8.8 is the outcome. What this graph really signifies is the operating line for implementing boundary controls, and all variations possible must lie upon this line.
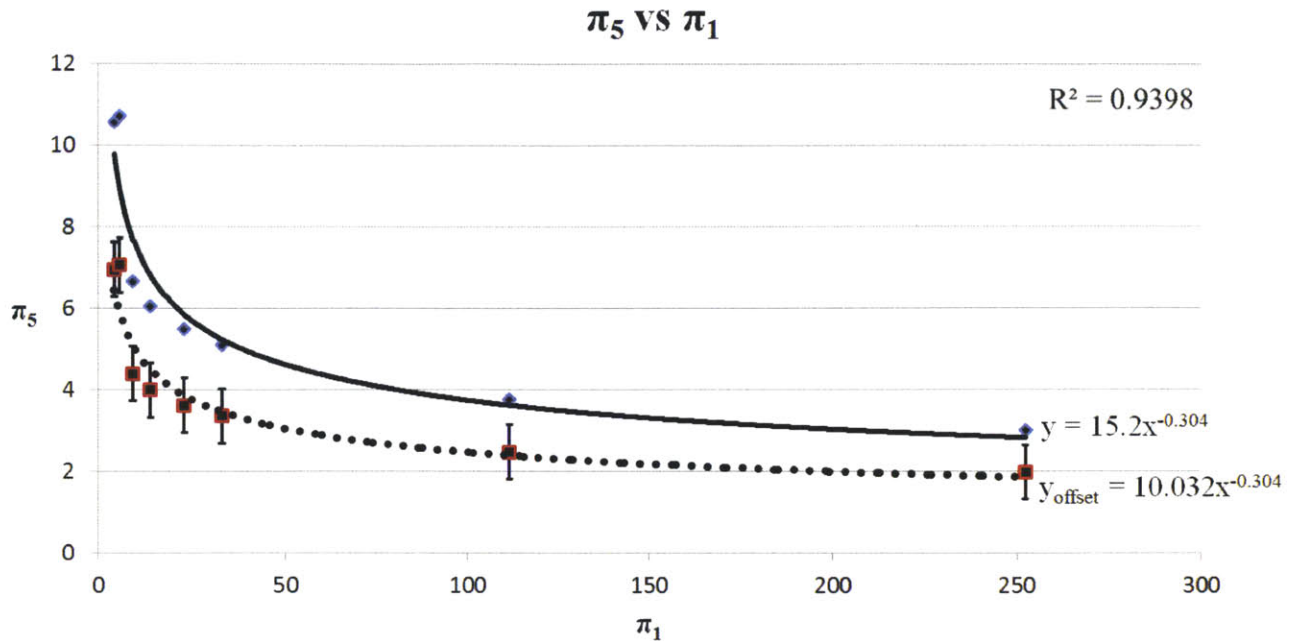
Figure 8.8:π_5 vs π_1

The largest standard error for this operating line was 6.8% and occurred at π_1 equal to 5.77, all other points had a standard error <3%. The y_{offset} indicates the π_5-π_1 relationship at the tip of the flexing portion of the beam and removes the effects of the extended area beyond the beam top (Figure 8.9). This is why on the non-offset line a π_1 value of 250 (essentially a hard stop) has a π_5 value of 3, instead of what would be the predicted value of 2 (boundary gap is half the total deflection). The y_{offset} equation when combined with the Pi terms becomes

Figure 8.9: Y vs Y_offset

$$\pi_5 = 10.032\pi_1^{-0.304} \quad \text{or} \quad \frac{\delta_O}{\delta_G} = 10.032 \left(\frac{k_c}{k_f}\right)^{-.0304}$$

These are the most significant equations in boundary control implementation, and represent a hard relationship between these four variables (δ_O, δ_G, k_c, k_f). Any combination of π_5 and π_1 must fall on this line. For any system, the designer will have a fixed k_f and δ_O, which allows him to choose either a δ_G which will dictate a specific k_c value, or choose a k_c value which will dictate a specific δ_G.
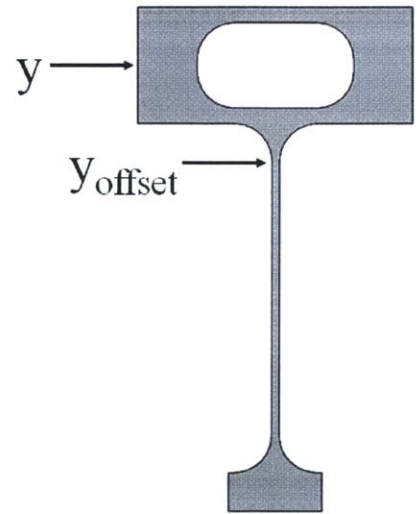
8.5 Which Variable to Control

With the items discussed in the previous section, the design can now tune the boundary control to give a specific output performance. The question then becomes which variable should we select as the driving value. As the δ_G in the π_5 term is adjusted the height value for the contact point needs to be adjusted to maintain position on the π_5-π_1 operating line. The smaller the δ_G value chosen, the lower the contact point needs to be placed (smaller L_a). The larger the δ_G value, the higher the contact point needs to be (larger L_a). The contact stress between the boundary control and the beam wall is highest the very top of the beam due to the tip being the max velocity found in the beam as well the Δt value being very small (causing a higher acceleration, thus higher contact force). However, as the contact point is lowered, the point of max stress in the beam (the bend around the contact point in most cases) sees an increase in overall stress. For this reason it is desirable for the δ_G value chosen to be the smallest value possible given the manufacturing or assembly tolerances, without causing the stress in the beam to exceed the max stress allowed in the material.

9.1 Practical Application Example

9.1.1 Initial Calculations

To demonstrate the application of this research we will apply it to a basic cantilever case study. Figure 9.1 shows a cantilever bending piezo (CMBP05 [43]) with a metal mass on the end. The yield stress of the PZT material is 55.4Mpa and has an elastic modulus of 60Gpa. The end user wants a factor of safety minimum of 2. The beam-mass combo is mounted on a machine that will be exposed to random vibration, and due to the nature of the piezo device is has a natural frequency within a high energy density zone of the vibration spectrum. The operation of the device means we cannot interfere with it as long as it is +/-50μm from the neutral position. Early analysis shows that the beam will deflect and break if the motion is not controlled. For a basic cantilever beam we know the stress is at a maximum where the moment is highest. If we take the second derivative of the deflection equation we get
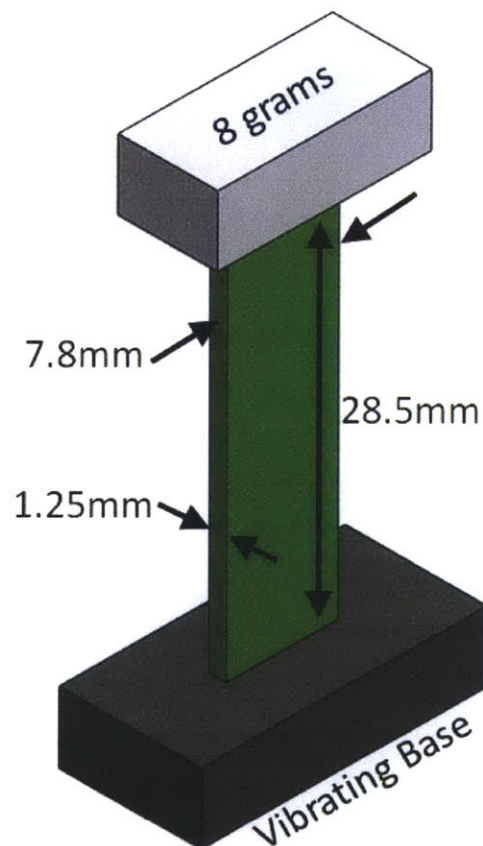
Figure 9.1: Practical Application Diagram

$$\delta = \frac{Fx^2(3L^3-x)}{6EI} \qquad \frac{d\delta}{dx}EI = \theta = \frac{-Fx(x-2L)}{2} \qquad \frac{d^2\delta}{dx^2}EI = M = -F(x-L)$$

This indicates the highest stress is at $x=0$, resulting in a stress value of

$$\sigma = \frac{My}{I} \quad \text{or} \quad \sigma_{max} = \frac{FLy}{\left(\frac{bh^3}{12}\right)}$$

In order to keep the stress below $0.5\sigma_{yield}$ (factor of safety of 2 desired by consumer) we must reduce the moment to 56.3N-mm, which corresponds to max cantilever deflection of 200μm. Now that we have the δ_O value we can determine if it is even possible to utilize boundary conditions to prevent failure in the device. Referring the operation line chart (Figure 9.2) and equation (see below) developed in the last chapter, we can determine the range of δ_G and k_c values we have as viable options.
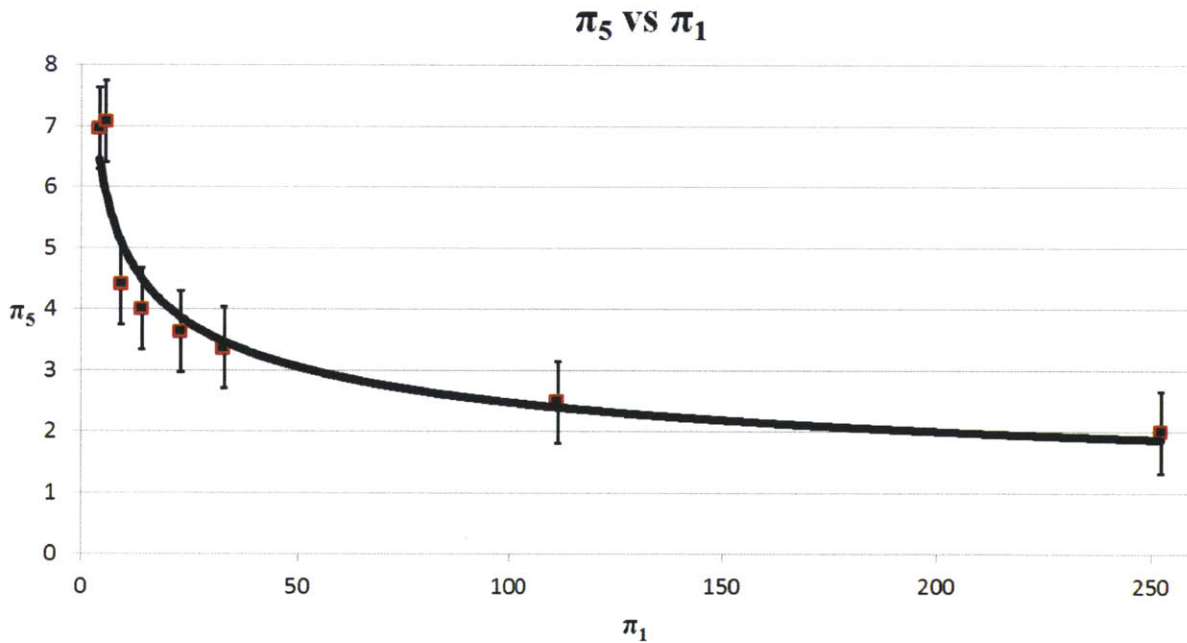
Figure 9.2: π_5-π_1 Operating Line

$$\pi_5 = 10.032\pi_1^{-0.304} \quad \text{or} \quad \frac{\delta_O}{\delta_G} = 10.032\left(\frac{k_c}{k_f}\right)^{-.0304} \quad \text{(I)}$$

If my δ_O=200μm, and my k_f=9.87N/mm as determined by the equation

$$k_f = 3EI/L^3$$

by inserting the known δ_O and k_f values into equation **(I)** we can determine the range of values possible for δ_G and k_c. As can be seen in Figure 9.3, the range is vast. To narrow it down, we know the k_c must be larger than k_f as the contact can only increase the beam stiffness. This means all k_c values below k_f can be eliminated.

$k_{c\ vs}\ \delta_G$

k_c
(N/mm)

δ_G (μm)
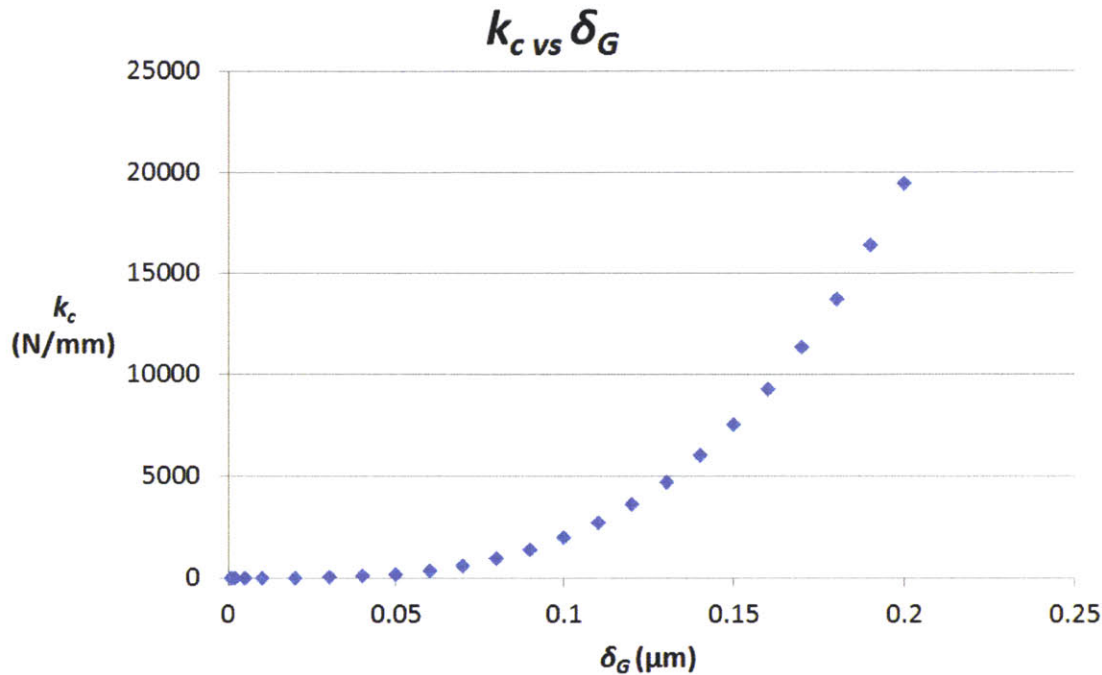
Figure 9.3: Range of kc and δG Values

Next we can assume anything contacting the top 10% of the beam is essentially a hard stop. To determine this k_c value we use

$$k_c = \frac{12EI}{4L^3 - 3LL_a(2L_a + 3L_b) + L_a^2(2L_a + 3L_b)} \quad \textbf{(II)}$$

with an L_a=0.9L, which is L_a=25.65mm, which results in kc=1.2kN/mm. If we remove the upper and lower portions of the values and we are left with Figure 9.4.
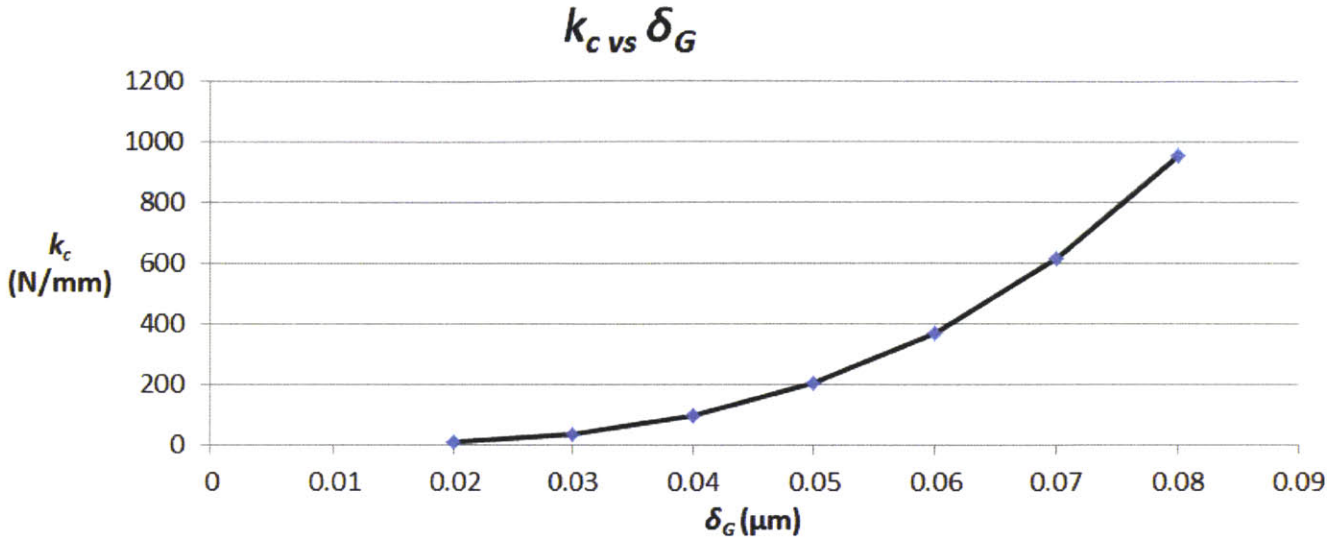
Figure 9.4: Useable k_c and δ_G Values

To narrow the options even more we must determine which of these points is even physically possible. To do this we can start with the smallest allowable gap size, which is 0.02mm, and results in k_c=9.98 (using Equation **(I)**). Using the stiffness equation **(II)** we find that this corresponds to a L_a=0.13mm (contact height), which reveals an impossibility since in the free deflected beam that beam height never reaches 0.02mm deflection. We need to find where the intersection point between possible usable δ_G and k_c values intersect with the physical deflection of the beam. This occurs when the δ_G value which produces a k_c is less than the δ at that same height on the beam. We can find this point by setting $\delta_G=\delta_{(La)}$ and substituting in all known values, this process is detailed below

$$\delta = \frac{Fx^2(3L^3-x)}{6EI} \quad \text{becomes} \quad \delta = \frac{FL_a{}^2(3L^3-L_a)}{6EI}$$

and

$$\frac{\delta_O}{\delta_G} = 10.032\left(\frac{k_c}{k_f}\right)^{-.0304} \quad \text{becomes} \quad \frac{0.2}{\delta_G} = 10.032\left(\frac{k_c}{9.87}\right)^{-.0304}$$

which can be rearranged to produce

$$\delta_G = 0.00994k_c^{0.304} \text{ (III)}$$

Substituting in the equation for k_c results in

94

$$\delta_G = 0.00994 \left(\frac{12EI}{4L^3 - 3LL_a(2L_a + 3L_b) + L_a{}^2(2L_a + 3L_b)} \right)^{0.304}$$

setting $\delta_G = \delta_{(La)}$ results in

$$\frac{FL_a{}^2(3L^3 - L_a)}{6EI} = 0.00994 \left(\frac{12EI}{4L^3 - 3LL_a(2L_a + 3L_b) + L_a{}^2(2L_a + 3L_b)} \right)^{0.304}$$

Inserting the proper values with F=1.94 (corresponds to the max deflection of 200μm), we find La=0.26mm, which indicates the very first height we can implement a boundary control. This point corresponds to a k_c value of 10.08N/mm and δ_G=.02. In this case the intersection point is just barely higher than our minimum possible k_c and δ_G values, so we will continue to use Figure 9.4.

9.1.2 Bending Stress After Contact

To further narrow down our options, we must now look at the contact stress and beam stress after contact. If we chose a max deflection such that the stress in the base of the beam is $0.5\sigma_{yield}$, we know that upon the moment of contact the base will have the highest stress. However, as the beam bends around the contact point the stress in the base of the beam is relieved and the contact point becomes the point of highest stress. This stress increases as the height of the boundary control is decreased. To find the lowest useable point, we can combine the δ_G and k_c relationship with the stress equation for the beam, this process is seen below

The stress in the beam will be the sum of the stress of the three beam conditions discussed in Section 4.1.3. The second derivatives of these beam equations at L_a are

$$M_I = -F'(L_a - L) \text{ and } M_{II} = -F''(L_a - L)$$

and

$$M_{III} = -\frac{F'(L_a - 3L)(L_a - L_a)}{2L_a}$$

We notice the M_{III} value is equal to zero be default, which makes sense since it is essentially just the tip of a cantilever beam. We also know that

$$F' = d\frac{6EI}{L_a^2(3L-L_a)} \quad \text{or with } \delta_G \text{ substituted for } d \quad F' = \delta_G\frac{6EI}{L_a^2(3L-L_a)}$$

and if we substitute the relationship between δ_G and L_a, equation **(III)** with the full k_c equation substituted in we get

$$F' = 0.00994\left(\frac{12EI}{4L^3 - 3LL_a(2L_a + 3L_b) + L_a^2(2L_a + 3L_b)}\right)^{0.304}\frac{6EI}{L_a^2*(3L-L_a)}$$

and

$$F'' = F - F'$$

although the equations seem messy, combining the full M_I and M_{II} values produces

$$M_{eq} = -F'(L_a - L) - F(L_a - L) + F'(L_a - L)$$

which simplifies to

$$M_{eq} = -F(L_a - L)$$

the combined stress equation at the contact point is then

$$\sigma_{ContantPoint} = \frac{-F(L_a-L)y}{I} \quad \textbf{(IV)}$$

with y being the distance between the neutral axis and outermost fiber.

Equation **(IV)** demonstrates that the bending stress is greatest when the difference between L and L_a is the greatest. However, it also shows that the bending stress at the contact point can never exceed the bending stress found in the original cantilever beam. Once boundary contact is achieved, the δo-δ_G (π_5) limits the deflection such that the stress can never rise to a level found in the original cantilever beam.

9.1.3 Contact Stress

The last consideration is the contact stress between the boundary point and the beam wall. To adequately determine the contact stress, we need to know the acceleration at max deflection, the moment when the tip mass has zero motion (Note: there are a many ways to determine this, the process used in this thesis is a simplified conservative process and will not necessarily give exact contact stress values, rather it is based upon "worst case" assumptions and produces a theoretical maximum contact stress).

First we will check the point of max contact stress, which will always be the highest possible contact point on the beam. For the contact stress we need to determine both the static force and the force required to accelerate the beam at it furthest deflection point. The easiest way to do this is by determining when this contact stress would be the highest, which should be when the beam is resonating. For this beam we can determine the natural frequency either by precise FEA, or use the simplified equation

$$fn = \left(\frac{1}{2\pi}\right)\sqrt{\frac{k_f}{m}} \text{ (Hz)}$$

This gives us a natural frequency of 176Hz. This means each cycle at resonance will take 5.7ms. At the highest contact point (0.9L) we have k_c=12kN/mm which results in π_1=129, and corresponds on Figure 9.2 with π_5=2.29 and therefore δ_G=87.3μm. A conservative estimate is to determine what the tip deflection at the point of contact is using the equation

$$\delta = \frac{Fx^2(3L^3-x)}{6EI} \quad \text{rearranged to solve for } F \quad F = \frac{\delta 6EI}{x^2(3L^3-x)}$$

and substitute L_a for x, and δ_G for δ

$$F = \frac{\delta_G 6EI}{L_a{}^2(3L^3 - L_a)}$$

and use this F value to solve for tip deflection when contact occurs

$$\delta = \frac{\left(\frac{\delta_G 6EI}{L_a{}^2(3L^3-La)}\right)L^3}{3EI}$$

which simplifies to

$$\delta = \frac{-2\delta_G L^3}{L_a^2(L_a-3L)}$$

resulting in tip deflection of 102μm when the beam wall contacts the boundary point. If we look at the total motion of the tip (Figure 9.5) we find that this means for each cycle the tip passes through the **B** zone 4 times and the **A** zone twice. This results in a ratio of 2:1 for amount of time the tip deflection is in contact with the boundary point. This is a conservative assumption since in reality the center zone is the highest velocity region, meaning it would
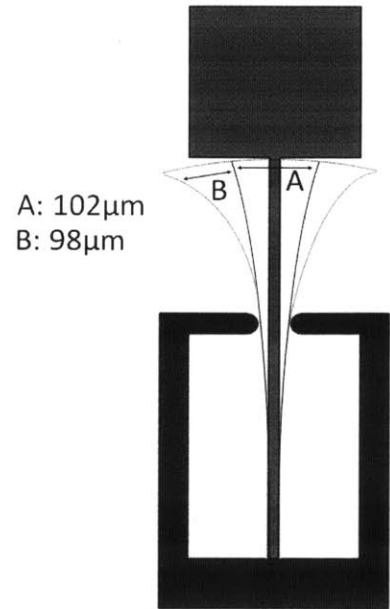

A: 102μm
B: 98μm

Figure 9.5: Deflection Zones

spend less time there and more time in contact with the boundary controls. Using this basic assumption we can then determine that the tip mass goes from its max velocity to a zero velocity in the span of 98μm, which accounts for ~1/6th of the total time in a full cycle. If the full cycle takes 1/(176Hz) or 5.7ms, we can use 1/6th of this value to determine the $\varDelta t$ used to calculate the acceleration of the tip mass. Lastly, we need to determine the velocity of the tip prior to impact. Rather than determining the exact velocity at the point of contact, we will use the max velocity found at the neutral point. Similar to the assumptions prior to this, it assumes a worse case than will be found in the actual system. To determine the max velocity we use the equation

$$V_{max} = \frac{\delta_O}{2}\sqrt{\frac{k_f}{m}}$$

this gives us a V_{max}=0.11m/s, which we can then combine with $\varDelta t$=(1/6)5.7ms to determine acceleration

$$V_f = V_{max} + at$$

with V_f=0 at the point of max deflection, this give us a=-12m/s^2, which we can then use with

$$F_{Inertial} = ma$$

to find the force required to achieve this acceleration is 0.94N, which we will combine with 1.94N static force to determine the equivalent force at the contact point, F_e=2.88N we will assume this is the only force acting on the beam.

Now we must determine the contact stress. This stress will be greatly affected by the radius of the contact surface and whether we choose a point contact or a line contact. As discussed earlier in the thesis, a line contact is preferred but is only possible when a very high level of precision is possible in aligning the parallel surfaces. For the case of this research, we will use a steel ball contact with a radius of 50mm (see Section 3.1.3 for a deeper look at contact stresses). To determine the contact stress we will start by determining the contact area [44]

$$a = \left(\frac{3F_{Inertial}\left(\frac{1 - v_1^2}{E_1} + \frac{1 - v_2^2}{E_2}\right)}{4\left(\frac{1}{R_1} + \frac{1}{R_2}\right)}\right)^{\frac{1}{3}}$$

With v, E, and R being Poisson's ratio, Young's Modulus, and radius of the two contact items respectively. Using the proper values we get a contact area of 0.127mm^2. To determine pressure we use [44]

$$p = \frac{3F}{2\pi a^2}$$

inserting the proper values we get a p=85.8N/mm^2. From here we can determine the max shear stress using [44]

$$\tau = 0.31p$$

which gives us τ=26.6Mpa, which is just above the 27.7Mpa factor of safety of 2 yield strength of the PZT material. This demonstrates the inability to use a hard stop in this application, which would cause a failure in the piezo as soon as resonance was achieved.

To shorten the contact stress process, we can do the last section in reverse. Determine what p value would give you a factor of safety of 2 with respect the shear stress, and continue to back calculate until you determine a suitable contact height.

In this case, we as the designer have established that we have the option to use essentially the entire range contained in Figure 9.4, and can adjust our k_c and δ_G values based upon other factors such as manufacturing, size constraints, etc.

10

Recap and Future Work

10.1 Research Recap

Compliant mechanisms continue to see expanded use as mechanical systems become more complex, smaller, and more precise. The benefits of compliant system are their simplicity, ease of manufacturing and assembly, and high level of precision. However, these compliant systems are severely limited in application where they can be subjected to high vibrational forces. This is due to the conflict between designed stiffness and sensitivity to frequencies where external vibration and compliant mechanism natural frequency overlap. Space bound applications subjected to launch vibration are a primary example of this conflict. The purpose of this thesis was to develop a deliberate design approach that an engineer could use to mitigate failure sensitivity without causing the fundamental operation of the compliant mechanism to be compromised. By developing, testing, and proving a method of implementing boundary controls this research expands the range of applications which compliant mechanism based systems can be applied.

10.2 Research Contribution

The design tools in this thesis will allow an engineer to intelligently design a boundary control into a pre-existing or pre-engineered cantilever compliant stage to prevent catastrophic failure of the stage if it is subjected to vibrational forces. By analyzing the cantilever compliant stage in the context of its basic variables this thesis shows the engineer which variables affect the survivability of the stage and how to adjust these variables to prevent the stage from deflecting to the point of failure. The Buckingham Pi theory combined with test data revealed the correlations which can be used to prevent both failures due to excess stress in the cantilever beam as well as

stress caused by the contact between the beam and boundary control. With the processes detailed in this thesis engineers can now implement the boundary controls within the context of manufacturing, assembly, or other auxiliary limitations. This research has also laid the foundation for future work in boundary control implementation for more complex flexure systems.

10.3 Future work

10.3.1 Complex Flexures

This research only dealt with cantilever flexures and sought to establish the foundation for boundary control use in the field of flexures. However, cantilever beams are the most basic flexure type and are often used with different end conditions as building blocks for more complex flexures (parallel, four-bar, etc.). In order to adapt this research to a broader spectrum of flexure technologies many more tests would have to be done on specific flexure designs.

10.3.2 Greater Mass/Frequency Ranges

Due to the use of the Buckingham Pi, and the number of Pi terms involved, the range of variables able to be tested needed to be condensed. The research was intended as a proof-of-concept and roadmap for future study. It does not necessarily encompass the full range of dynamics that may occur. To build a more comprehensive set of data a much more vast variable range would need to be used and would require more time than was available for this research.

10.3.3 Higher Mode Shapes

This research is limited to the resonant behavior of a cantilever beam in its first mode shape only. Even with the low natural frequency of the beams tested, the second mode shapes occurred above the maximum frequency range of the vibrating platform. In order for second and third modes to be studied a more responsive and capable vibration platform is required.

10.3.4 Multi Degree of Freedom Systems

This research dealt with a simplified system with a single degree of freedom. Theoretically this should be able to apply to other degrees of freedom with the same motion type

(i.e. linear motion, not torsion). A more complex vibration platform and test rig would be required to study flexures involving multiple linear motions or rotational motion.

SPECIAL THANKS

This research first started as an engineering project for Lincoln Labs under the direction of Mr. Joe Scozzafava and Professor Marty Culpepper, both of which provided great direction and expectation for the work I was doing. From the engineering design came the novel research into boundary controls.

Upon starting work on the nanopositioner I had very little experience in machining or fabricating and would like to thank Bob Panas and Aaron Ramirez for teaching me everything from developing tool paths and manufacturable CAD designs to milling practices and proper machine use.

I would like to thank the entire PCSL family who supported me and were there when I had questions and provided guidance or expertise when I asked, and were just a great bunch of people to work with; Prof. Marty Culpepper, Maria Tellaria, Bob Panas, Aaron Ramirez, Sourabh Saha, Josh Nation, Brandon Evans, Marcel Thomas, Charlie Wheeler, and Lauren Chai.

Special thanks to John Kuconis who goes out of his way each year to give students like myself from Service Academies the opportunity of a lifetime and secures funding for each and every one to ensure they are able to complete their program without extra financial burden.

Thanks to the entire Lincoln Lab team who helped me over the last two years. Thanks to Allan Lush for his assistance with FEA theory and application. Special thanks to the three wonderful secretaries that showed me incredible patience and guided me through all the administrative processes required to complete my work; Joanna Erbafina, Paula Lach, and Noreen Arakelian.

REFERENCES

[1]   NASA, "Lunar Laser Communications Demonstration," accessed Jul. 2014,
      <http://esc.gsfc.nasa.gov/267/271.html>.

[2]   NASA, "Lunar Laser Communications Demonstration," accessed Jul. 2014,
      <https://solarsystem.nasa.gov/missions/docs/LLCDFactSheet.final.web.pdf>.

[3]   D. M. Boroson et al. "The Lunar Laser Communications Demonstration (LLCD)." Space
      Mission Challenges for Information Technology, 2009. SMC-IT 2009. Third IEEE
      International Conference on. 2009. 23-28.

[4]   D. L. Clark, M. Cosgrove, R. VanVranken, "Application of a Single Area Array Detector
      for Acquisition, Tracking and Point-Ahead in Space Optical Communications," NASA,
      Rochester, NY, 1989.

[5]   Piezo Systems, INC., "Introduction to Piezo Transducers," accessed Jul. 2014,
      <http://www.piezo.com/tech2intropiezotrans.html>.

[6]   "Minotaur User's Guide," Manual, Orbital Sciences Corporation, USAF Kirtland AFB,
      NM, 2002.

[7]   Noliac, "Plate Bender 3 (CMBP03)," Datasheet, accessed Jul. 2014,
      <http://www.noliac.com/Default.aspx?ID=739&NPMode=View&ProductID=27>.

[8]   S. Clark, "Minotaur rocket poised to send research to new heights," accessed Jul. 2014,
      <http://spaceflightnow.com/minotaur/stps26/101118preview/>.

[9]   P. B. De Selding, "Space Forecast Predicts Satellite Production Boom," accessed Jul.
      2014, <http://www.space.com/6839-space-forecast-predicts-satellite-production-
      boom.html>.

[10] S. Kota, K. J. Lu, K. Kreiner, B. Trease, J. Arenas, J. Geiger, "Design and Application of
      Compliant Mechanisms for Surgical Tools," *Journal of Biomechanical Engineering*, vol
      127, pp. 981-989, 2005.

[11] Wulfsberg, J.P., et al. "A Novel Methodology For The Development Of Compliant
      Mechanisms With Application To Feed Units." *Production Engineering - Research And
      Development*, vol. 7.5, pp. 503-510, 2013.

[12] Kumar, G. Arun, and P. S. S. Srinivasan. "Design Of Compliant Mechanisms - A
      Topology Optimization Approach For New Age Industries And Engineering Support."
      CURIE Journal, vol. 3.3/4, pp. 10-19, 2010.

[13] D. C. Freeman, "Nonlinear Springs With Applications To Flow Regulation Valves And
      Mechanisms," n.p.: c2008., 2008. MIT Barton Catalog. Web. Aug. 2014.

[14] C. T. Mueller-Falcke, "Switchable Stiffness Scanning Microscope Probe," n.p.: c2005.,
      2005. MIT Barton Catalog. Web. Aug. 2014.

[15] nPoint, "Product nPXY60-258," Datasheet, accessed Jul. 2014,
      <http://www.npoint.com/products/nanopositioning-stages/item/72-npxy60-258.html>.

[16] Physik Instrumente, "P-612 XY Piezo Nanopositioning System," Datasheet, accessed Jul.
      2014, <http://www.physikinstrumente.com/en/products/prdetail.php?sortnr=201740>.

[17] Nanotechweb, "PZ 250 CAP WL High Precise Wafer," Datasheet, accessed Jul.2014,
      <http://nanotechweb.org/cws/product/P000030801>.

[18]   J. B. Hopkins, M. L. Culpepper, "Synthesis of Precision Serial Flexure Systems Using Freedom and Constraint Topologies (FACT)," *Precision Engineering*, vol. 35, pp. 638-649, 2011.

[19]   B. Black, M. Lopez, A. Morcos, "Basics of Voice Coil Actuators," *Power Conversion Intelligent Motion*, July, pp. 44-46, 1993.

[20]   H2W Technologies, "Non-Comm DC Voice Coil Linear Actuator," Datasheet, accessed Jul. 2014, <http://www.h2wtech.com/Products/ShowProduct?productid=2>.

[21]   Noliac, "Piezo Design Tutorial: Fundementals of Piezoelectric Actuators." Informational Pamphlet, accessed Jul. 2017, <http://www.piezo.ws/piezoelectric_actuator_tutorial/Piezo_Design_part3.php?>.

[22]   Piezo Systems Inc., "Standard Quick-Mount Piezoelectric Bending Actuators," Product Catalog, accessed Jul. 2014, <http://www.piezo.com/prodbm7qm.html>.

[23]   Physik Instrumente, "PL112-PL140 PD410 PICMA® Bender Actuator," Product Catalog, accessed Jul. 2014, <http://www.physikinstrumente.com/en/products/prdetail.php?sortnr=103000>.

[24]   Noliac, "Plate Benders," Product Catalog, accessed Jul. 2014, <http://www.noliac.com/Plate_benders-57.aspx>.

[25]   Matweb, "Aluminum 6061-T6," Datasheet, accessed Jul. 2014, <http://www.matweb.com/search/DataSheet.aspx?MatGUID=1b8c06d0ca7c456694c7777d9e10be5b>.

[26]   MEMSnet, "Material: Lead Zirconate Titanate (PZT)," Property Sheet, accessed Jul. 2014, < https://www.memsnet.org/material/leadzirconatetitanatepzt/>.

[27]   Sporting Good Review, "Schutt Adult ION 4D Helmet Review," Online Article, accessed Jul. 2014, < http://www.sportinggoodreviews.com/schutt-adult-ion-4d-football-helmet-review/>.

[28]   Jeff ClickHomes, "Silence of the Slams," Online Article, accessed Jul. 2014, < http://jeffclickhomes.com/blog/wtff-silence-of-the-slams/>.

[29]   CellPhone Beat, "Useful Tips to Choose an Ideal Cellphone Case," Online Article, accessed Jul. 2014, < http://www.cellphonebeat.com/tips-choose-ideal-cellphone-case.html>.

[30]   Korea JoongAng Daily, "Impact of Airbags Focus of New Camry Ad," Online Article, accessed Jul. 2014, < http://mengnews.joins.com/view.aspx?gCat=050&aId=2952791>.

[31]   Circle Track, "Race Safer – Helmets and Head Restraint Gear," Photo Gallery, accessed Jul. 2014, <http://www.circletrack.com/techarticles/1306_race_safer_helmets_head_restraint_gear/photo_11.html>.

[32]   Jae-Sung, Kwon, et al. "*Outgassing Characteristics Of A Polycarbonate Core Material For Vacuum Insulation Panels,*" Vacuum 85.8, pp. 839-846, 2011.
        Taggart & Sons Automotive, "Shock and Strut Suspension Service," Online Article, accessed Jul. 2014, < http://www.taggartautorepair.com/shock_and_strut_suspension_service.asp>.

[33]   Taggart & Sons Automotive, "Shock and Strut Suspension Service," Online Article, accessed Jul. 2014, <http://www.taggartautorepair.com/shock_and_strut_suspension_service.asp>.

[34]   ISOTECH, "Model DS 03-12, Oil Damper," Product Catalogue, accessed Jul. 2014, < http://catalog.isotechinc.com/item/gas-springs/oil-dampers/d-04-12>.

[35]   Tech Products Corporation, "Technical Section: Vibration and Shock," Technical Manual, accessed Jul. 2014, <http://www.fabreeka.com/documents/file/Vibration AndShock.pdf>.

[36]   D. L. Hall, "Understanding SHOCK LOADS." *TD&T: Theatre Design & Technology*, vol. 49.2, pp. 46-51, (2013).

[37]   A. H. Slocum, "Precision Machine Design," Dearborn, Michigan: Society of Manufacturing Engineers, 1992.

[38]   T. A. Philpot, "Mechanics of Materials: An Integrated Learning System. Hoboken", NJ: J. Wiley, 2008. Print.

[39]   E. Kausel, "Advanced Structural Dynamics," Student Guide, MIT CopyTech, 2013.

[40]   Brown University, "Sensors and Sensing", Online Guide, accessed Aug. 2014, <http://cs.brown.edu/~tld/courses/cs148/02/sensors.html>.

[41]   B. R Munson, D. F. Young, T. H. Okiishi, "Fundamentals of Fluid Mechanics," John Wiley & Sons, 1990.

[42]   P. A. Lagace, "Solutions for Single Spring-Mass Systems," Online Course Text, MIT OpenCourseWare, accessed Aug. 2014, < http://ocw.mit.edu/courses/aeronautics-and-astronautics/16-20-structural-mechanics-fall-2002/lecture-notes/unit20.pdf>.

[43]   Noliac, "Plate Bender 5 (CMBP05)," Datasheet, accessed Jul. 2014, < http://www.mmech.com/noliac-actuators/plate-benders/cmbp05>.

[44]   L. C. Hale, "Contact Mechanics," Online Course Text, MIT OpenCourseWare, accessed Aug. 2014, <http://ocw.mit.edu/courses/mechanical-engineering/2-76-multi-scale-system-design-fall-2004/readings/lec12cont_read.pdf>.